INFORMATION TO USERS

This manuscript has been reproduced from the microfilm master. UMI films the text directly from the original or copy submitted. Thus, some thesis and dissertation copies are in typewriter face, while others may be from any type of computer printer.

The quality of this reproduction is dependent upon the quality of the copy submitted. Broken or indistinct print, colored or poor quality illustrations and photographs, print bleedthrough, substandard margins, and improper alignment can adversely affect reproduction.

In the unlikely event that the author did not send UMI a complete manuscript and there are missing pages, these will be noted. Also, if unauthorized copyright material had to be removed, a note will indicate the deletion.

Oversize materials (e.g., maps, drawings, charts) are reproduced by sectioning the original, beginning at the upper left-hand corner and continuing from left to right in equal sections with small overlaps.

Photographs included in the original manuscript have been reproduced xerographically in this copy. Higher quality 6" x 9" black and white photographic prints are available for any photographs or illustrations appearing in this copy for an additional charge. Contact UMI directly to order.

ProQuest Information and Learning
300 North Zeeb Road, Ann Arbor, MI 48106-1346 USA
800-521-0600

Regenerating the Sampling Interface of Modular Chemical Sensing Systems

Heather Colburn Edberg

A dissertation submitted in partial fulfillment of the requirements for the degree of

Doctor of Philosophy

University of Washington

2002

Program Authorized to Offer Degree: Chemistry

UMI Number: 3041019

ProQuest Information and Learning Company
300 North Zeeb Road
P.O. Box 1346
Ann Arbor, MI 48106-1346

In presenting this dissertation in partial fulfillment of the requirements for the Doctoral degree at the University of Washington, I agree that the Library shall make its copies freely available for inspection. I further agree that extensive copying of the dissertation is allowable only for scholarly purposes, consistent with "fair use" as prescribed in the U.S. Copyright Law. Requests for copying or reproduction of this dissertation may be referred to Bell and Howell Information and Learning, 300 North Zeeb Road, Ann Arbor, MI 48106-1346, to whom the author has granted "the right to reproduce and sell (a) copies of the manuscript in microform and/or (b) printed copies of the manuscript made from microform."

Signature: Heather C. Ebbing

Date: 2/24/02

University of Washington
Graduate School

This is to certify that I have examined this copy of a doctoral dissertation by

Heather Colburn Edberg

and have found that it is complete and satisfactory in all respects, and that any and all revisions required by the final examining committee have been made.

Chair of Supervisory Committee:

Lloyd W. Burgess

Reading Committee:

Lloyd W. Burgess

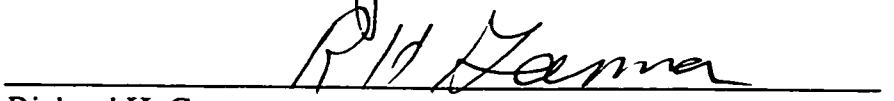

Richard H. Gammon

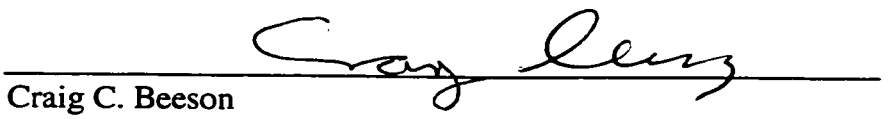

Craig C. Beeson

Date: 27 Feb. 2002

University of Washington

Abstract

Regenerating the Sampling Interface of Modular Chemical Sensing Systems

Heather Colburn Edberg

Chair of the Supervisory Committee:

Research Professor Lloyd W. Burgess
Chemistry

This dissertation describes modular chemical sensing systems (MCSS) and how the sampling interfaces of these systems can be regenerated. By regenerating the sampling interface, the reproducibility of the sensing system's measurements can be improved over traditional stationary sampling interfaces. The first modular chemical sensing system explored in this work is a chemiluminescent biosensor with fiber optic detection. The concept of *in situ* replacement the part of the sensor that imparted selectivity and pre-concentration, in this case the antibody layer, grew out of this work after conventional immobilization strategies failed and non-covalent immobilization was explored. This led to exploration of other systems or system components that can be regenerated to increase the stability of a chemical sensing system over time.

These other systems include a dissolved oxygen sensing system for marine deployment, the liquid core waveguide, and supported liquid membrane sampling interfaces. The oxygen sensing system's sampling interface is an electrolyte-filled

tubular membrane. The electrolyte is renewed with each measurement, thereby renewing the sampling interface of the system. Membrane biofouling is prevented by periodically illuminating the tube with UV radiation. The liquid core waveguide can be used as both a detector and sampling interface. It is a semi-permeable membrane in which the core material can be renewed with each measurement, regenerating the sampling interface. In addition, it is a long-path optical cell that can be used for sensitive absorbance-based or Raman detection. Supported liquid membranes were also explored in this work as a sampling interface for two sensing systems, the FlowProbe and the liquid core waveguide. Supported liquid membranes provide one-step extraction from a bulk matrix where the reagent acts as the sink for the extracted species. Renewing this reagent regenerates the sampling interface. Additionally, *in situ* replacement of the supported liquid membrane was explored.

Table of Contents

List of Figures

List of Tables

Acknowledgements

This body of work would not have been possible without the contribution of others. I would like to thank my advisor Lloyd Burgess as well as my committee, Richard Gammon, Craig Beeson, and Bill Parson. In addition, I would like to thank Bruce Kowalski for taking me on as an advisee when I first started. Thanks to the past and present members of the Kowalski and Burgess groups for their beneficial discussions.

This work is the summation of several collaborative efforts. The first of which, the chemiluminescent fiber optic biosensor was in collaboration with Clem Furlong and his research group in UW's Medical Genetics Department. The biosensor work was funded by the Washington SeaGrant. The second major collaborative effort was the oxygen sensing system in collaboration with Professor Steve Emerson's research group in the UW's Oceanography Department. I would like to thank Steve for his guidance with the project. A special thanks to Peter Kauffmann for all of his efforts in the design and construction of the prototype and electronics. In addition, thanks go to Chuck Stump, Vernon Brock, and Julia Lynton for their sampling and Winkler titration skills. The Oxygen sensor work was also funded by the Washington SeaGrant.

A huge thanks goes to Dr. Brian Marquardt for his aid in the liquid core waveguide development, particularly optical-train design and alignment. I also want to acknowledge Dr. Leanna Levine from Spectrum Laboratories for the supported

liquid membrane modules and her helpful discussions with that phase of the project. This work was funded in part by the Center for Process Analytical Chemistry (CPAC).

Thanks to the folks at TraceDetect for the employment opportunity and the understanding during my final phase of graduate school. In particular, thanks to Joel Reiter for editing several chapters.

On a personal note, thanks to all of my family and friends for their support through my graduate career. In particular, to my husband Kyle who has always been there for me. As trivial as it may sound, thanks to my dog Abbie for always being excited when I return home and making me smile. Thanks to Dad and Jan for their moral support, and my siblings Dawn, Bryan and Arin for goading me along. Many thanks to the Edberg family who have made me part of their family and their moral support throughout graduate school.

Dedication

I dedicate this in fond memory of Dr. Robert D. Bocksch, professor emeritus at Whitworth College, who passed away in May 2001. Dr. B was a kind advisor, mentor and friend. He will be missed.

Chapter 1 – Modular Chemical Sensing Systems (MCSS)

1.1 - Introduction

Chemical sensing systems play an important role in modern analytical chemistry by filling a need in process measurement technology as well as environmental monitoring technology by taking the place of conventional laboratory measurements that are both costly and time-consuming. Due to the fact that they replace conventional analyses, for the same amount of time and/or money, chemical sensing systems provide increased data density in real-time to better understand the process being studied. This additional data density is important for process control situations and modeling of environmental events.

A sensing system's ability to make stable and robust measurements is also an important factor in the decision to replace a conventional analysis. If the system is not stable and requires a lot of maintenance, the economic benefit of placing the sensor is not realized. Sensor failures in key operations can cause the operators to revert back to conventional lab-based analyses as well as put up a psychological barrier to further sensor installations.

Recently, there has been a move away from the mode of thinking of a sensor as a stand-alone device that is dipped into the process. To have a stable sensor measurement there are components that have to be added, creating a sensing system instead of a solitary sensing device. These components often include supporting software and electronics, fluid delivery and handling, and sampling devices. By

changing the approach to chemical sensing system design, solutions from other chemical sensing systems, when thought of as individual modular components, can be applied in different sensing system scenarios. Each combination of components represents a new approach to solving a chemical analysis problem.

What are some typical modules for a chemical sensing system? Some key modules may include sampling, fluidics, and detection. The sampling module can take a variety of configurations, while fluidics will include both reagent reservoirs, and fluid delivery. Detection components are what are traditionally thought of as the sensors themselves. They convert the chemical analyte signal to a measurable signal such as a voltage or current. Sometimes one module addresses one or more functionality (i.e. sampling & detection). An example of this would include an analyte-specific reagent chemistry that reacts selectively with the otherwise undetectable analyte and produces a signal. One reagent chemistry example is a complexation reaction that converts analyte to a colored species so that the concentration can be determined with absorbance spectroscopy. Phenanthroline reacting with iron is one such complexation reaction.

Figure 1.1 shows a schematic of a modular chemical sensing system employing a pump and multi-port valve for fluid transfer, a sampling/reaction region, and a detector. The supporting software and electronics can control the fluid transfer as well as the detection, data collection, data storage, and sometimes even data analysis. The modules presented in this figure are typical of stand-alone chemical sensing systems, but are not all required for some chemical sensing systems.

1.2 - Background - Renewable Reagent Sensing

In the early 1990s, the Burgess research group developed renewable reagent fiber optic chemical sensing. Previous fiber optic chemical sensors utilized reagents that were immobilized on the optical fibers themselves. Immobilized reagents have to be both stable and reversible. The reagent also needs to be sensitive enough to follow a transient analyte concentration change. The immobilization chemistry must also be stable and cannot interfere with the measurement. These requirements precluded many possible reagent chemistries. With a renewable-reagent sensing scenario, the chemical reagent is exchanged after each measurement, opening up many more possibilities for reagent chemistries including irreversible reactions and reactions that were previously impossible due to the immobilization strategies.

The first renewable reagent optical chemical sensors detected sodium hydroxide, ammonia and chloride.[1,2,3] Further optical sensors were developed by Burgess and co-workers to detect chlorinated hydrocarbons[4] and heavy metals (specifically Pb and Cd)[5]. In addition, DeGrandpre developed a renewable reagent fiber optic sensor for determining the partial pressure of CO_2 in marine environments.[6,7,8] The renewable reagent fiber sensor work led to the development of

---

1 R.J. Berman, G.D. Christian, L.W. Burgess, Anal. Chem., Vol. 62, (1990), 2066-2071.
2 R.J. Berman, Ph.D. Dissertation, University of Washington, Seattle, WA, (1990).
3 R.J. Berman, L.W. Burgess, Proc. of SPIE – Chem., Biochem., and Env. Fiber Sens. II, Vol. 1368, (1991), 25-35.
4 J.M. Henshaw, L.W. Burgess, Proc. of SPIE – Chem., Biochem., and Env. Fiber Sens. III, Vol. 1587, 39-47.
5 Z. Lin, L.W. Burgess, Anal. Chem., Vol. 66, (1994), 2544.
6 M.D. DeGrandpre, Anal. Chem., Vol. 65, (1993), 331-337.
7 M.D. DeGrandpre, T.R. Hammar, S.P. Smith, F.L. Sayles, Limnol. Oceanogr., Vol. 40, No. 5, (1995), 969-975.
8 M.D. DeGrandpre, M.M. Baehr, T.R. Hammar, Anal. Chem., Vol. 71, No. 6, (1999), 1152-1159.

several chemical sensing systems based upon this technology including the FlowProbe™ and the liquid core waveguide.

The FlowProbe™ integrated the reagent-based chemistry, fiber optic spectroscopic detection, and membrane sampling into a 0.5" O.D. probe head. In addition to the probe head, the complete sensing system included other modules. These modules were reagent delivery and storage, a light source, spectrometer and supporting and electronics (Figure 1.2).[9] The liquid core waveguide system incorporated similar modules, but unlike the FlowProbe™ it was not restricted by the short pathlength that limited the detection limits in sensors like the FlowProbe™.[10]

1.3 – Important Components in MCSS

Many chemicals are not detected directly, but employ a chemical reaction to convert the analyte into a detectable species. Most sensing systems require a 'dynamic' mechanism to separate the analyte from the bulk medium or convert the undetectable analyte species into a detectable species. This conversion is addressed by various components in the system, including reagents and sampling interfaces. One such mechanism is to renew the reagent, but renewing the reagent requires reagent storage and delivery.

As mentioned above, to convert a traditional sensor to a stand-alone sensing system, various components need to be present to make a measurement system that is

---

9 L.K. Moore, D.J. Veltkamp, J.L. Cortina, Z. Lin, L.W. Burgess, Sensors & Actuators B, Vol. 38-39, (1997), 130-135.
10 K. Hong, Ph.D. Dissertation, University of Washington, Seattle, WA (1995).

accurate and stable for long-periods of time. Fluid handling is the mechanical backbone of most stable sensing systems, while detectors measure the detectable species. In addition, sample handling and conditioning is an important component to ensure that the measured sample is representative of the bulk matrix.

1.3.1 - Fluidics

Fluid handling and reservoirs are necessary for most renewable reagent applications. In addition to simply moving fluids around, the fluid handling part of a sensing system can help reduce the amount of waste generated per analysis and the overall size of a sensing system. For example, the FlowProbe™ is small compared to many sensing systems capable of making similar absorbance-based measurements. The probe-head detection volume is 3 μL. Reagents and wash solutions are pumped into the probe head through standard, commercially available 1/16" O.D. tubing and fittings. The stainless steel bellows reagent reservoirs are also the pumps in the analyzer system. A commercial analyzer may typically have a 25 mL or larger detection volume, resulting in almost 4 orders of magnitude more waste generated per measurement over the FlowProbe™.

Components used for fluid handling and delivery are pumps, valves for switching between reservoirs or flows, as well as tubing that acts as the conduit between these components. Fluid handling is a basic part of most chemical sensing systems used for long-term reproducible sensing systems by providing the mechanics to replace reagents, make reference and baseline measurements as well as periodic calibrations.

1.3.2 – Reagent Chemistries

Reagent chemistries employed in modular chemical sensing systems span a wide range of analytes and detection methods. The reagents may be as simple as a buffer or salt solution, or as complex as a metal-specific complexation reaction. When used in a renewable reagent configuration, the possibilities are numerous. Some examples of absorbance detection reagent chemistries employed include acid-base indicators for the presence of acid or base either in solution or headspace[11] and the Fujiwara reaction between chlorinated hydrocarbons in a caustic pyridine solution.[12] There are also water-soluble metal-specific reagents that form highly colored complexes suitable for spectrophotometric detection. One such reagent is bathocuproinedisulphonic acid for the analysis of Cu^{+1} ions.[13]

Other optical detection mechanisms that may employ a reagent include chemiluminescence, phosphorescence, and fluorescence. In the case of phosphorescence and fluorescence, the degree of quenching in the presence of analyte can be used to quantify the analyte concentration. This is the case for many dissolved oxygen determinations via fluorescence or phosphorescence. The difference between chemiluminescence and phosphorescence or fluorescence is the excitation energy is provided through the chemical reaction itself rather than from an outside source such as a lamp or laser. In the case of a chemiluminescent reaction, the analyte can be the oxidizer to drive the luminol reaction, so the reagent employed is a basic solution

---

11 R.J. Berman, Ph.D. Dissertation, University of Washington, Seattle, WA (1990).
12 J.M. Henshaw, Ph.D. Dissertation, University of Washington, Seattle, WA (1993).
13 D. Blair, H. Diehl, Talanta, Vol. 7 (1961), 163-174.

containing luminol and hydrogen peroxide.[14] The chemiluminescent reagent may be more complicated, but the instrumentation for a sensing system built around a chemiluminescent reaction will be less complicated because an external light source is not necessary.

For other modes of detection (e.g. electrochemical), the reagent chemistry does not need to produce a change in the light transmission characteristics of the sample. For many electrochemical measurements, the analyte can be measured directly, and the reagent may be as simple as a salt or buffer solution to control the sample's ionic strength and pH. If the analyte is not directly detected via electrochemical methods, it can be rendered electroactive with the addition of a complexing reagent. Wang and co-workers demonstrated an example of a renewable reagent sensing system employing a complexation reaction and adsorptive stripping voltammetry to detect chromium by complexing it with diethylenetriaminepentaacetic acid (DTPA).[15] The sensing system incorporated fluidics with an electrochemical cell for the Cr determination.

1.3.3 – The Sampling Interface

The sampling mechanism in a chemical sensor is a selective component that samples the analyte(s) from the bulk matrix. The sampling interface may be a physical mechanism that selectively removes the analyte, or a chemical mechanism that selectively reacts to the analyte, or a combination of both for increased specificity. Membranes and sorbent coatings are two types of sampling components that

---

14 I. Durrant, Nature, Vol. 346, (1990), 247.
15 J.Wang, J. Wang, J. Lu, B. Tian, D. MacDonald, K. Olsen; Analyst, Vol. 124, (1999)349-352.

physically remove or extract specific compounds or classes of compounds from a bulk medium.

Membranes, as applied to sensing systems for sampling, can be either liquid or solid, and they are semi-permeable in nature. Molecules of a given type will selectively pass through the membrane. For example, Teflon™ membranes are hydrophobic, so water molecules will not diffuse through a Teflon™ membrane; however, non-polar molecules will. Membranes can be tubular or flat. In 1992 Wolcott patented the concept of a long, coiled, tubular membrane as a sampling interface for GC.[16]

A sorbent coating is a physical sampling mechanism with chemical selectivity. An example of a sorbent coating is a coating on a sensor to increase the sensor's chemical selectivity over its response to the bulk. Sorbent coatings are used in combinations in arrays of sensors for detection of vapors in gas streams. The analyte is absorbed into the coating, changing the intrinsic response of the sensor. The analyte is usually desorbed out of the coating thermally.

Both membranes and sorbent coatings are subject to degradation and failure over time. This degradation may be due to exposure to the chemicals in the bulk matrix or the analysis, or due to fouling. Membrane fouling is often responsible for sensor failures or erroneous results.

Chemically selective sampling mechanisms could include an immobilized reagent or a renewed reagent such as those mentioned above. The reagent imparts

---

16 D. Wolcott, U.S. Patent 5,317,932 (1997).

selectivity to many chemical sensor applications by reacting only with specific compounds or classes of compounds. An example of an immobilized reagent is an immobilized antibody layer that selectively reacts with a specific analyte (antigen). This type of biolayer has a high degree of selectivity.

Chemical sensing systems that employ both a physical and chemical means of analyte selectivity are the most powerful. One example would be a membrane that is selective, and a reagent that converts the analyte to inhibit diffusion back across the membrane, such as protonation of a polar organic molecule. A specific example of this type of sensing system is the FlowProbe™ that was applied to various analytes by changing the membrane chemistry and the sampling interface including the application for detection of Cu^{+1} ions with the bathocuproinedisulfonic acid reagent and a cation-exchange membrane.[17] Another example is the pCO_2 sensor reported by DeGrandpre and coworkers that utilizes a coiled, tubular polymer membrane equilibration coil and an acid-base indicator solution to determine the pCO_2 in a marine environment.[18] The CO_2 reacts with water to form H_2CO_3 as well as its dissociation products, acidifying the solution and causing a color change.

The sampling interface is often exposed to harsh environments that can cause it to fail over time. The classic example of this is a membrane interface developing a leak or fouling, rendering the entire sensing system useless until the membrane is changed. Regenerating the sampling interface can extend the useful lifetime of a

---

17 L.K. Moore, D.J. Veltkamp, J.L. Cortina, Z. Lin, L.W. Burgess, Sens. & Act. B; Vol. 38-39, (1997), 130-135.
18 M.D. DeGrandpre, M.M. Baehr, T.R. Hammar; Anal. Chem.; Vol. 71, (1999), 1152-1159.

sensing system before the system requires maintenance. Examples of regenerating the sampling in the above systems include replacing the reagent by either stripping out an immobilized reagent layer and replacing it *in situ*, or renewing the reagent. Another example would be replacing a liquid membrane material without physically removing the membrane support from the system.

1.3.4 Detection

Typical chemical sensing systems may use optical, electrochemical, acoustic, or thermal sensing devices for analyte detection. As previously mentioned, most chemicals are not directly detected, so the chemical signal must be converted to a measureable signal. The measureable signal can be a voltage or current, or a color change. For example, a molecule that is colored (e.g. acid-base indicator), can be measured directly with visible absorbance spectroscopy and an analyte that is not colored, such as a metal ion, can be reacted with a complexing agent to form a colored species.

Forms of optical chemical detection include various types of spectroscopy, (e.g. UV/Vis, IR, Raman, fluorescence). With the increased availability of small optical components such as fiber optics and spectrometers, spectoscopic methods can be easily incorporated into sensing devices. Other forms of optical detection do not require wavelength specificity, but rather measure total light intensity. Chemiluminescence is one example in which overall light intensity is the measured element. One photomultiplier tube is sufficient for light detection, as opposed to a dispersive or scanning spectrograph.

Various forms of electrochemical detection have also been implemented into chemical sensing systems. These forms include potentiometry, voltammetry, amperometry, and coulometry to name a few. Potentiometry measures the potential of a solution under a given set of conditions. An example of a pontentiometric measurement is an ion-selective electrode measurement of copper. Voltammetry is defined as a measurement in which a varying potential is applied between electrodes in solution and the resulting current is measured. When sample is pre-concentrated on the working electrode before the potential is varied and the current measured, this technique is called stripping voltammetry. An amperometric measurement determines the current associated with a given concentration of analyte whereas a coulometric measurement is made at a set potential and the change in current over time is determined. All electrochemical measurements require a complete circuit through the solution of interest via a series of electrodes. These electrodes may be as simple as wires immersed in the solution or as complex as ion-selective electrodes.

Other modes of detection in a chemical sensing system include acoustic sensors such as SAW (Surface Acoustic Wave) devices, ultrasonic transducers, thermocouples and thermistors. These devices are often inferential, meaning that their signal changes in contact with analyte, but the signal change usually needs to be well characterized.

1.3.5 – Software and Supporting Electronics

Software and supporting electronics are a key component to a functional chemical sensing system. The software can control the fluidics by controlling valve

switching, pump flow rates, data collection and storage, and even data analysis. The supporting electronics include conduits to power the various fluidics and detection components, as well as signal conditioning electronics. For a full-featured, commercialized system, this component is the most important but also the most difficult and expensive to create with a high degree of usability for a wide range of potential users.

For research-based, development systems, the software and electronics components are rather crude in comparison. The software is usually as simple as possible with a minimum number of features, but allowing for complete control of the instrument. This system can be as simple as a computer downloading a BASIC program via a serial interface to an inexpensive datalogger to control the entire sensing system including data collection, as in the dissolved oxygen sensing system presented below and in chapters 3 and 4. This solution can also be as complex as the LabView-based software for control of the FlowProbe™ sensing system for fluidics control, data collection and even chemometric data analysis. Both of these systems contained a minimum of customized, integrated electronics and were a combination of various commercially available modules.

1.4 - This work: MCSS where the sampling interface can be regenerated

This work will address making specific modular chemical sensing systems (MCSS) in which the sampling and reagent components can be regenerated in order to improve the robustness and long-term stability of the measurement. The sensing

systems explored and developed in this work include a chemiluminescent fiber optic biosensor, an oxygen electrode system for dissolved oxygen measurements in marine environments, liquid core waveguides as both a detection cell and a membrane sampling interface, and supported liquid membranes as sensing system sampling interfaces.

1.4.1 - Chemiluminescent fiber optic biosensor

Chapter 2 describes the chemiluminescent fiber optic biosensor. This sensor involves the use of an analyte-specific protein immobilized on the inside surface of a glass tube. The protein layer acts as an analyte pre-concentration/sampling mechanism while the scintillating optical fiber inserted inside of the tube couples the chemiluminescent signal generated by the horseradish peroxidase/luminol chemiluminescent reaction to the photomultiplier tube. The principle behind the measurement is a competition immunoassay where the measured chemiluminescent signal is inversely proportional to the analyte concentration.

Fluid handling (i.e. pumps and a 3-way solenoid valve) is integrated into the sensing system to renew the chemiluminescent reagent between measurements and flush out the sensor with buffer. The pumps and valve were automated with relay switches and software. The signal from the PMT was collected using an analog to digital interface card and a PC computer. Degraded protein layers are renewed by chemical removal followed by construction of a new layer *in situ* by adding additional fluidics reservoirs to the sensor system to incorporate the stripping reagent as well as the reagents required for replacing the protein layers.

1.4.2 – Dissolved oxygen sensing system

Chapters 3 and 4 present the development of a renewable reagent electrochemical oxygen sensor for long-term deployment in marine environments, followed by the construction and testing of the autonomous prototype sensing system. The sensor performs a coulometric measurement as opposed to the amperometric measurement performed by a Clark electrode. To increase the measurement stability of the system, the membrane equilibration portion was separated from the measurement portion of the instrument. This two-stage measurement allows for complete reduction of oxygen in the cell without kinetic dependence on membrane transport of oxygen. The complete reduction also allows measurement of the absolute O_2 concentration inside of the cell.

This system is also modular in nature. The reagent reservoir and pump is connected to a long silicone equilibration coil. In the prototype instrument, the reservoir and pump are incorporated into the same module. The electrolyte in the equilibration coil acts as the sampling component of the system. This electrolyte comes into equilibrium with the external environment before it is moved into the measurement cell for detection. Each measurement is made with fresh electrolyte, so the sampling interface is renewed between measurements. The silicone coil was protected from biofouling by exposing it to UV radiation from a mercury vapor lamp. Separating the sampling part of the measurement from the detection part of the measurement removes the kinetic dependence of the measurement upon the diffusion of oxygen through the membrane interface.

Oxygen is detection by reduction at the platinum electrode when a voltage is applied across the platinum and silver/silver chloride electrode. The current generated by the reduction of oxygen is proportionate to the number of O_2 molecules present in the electrode cell. The current is passed through a current to voltage converter and detected, integrated, and stored by a datalogger operating under a BASIC computer program.

1.4.3 - Liquid Core Waveguides

Chapter 5 describes the liquid core optical waveguide systems that were addressed in this work. The waveguide is simply a fiber optic with a liquid core. The core material must have a higher refractive index than the cladding material to meet the conditions for total internal reflection. In this case, polymer tubes were used as cladding materials, particularly Teflon™ AF. The core material can be either reagent-based or a passive phase for analyte detection. The cladding may be used as a membrane phase for separation of analyte from the bulk. In addition, the reagent core material can be renewed for subsequent measurements. Development of an LCW sensor for the detection of hydrochloric acid vapor and CO_2 is discussed.

A liquid core waveguide can be used as simply a long-path detection cell for absorbance spectroscopy or Raman spectroscopy; however, if the cladding material is a polymeric material, the cladding will act as a semipermeable membrane as well. This turns a detection module into both a detection module and a sampling module. By incorporating fluid handling into the instrumentation, the core material can be renewed, so the sampling interface is renewed in between measurements preventing

any instability due to reagent degradation. By performing injections of reagent into the core of the waveguide as opposed to a continuous reagent flow, the system can be referenced before and after each measurement correcting for drift in either the light source or detector as well as fouling that may occur.

1.4.4 - Supported Liquid Membranes

Chapter 6 describes the supported liquid membrane (SLM) systems explored in this work. SLMs are membrane systems employing a liquid polymeric phase supported on a porous polymeric support. The liquid phase is selective for specific coumpounds or classes of compounds. These membrane systems have been explored for use in chemical sensing systems as a membrane interface for the FlowProbe™. The *in situ* regeneration of the SLM was also investigated. Commercially available supported liquid membrane modules were also explored as the sampling interface with the liquid core waveguide as the detection cell. Some basic strategies for removing the liquid membrane material and replacing it *in situ* were also explored.

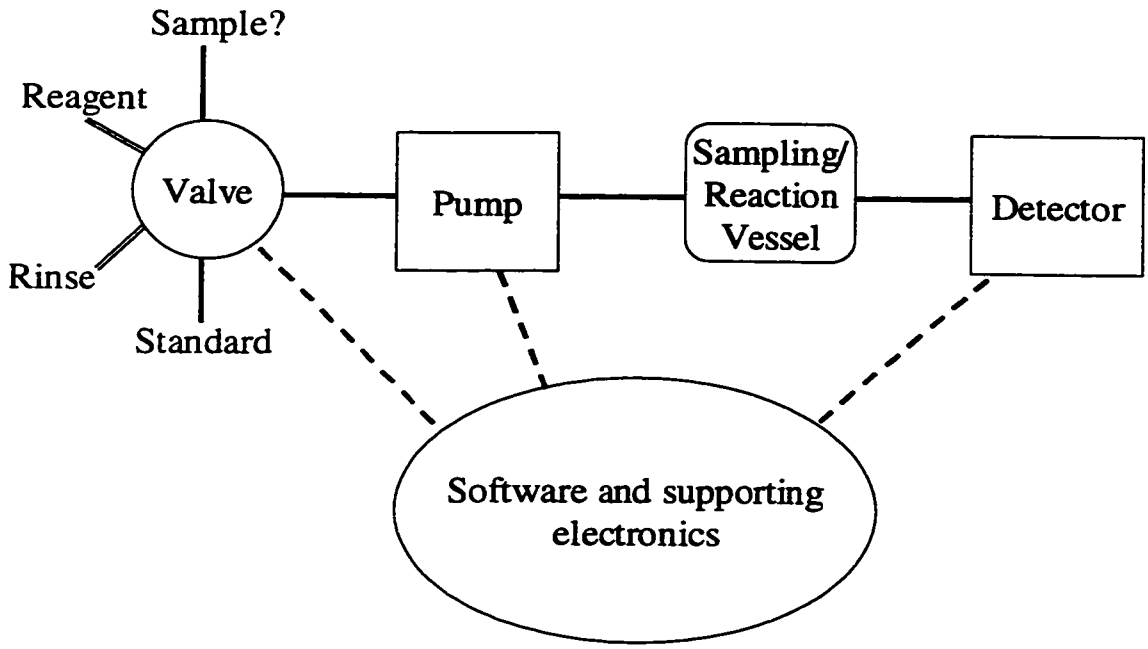

Figure 1.1 - Schematic of a Modular Chemical Sensing System (MCSS). MCSS usually incorporate fluid-handling to lengthen the stable lifetime of a detection module and take a laboratory measurement out of the laboratory.

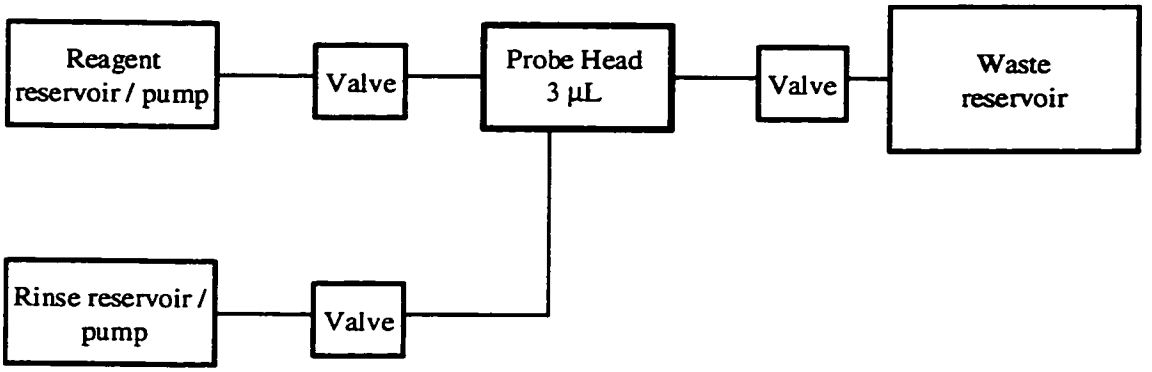

Figure 1.2 – Schematic of the FlowProbe ™ system. The valves (12 volt solenoid valves) are controlled by the LabView software that also controls the light source, spectometer, data collection and data analysis. The reagent bellows reservoirs are combined reservoirs and pumps.

Chapter 2 - Chemiluminescent Fiber Optic Biosensor

2.1 - Introduction

This research reported here is based upon a fiber optic biosensor with a chemiluminescent immunoassay sampling mechanism. The protein layer is immobilized, and reacts with the sample. The antibody is selective for the analyte of interest. The sensing system development is described as well as protein layer deposition techniques. In addition, cycling of single protein layers, and *in situ* removal/redeposition schemes are described.

Optical fibers have long been used to collect chemiluminescent emissions.[1,2,3,4] Most of the literature describes the use of fiber optics for chemiluminescence collection in conventional well-plate assays. There is no discussion of incorporation of the assay into the sensor itself by either cycling or *in situ* renewal of the protein chemistry involved in the assay. The research reported here demonstrates cycling of a chemiluminescent assay as well as *in situ* removal and deposition of the protein layer.

Ligler and co-workers have developed various continuous-flow, antibody-based fluorescence biosensors for the detection of analytes such as explosives and biowarfare agents. Most of these sensors are based upon a competition immunoassay in which the down-stream fluorescent signal is detected, and is directly proportional to

---

1 T. M. Freeman, W.R. Seitz; Anal. Chem.; Vol. 50, No.9, (1978), 1242-1246.
2 M.V. Cattaneo, K.B. Male, J.H.T. Luong, Biosensors & Bioelectronics, Vol. 7, (1992), 569-574.
3 J. Hlavay, S.D. Haemmerli, G.G. Guilbault, Biosensors & Bioelectronics, Vol. 9, (1994), 189-195.
4 X. Zhou, M.A. Arnold; Anal. Chim. Acta; Vol. 304, (1995), 147-156.

the analyte concentration.[5,6] The same researchers have also demonstrated that immobilized antibody layers can be regenerated without complete removal of the antibody layer.[7] This work takes off from where previous work ends to produce a practical and renewable sensor technology.

The sensing system reported here is based upon a competition immunoassay with a chemiluminescence reaction as the transduction mechanism. Equations 2.1 and 2.2 demonstrate a chemiluminescent reaction. Chemiluminescence occurs when a chemical reaction causes a molecule to reach an excited state that subsequently relaxes to the ground state, emitting light in the process. The basic textbook reaction involves luminol, an oxidizing agent such as $K_3Fe(CN)_6$, and hydrogen peroxide in the presence of base. The hydrogen peroxide is oxidized into hydroxyl radicals that react with luminol resulting in blue-green light emission (Figure 2.1).

$$A + B \xrightarrow{catalyst} C^* \qquad (2.1)$$

$$C^* \longrightarrow C + h\upsilon \text{ (light)} \qquad (2.2)$$

A competition immunoassay is based upon an immobilized antibody layer bound with labeled antigen (Figures 2.2a and 2.2b). In the case of our chemiluminescent reaction, the antigen is labeled with horseradish peroxidase (HRP), an enzyme with an iron-containing heme functional group that reacts with the

---

5 J.P. Whelan, A.W. Kusterbeck, G.A. Wemhoff, R. Bredehorst, F.S. Ligler; Anal. Chem.; Vol. 65, (1993), 3561-3565.
6 L.C. Shriver-Lake, K.A. Breslin, P.T. Charles, D.W. Conrad, J.P. Golden, F.S. Ligler; Anal. Chem.; Vol. 67, (1995), 2431-2435.
7 D. Wijesuriya, K. Breslin, G. Anderson, L. Shriver-Lake, F.S. Ligler; Biosensors & Bioelectronics; Vol. 9, No. 8, (1994), 585-592.

chemiluminescent reagents (in this case, luminol and hydrogen peroxide). This layer is reacted with luminol and H_2O_2 and the baseline chemiluminescence is recorded. The layer is flushed with sample containing the analyte (unbound antigen). The analyte competes for binding sites on the antibody, thereby displacing some of the HRP-labeled antigen (Figure 2.2c). The layer is reacted again with the chemiluminescent reagents and the change in signal recorded. The decrease in chemiluminescent signal is proportional to the analyte concentration. After this readout, the antibody layer can be regenerated by removing the bound analyte. The antibody layer releases bound antigen when flushed with pH = 2 glycine buffer.

Many chemiluminescent bioassays utilize HRP and luminol to generate the chemiluminescent signal. The HRP is covalently attached to a carrier protein in the reaction. The chemiluminescent signal generated from the HRP/luminol reaction is a transduction of the binding of the biomolecule of interest. The HRP reaction is similar to the luminol chemiluminescent reaction described above. The heme group in the active site of the HRP enzyme acts as the oxidizing agent to produce hydroxyl radicals, and the luminol reaction proceeds as described.[8] In both cases, the iron-containing reagent reacts via an oxidation/reduction reaction to form hydroxyl radicals that react with the luminol molecule to produce light.

Two different protein immobilization methods were utilized in this study. The first of these methods was silane coupling. Silane coupling is the reaction of an organo-silane compound with a glass surface via a condensation reaction. The

---

8 I. Durrant, Nature, Vol. 346, (1990), 247.

attached organo-silane molecule, usually a trialkoxysilane, has a terminal functional group that can be used to attach the desired molecule or protein to be immobilized. The trialkoxysilane is hydrolyzed in aqueous alcohol to form reactive silanol groups (Figure 2.3). This solution is reacted with a clean glass surface and a condensation reaction occurs between the silanol groups in solution and on the glass surface. The functionalized surface is rinsed and allowed to cure.[9]

A second technique, glutaraldehyde entrapment with non-covalent immobilization was also explored in this work. This method involves the homo-bi-functional cross-linking agent glutaraldehyde. The two aldehyde groups on the glutaraldehyde molecule react with a protein's amino groups, cross-linking the protein to itself and other protein molecules, to form a thick, viscous gel that solidifies upon solvent evaporation (Figure 2.4).[10] Thin layers of the viscous protein gel may be formed on the inside walls of tubes analogous to the work performed by Lucy and co-workers.[11,12,13] These researchers demonstrated that by flowing a small amount of viscous material through a tube followed by a less viscous fluid or air segment, the more viscous material forms a thin layer on the inside walls of the tube. Recent research in the Ruzicka-Christian group has used these types of layers as an analyte pre-concentration method.[14,15]

---

9 B. Arkles, "Silane Coupling Agent Chemistry", Hüls Technical Note, (1991), 59-64.
10 M.S. Abdel-Latif, G.G. Builbault, in Biosensor Technology Fundamentals and Applications, Marcel Dekkar, Inc.; New York, (1990), 285-289.
11 C.A. Lucy, F.F. Cantwell, Anal. Chem., Vol. 61, (1989), 101-107.
12 C.A. Lucy, K. Yeung, Anal. Chem., Vol. 66, (1994), 2220-2225.
13 C.A. Lucy, S. Varkey, Anal. Chem., Vol. 67, (1995), 3036-3041.
14 Y. Luo, R. Al-Othman, J. Ruzicka, G.D. Christian, Analyst, Vol. 121, (1996), 601-606.

Construction of the light collection and flow systems, as well as exploration of protein immobilization aided in meeting the overall goal to develop a sensing system to measure the chemiluminescent signal from a chemiluminescent-based competition immunoassay in which the antibody is immobilized on the inside surface of a glass capillary tube. This study entailed optimization of the fiber-optic collection of the chemiluminescent signal, protein immobilization, cycling studies, and regeneration of the protein, or sensing interface. This type of sensor is designed for use under flowing conditions where the chemiluminescence is measured directly inside of the tube as opposed to down-stream as in most biosensor applications. Additionally, the reaction may be cycled several times before the antibody layer must be regenerated.

2.2 – Construction of a Reusable Fiber Optic Chemiluminescent Probe

The aim of this project was to adapt a chemiluminescent bioassay into a chemical sensing system in which the reagent can be flowed through the sensing area. The first task was construction of a fiber optic probe to efficiently collect the chemiluminescent signal generated during the assay. The probe was incorporated into the sensing area of the flow system in a co-axial configuration. The first probe consisted of a bare-ended, aluminum-jacketed optical fiber (Fiberguide, Stirling, NJ) coupled into the glass capillary reaction tube. The output end of the fiber was coupled into a side-on photomultiplier tube (Hamamatsu, Japan), to measure the chemiluminescent signal (Figure 2.5). The flow system consisted of two small syringe

---

15 K.L. Peterson, B.K. Logan, G.D. Christian, J. Ruzicka, Anal. Chim. Acta, Vol. 99, (1997), 99.

pumps (FMI, Syosset, NY), a three-port solenoid valve (ASCO Products, Florham Park, NJ), 1/16" O.D. x 0.020" black FEP tubing (Upchurch Scientific, Oak Harbor, WA) to minimize light leakage into the sensing area, and low-pressure flangeless fittings (Upchurch Scientific), and a 1/16" O.D. glass capillary that would eventually be coated with the protein layer. The pumps and valves were computer controlled with relay switches. This system allowed for the flow of the chemiluminescent reagent on one channel and phosphate-buffered saline as a rinse solution on the other channel. A solution containing luminol, NaOH, $K_3Fe(CN)_6$, and H_2O_2 was pumped through the capillary cell and the chemiluminescent signal of luminol was observed. The luminol reaction produced a large amount of readily observable light but detection of the light was dependent upon emission with the acceptance cone of the fiber (Figure 2.6). The peak emissions varied from 20,000 counts on the photomultiplier tube to 120,000 counts.

The luminol chemiluminescent reaction with $K_3Fe(CN)_6$ as the oxidant, generates relatively large amounts of light, far more than most chemiluminescent assay reactions. The next experiment mimicked the actual assay reaction by flowing a mixture of an HRP-conjugated monoclonal antibody, luminol, and H_2O_2 through the tube. The weaker chemiluminescent signal was not observable with the bare fiber (Figure 2.7). To detect the weaker signal, a scintillation fiber was constructed.

The scintillation fiber consisted of a small piece (~ 5 cm) of a fluorophor-doped plastic fiber (Optectron, France) end-coupled to an aluminum-jacketed fiber. The fluorophor-doped fiber was chosen based upon its excitation/emission

characteristics; the luminol emission wavelength matched the excitation wavelength of the fiber (Figure 2.8). The scintillation fiber offered larger collection efficiency because the emitted chemiluminescent signal surrounding the whole length of the scintillation fiber excited the fluorophor in the fiber, and the fiber did not require a specific launch angle for collection of light. Conservatively, the scintillation fiber provided 100 times more sensitivity to the luminol chemiluminescence generated by the immobilized antibody layer. The fluorescent signal of the small piece of scintillation fiber was then coupled to the detector via the aluminum-jacketed fiber. The resulting signal generated from the immobilized antibody reaction described above was easily detected. The subsequent sensor included an antibody/enzyme layer immobilized on the interior of a glass capillary tube with a scintillating optical fiber inserted into the tube similar to the original configuration (Figure 2.9). Reagent flowed between the fiber optic and the interior of the capillary tube, and the chemiluminescent reaction occurred within the protein layer.

2.3 – Covalent attachment of proteins and antibodies via silane coupling

After the appropriate signal collection method was determined, initial experiments were begun to observe the behavior of the protein layer reactions and optimize the sensor system itself. Initially the chemical system used for this task consisted of fluorescein isothiocyanate (FITC) immobilized on the inside surface of glass capillaries using 3-aminopropyltriethoxysilane (Huls, Parsippany, NJ). FITC is a common amino-reactive label for proteins that readily reacts with an amino-

functionalized surface (Figure 2.10). After flushing the surface with buffer, it was incubated with HRP-conjugated anti-FITC monoclonal antibody, thereby immobilizing the antibody to the inside surface of the tube.

The tube was flushed with buffer and the scintillation fiber inserted. A chemiluminescent reagent containing luminol and H_2O_2 was flowed and the emitted light intensity measured. Initial cycling studies of these layers were performed manually by washing the tube with buffer followed by the chemiluminescent reagent. The chemiluminescent signal returned with subsequent cycles, although not to the same intensity as previous cycles. After five to seven cycles, no measurable signal was obtained, indicating that the protein layer was either no longer functional or no longer present in a large enough concentration to generate a measurable signal.

In an effort to preserve the scarce amounts of monoclonal antibody available, another covalent-attachment protein layer chemistry was devised for sensor optimization. The glass surfaces were functionalized with a sulfhydryl group by covalently binding 3-mercaptopropyltrimethoxysilane to the cleaned glass surface. The –SH group on the surface forms a thioether link with succinimidyl-4-(N-malimidomethyl)cyclohexane-1-carboxylate or SMCC. SMCC is a hetero-bi-functional cross-linking agent commonly used for cross-linking proteins. The HRP enzyme is cross-linked to the SMCC-functionalized surface (Figure 2.11).

The same types of cycling studies were performed as above, and the results also showed almost 50% degradation in signal by the third cycle (Figure 2.12). Clearly the layers lacked stability over subsequent cycles with reagent flow. We

postulated that the silane chemistry used to attach the proteins to the surface was not stable under the pH conditions of the experiment (pH ~ 7.0). Essentially, we were washing off the protein layer during the course of the experiment. This instability under neutral to basic pH conditions has been described in the literature.[16]

2.4 – Non-covalent protein immobilization via glutaraldehyde entrapment

Due to the instability of covalent attachment, we explored other methods of protein immobilization. Birnbaum and Nilsson have demonstrated that proteins reacted with glutaraldehyde produce a viscous cross-linked polymer of protein that can be applied mechanically to a sensor.[17] Based on previous work by Lucy and co-workers[11-13] on the deposition of extractive or reactive layers, we determined that the viscous cross-linked proteins could be mechanically deposited inside a capillary by flowing a small plug of the viscous polymer through a tube followed by a less-viscous liquid or air plug. The difference in viscosity between the two materials forces the higher viscosity material to the walls of the tube while the low viscosity material flows through the center.

The cross-linking reaction was first optimized to achieve uniform layers (Table 2.1). The optimal solution was one part HRP to ten parts bovine serum albumin (BSA) in a phosphate/acetate buffer (pH = 5.0) reacted with a small amount of 50% glutaraldehyde solution. As the mixture polymerized, a small amount was sent through the capillary followed by a small amount of air. The difference in viscosity

16 E.P. Plueddemann, Silane Coupling Agents, 2nd Ed.; Plenum Press, (1991), 242-247.
17 S., Birnbaum, S. Nilsson, Anal. Chem., Vol. 64, (1992) 2873.

between the air and the cross-linked material forced the protein layer to form on the capillary walls (Figure 2.13).

The layers were washed with buffer (pH = 7.0) and reacted with luminol and H_2O_2. We observed a strong chemiluminescent signal. Cycling studies were also performed using these layers and although the layers appeared to generate more signal overall, the chemiluminescent signal was not observable after approximately ten cycles degrading from more than 40,000 counts to less than 2,000 counts (Figure 2.14). The protein layers were easily removed using a solution of alcoholic KOH, making it possible to deposit and remove the protein layers *in situ*.

The cross-link method was applied to an antibody to determine its usefulness in an immunoassay. As before, BSA was dissolved in buffer with a small amount of fluorescein-conjugated BSA, followed by the 50% glutaraldehyde solution. The viscous gel layers were incubated with HRP-conjugated anti-FITC monoclonal antibody. The layer was reacted with chemiluminescent reagent yielding a very strong signal from one of the three layers while the other two provided no signal.

2.5 – Protein Layer Thickness Determinations

The thickness of the HRP/glutaraldehyde layers was measured using the Hewlett-Packard High Precision Reflectometer to determine the uniformity of the protein gel layer deposition. For comparison, the thickness of a layer of silicone oil (PDMS), deposited in a similar manner on the inside of a PTFE tube, was also measured. The reflectometer is useful for the thickness determination of non-

scattering thin films such as these, provided there is a difference in refractive index from one material to another. In the case of non-scattering thin films, the instrument scan shows discrete peaks representative of discrete reflections of the incident light back to the detector. A reflection occurs at the interface in which the refractive index changes. The distance between peaks is the optical thickness of the interface represented by the pair of peaks.

The approximate optical thickness of the protein layers was on the order of 70 microns (Figure 2.15). Optical thickness is defined as physical thickness of a material multiplied by the refractive index of the material. The refractive index of the protein gel material was unknown, so the physical thickness of the layer was not determined exactly. Assuming that the refractive index of the protein layers was similar to that of a buffer solution, (1.35), then the physical thickness of the protein layer was approximately 50 ± 10 μm. In the comparison system, the silicone oil layers (RI = 1.4053 as measured on the Milton Roy ABBE refractometer) were approximately 50 ± 10 μm in physical thickness . Thus we were able to determine layer thickness of these thin layers inside of capillary tubes (Figure 2.16).

2.6 – Conclusions

The work represented in this chapter was an important advance in biosensor technology. By utilizing non-covalent attachment of the active protein, it is possible to remove and replace the protein layer *in situ*. The ability to change the active protein layer, which acts as both the sampling and analyte signal transduction mechanism for

the sensing system, allows for a sensing system which can essentially be completely regenerated after the layer's useful lifetime. This also means that several different protein chemistries could be employed in a single sensing system. In addition, the renewable-reagent concept was employed in this sensing system as well. For each measurement, fresh chemiluminescent reagent was delivered to the protein layer followed by a rinse solution. The two concepts illustrated in this experiment, renewable reagent and regenerated sampling interfaces, combine to produce a robust, long-lived chemical sensing system.

To fully automate the system and render it useful for further study, the fluid handling components will need to be upgradeded and the protein layer removal/replacement incorporated for automated sampling interface regeneration. The system reported here is still a research-based experimental system and would require extensive development for commercial realization.

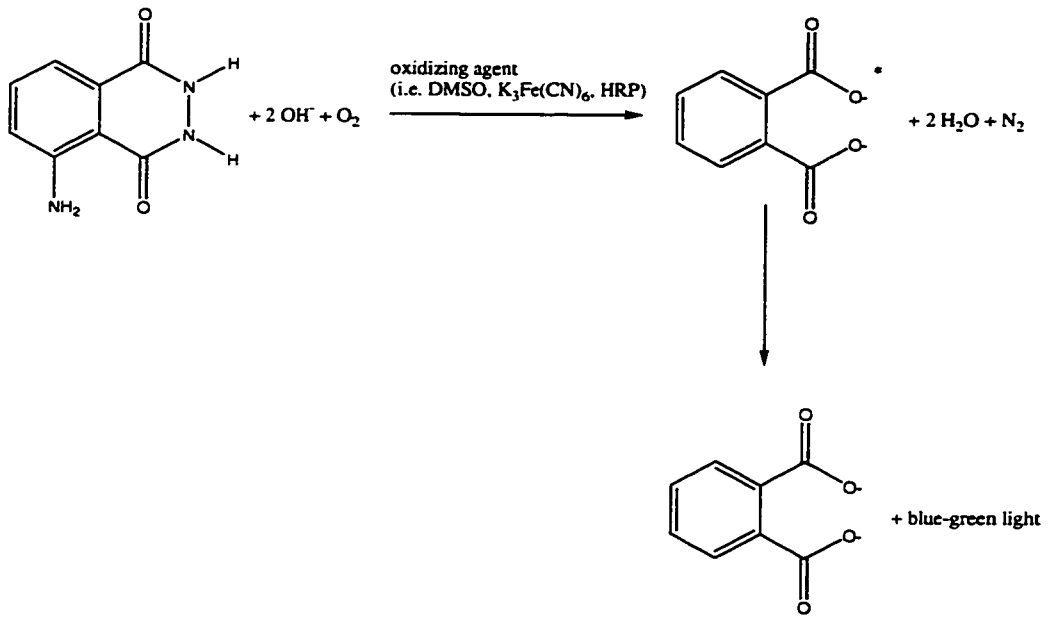

Figure 2.1 - Luminol chemiluminescent reaction: Luminol reacts with oxygen in the presence of base and an oxidizer to form the phthalate product in an excited state that emits light as it relaxes to the ground state.

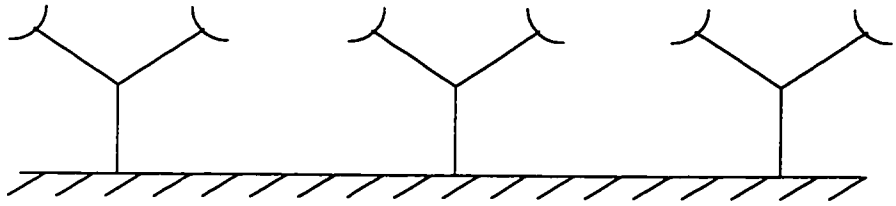

Figure 2.2a – Competition Immunoassay Step 1: Immobilization of the antibody layer.

$$HRP + luminol + H_2O_2 \longrightarrow light$$

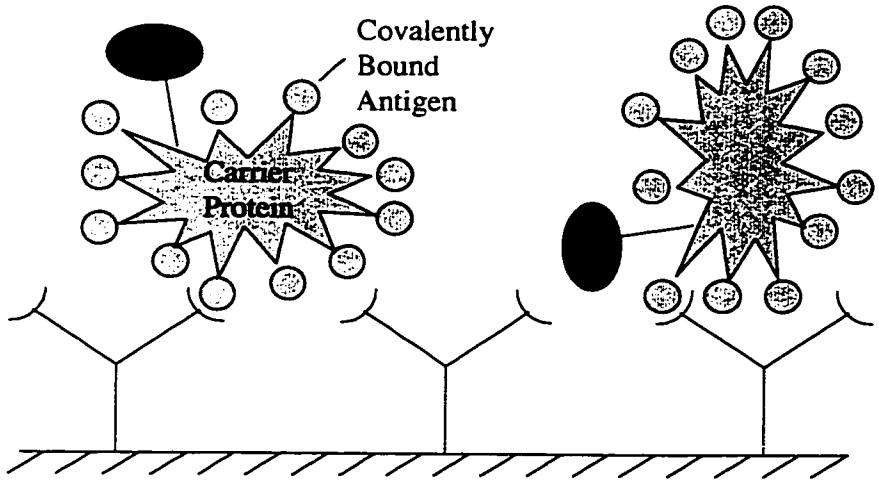

Figure 2.2b – Competition Immunoassay Step 2: Reaction of the carrier protein/antigen complex with the antibody layer. This layer is reacted with the luminol reagent to acquire the baseline signal.

$$HRP + luminol + H_2O_2 \longrightarrow light$$

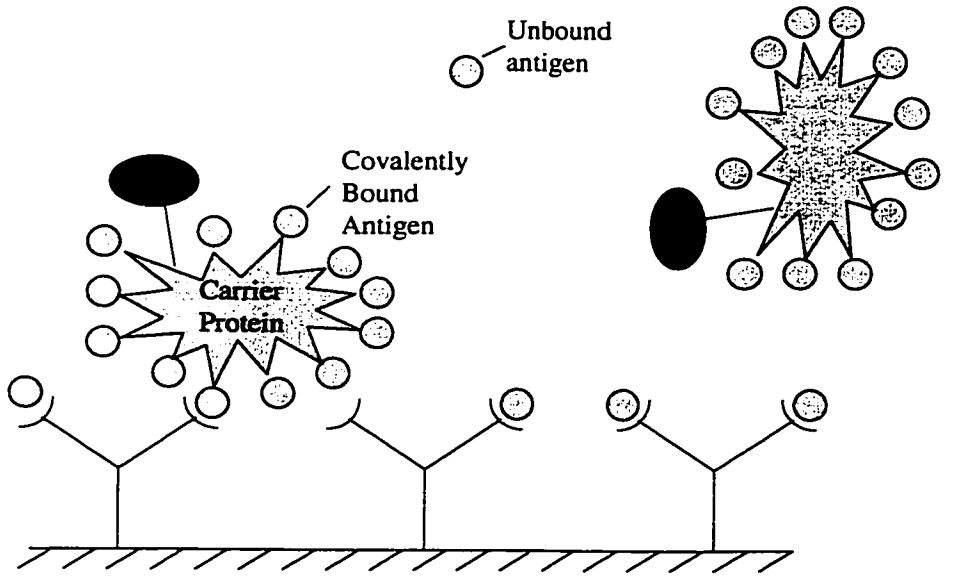

Figure 2.2c – Competition Immunoassay Step 3: Analyte (unbound antigen) is allowed to react with the antibody layer and competes with the carrier protein complex for the antibody binding sites. The luminol/H_2O_2 reaction is repeated. The decrease in the chemiluminescent signal is proportional to the analyte concentration.

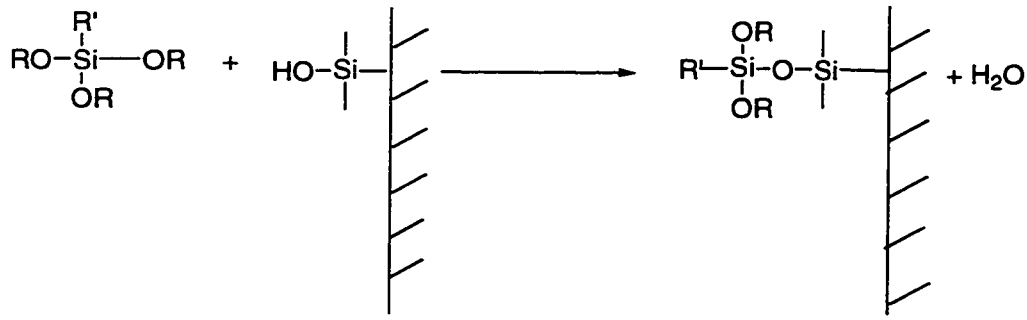

Figure 2.3 - Silane Coupling Reaction of a trialkoxysilane with a silanol group on a glass substrate. R' is the desired functional group for the surface.

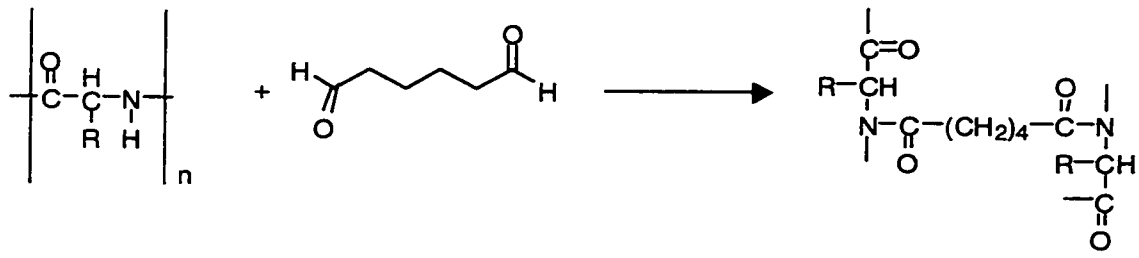

Figure 2.4 - Glutaraldehyde cross-linking – an amino acid within a protein reacting with glutaraldehyde to cross-link to another amino acid. The R represents the amino acid side-chain. This crosslinking reaction is independent of side-chain.

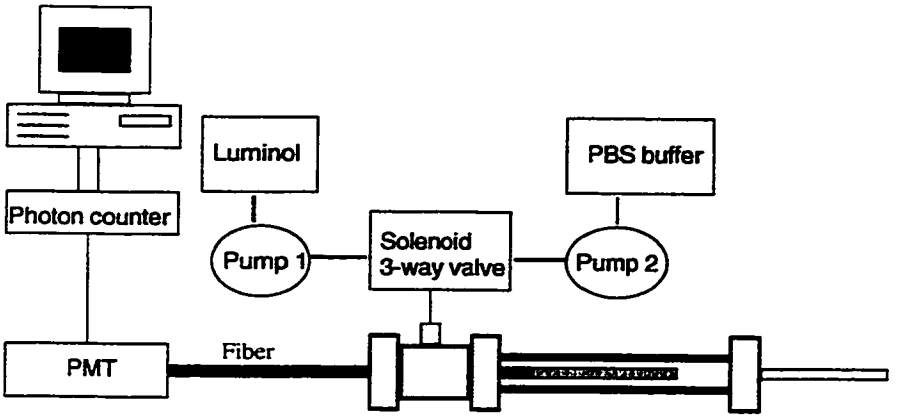

Figure 2.5 - Regenerable biosensor schematic (not to scale). The reagents were delivered with small-volume piston pumps, through a three-way solenoid valve . The pumps and valve were controlled via relays. 1/16" black FEP tubing and low-pressure flangeless fittings were used.

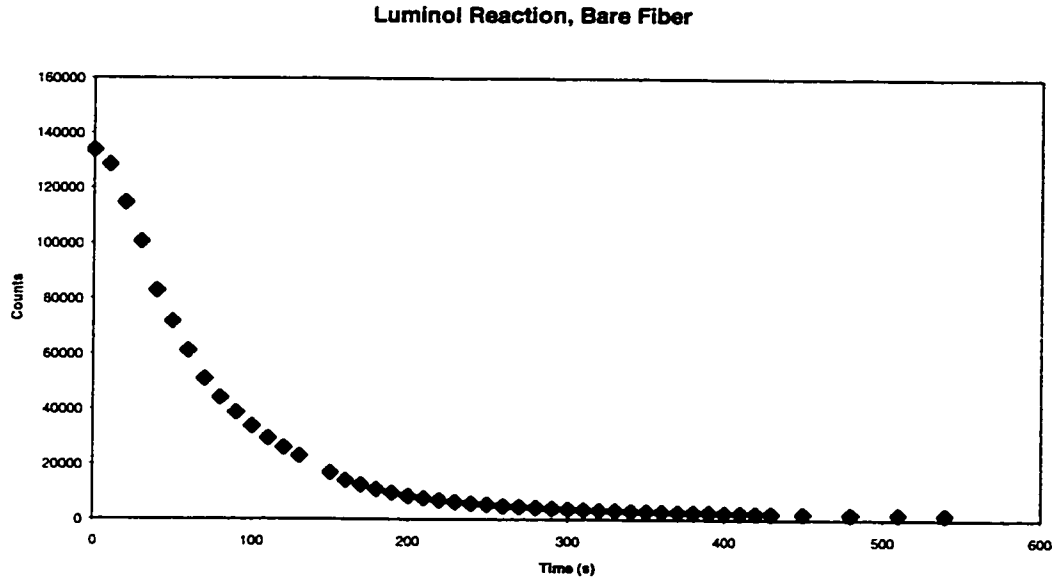

Figure 2.6 - Observation of luminol chemiluminescence via a bare optical fiber. Approximately 10 μL of a mixture of luminol, H_2O_2, and $K_3Fe(CN)_6$ was flowed into the capillary cell of the system shown in Fig. 2.5, and the photon count was monitored on the PMT as the chemiluminescent reagents were depleted.

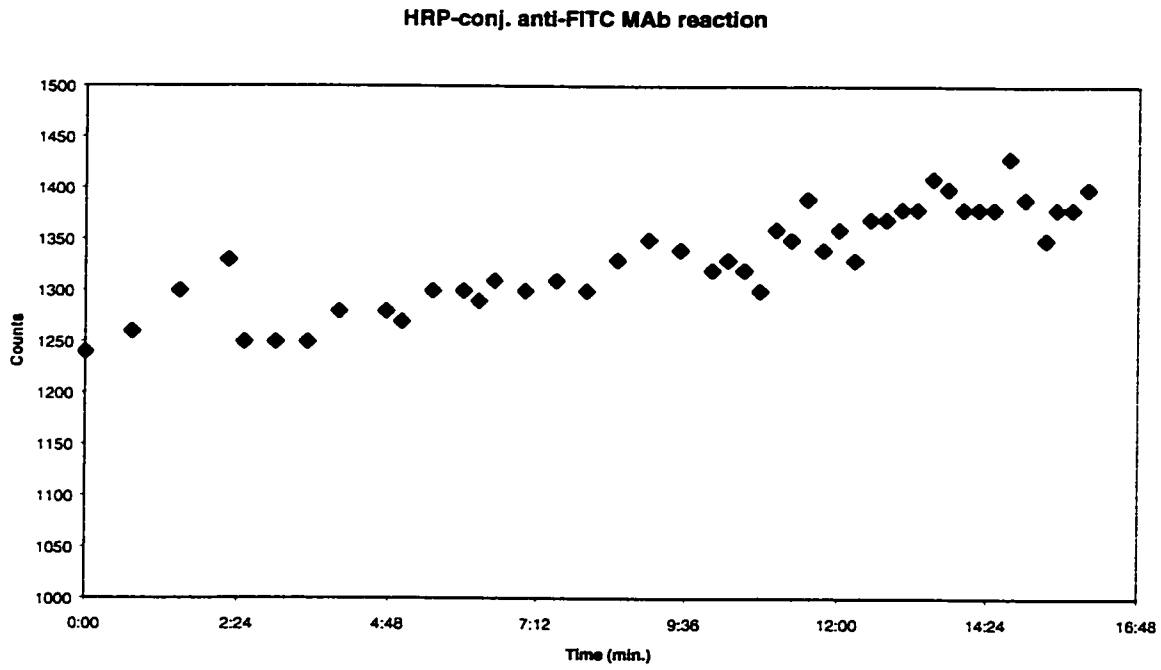

Figure 2.7 - No observable signal of bound antibody chemiluminescent reaction via a bare optical fiber. The signal was at the dark level for the PMT used.

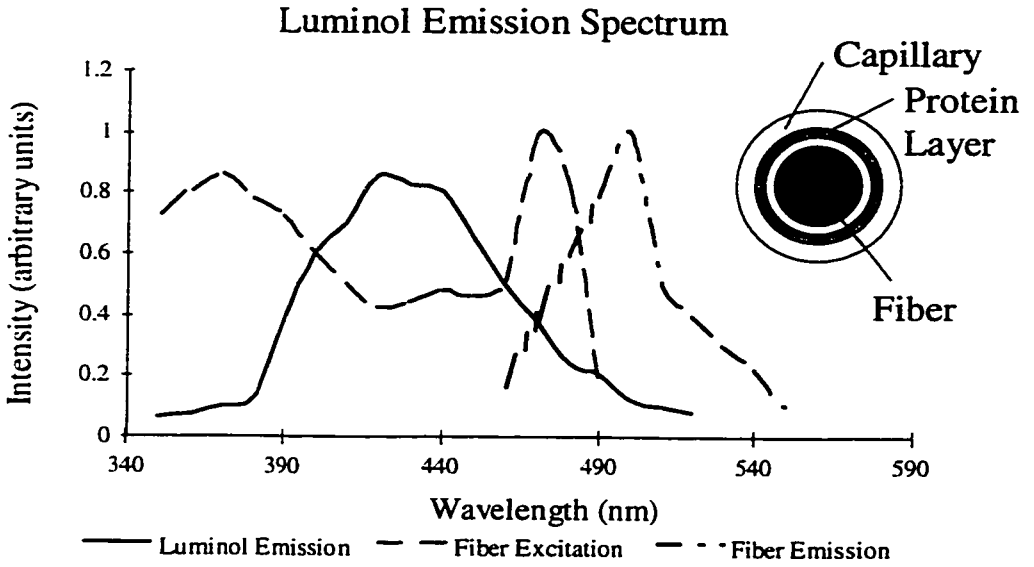

Figure 2.8 - Excitation/Emission spectra of the fluorophor-doped optical fiber compared to the luminol emission spectrum. The schematic at top-right shows a cross-section of the fiber inside of the capillary. The protein layer, when reacted with chemiluminescent reagents emits light that excites the fluorophor of the fiber. The fluorescent signal is collected by the end-coupled aluminum-jacketed fiber.

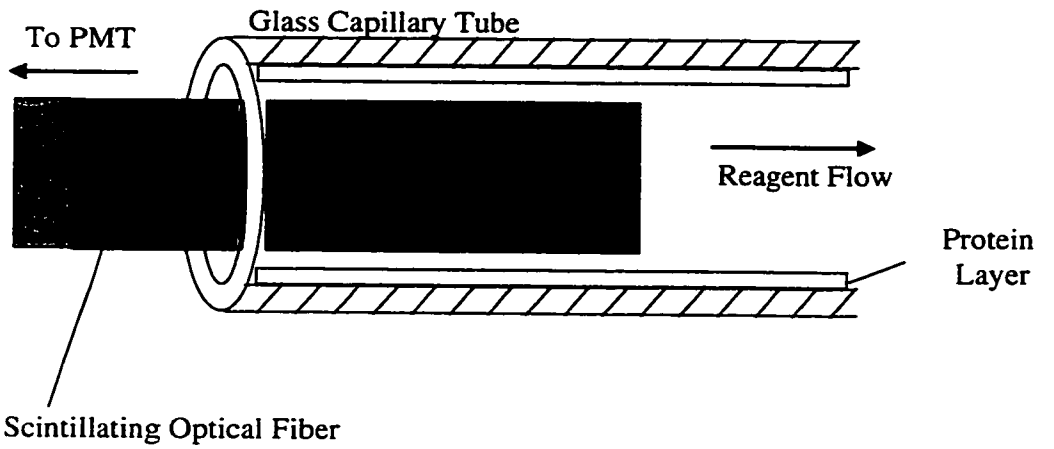

Figure 2.9 - Detail View of the Scintillation Probe inside of the sensor tube. Reagent flows around the fiber through the tube. The scintillation fiber is sensitive to light emission along its length.

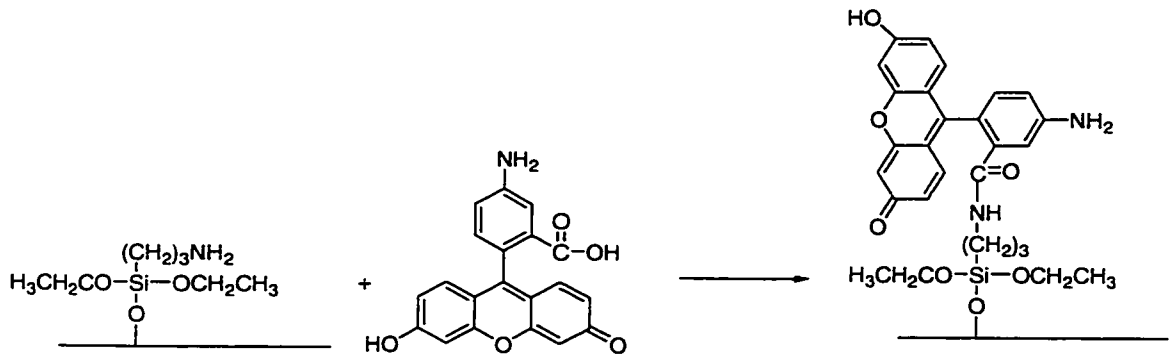

Figure 2.10 - Covalent attachment of fluorescein isothiocyanate (FITC) via a silane coupling agent. Aminopropyltriethyoxysilane is attached to a clean glass surface. The amino group reacts with FITC to immobilize the FITC molecule to the surface.

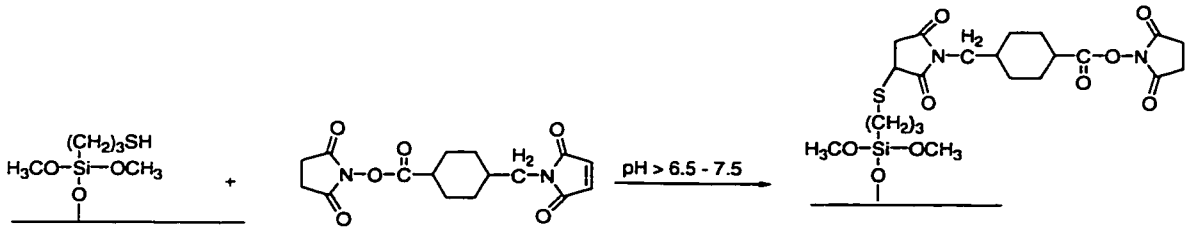

Figure 2.11 – Covalent coupling of SMCC to a glass surface by reacting the 3-mercaptopropyltrimethoxysilane functionalized surface with SMCC around neutral pH.

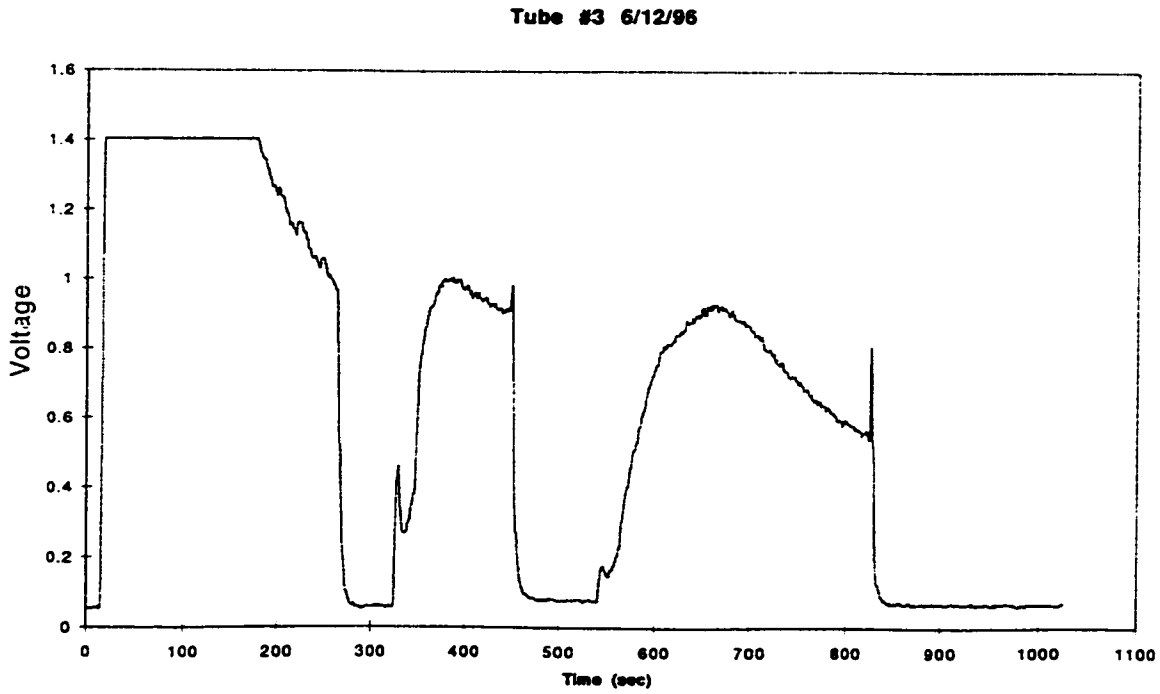

Figure 2.12 - Cycling of silane coupled tube – This plot shows three cycles of the tube with the PMT recording the light produced in volts. A cycle begins by flowing a small amount of the luminol reagent into the capillary tube and stopping the flow. The signal of the first cycle saturates the detector, and begins to decay as the chemiluminescent reagents are expended. The sharp decrease in signal indicates introduction of buffer in the capillary, removing reagent from the cell. The sharp spikes are indicative of the dead-volume and the luminol reagent contained within that dead-volume in the system.

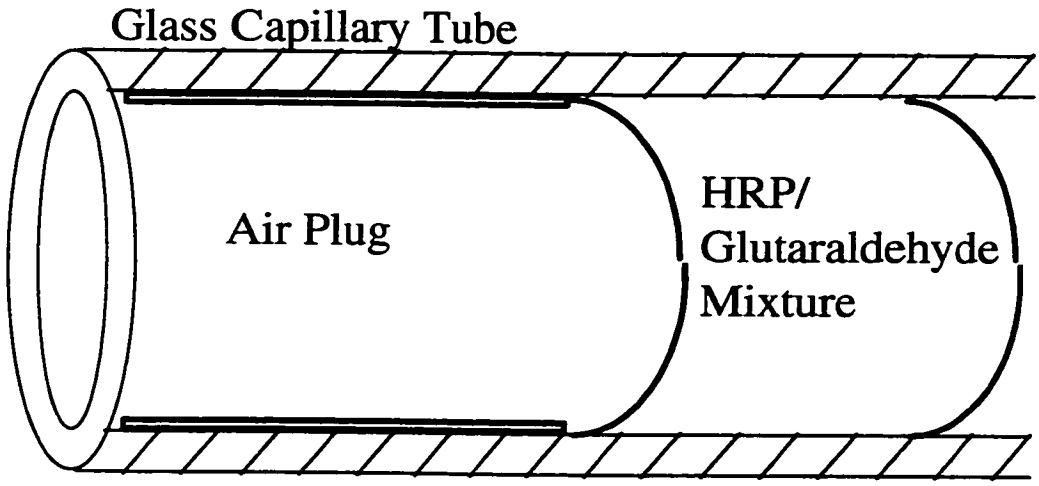

Figure 2.13 - Schematic of non-covalent protein immobilization.

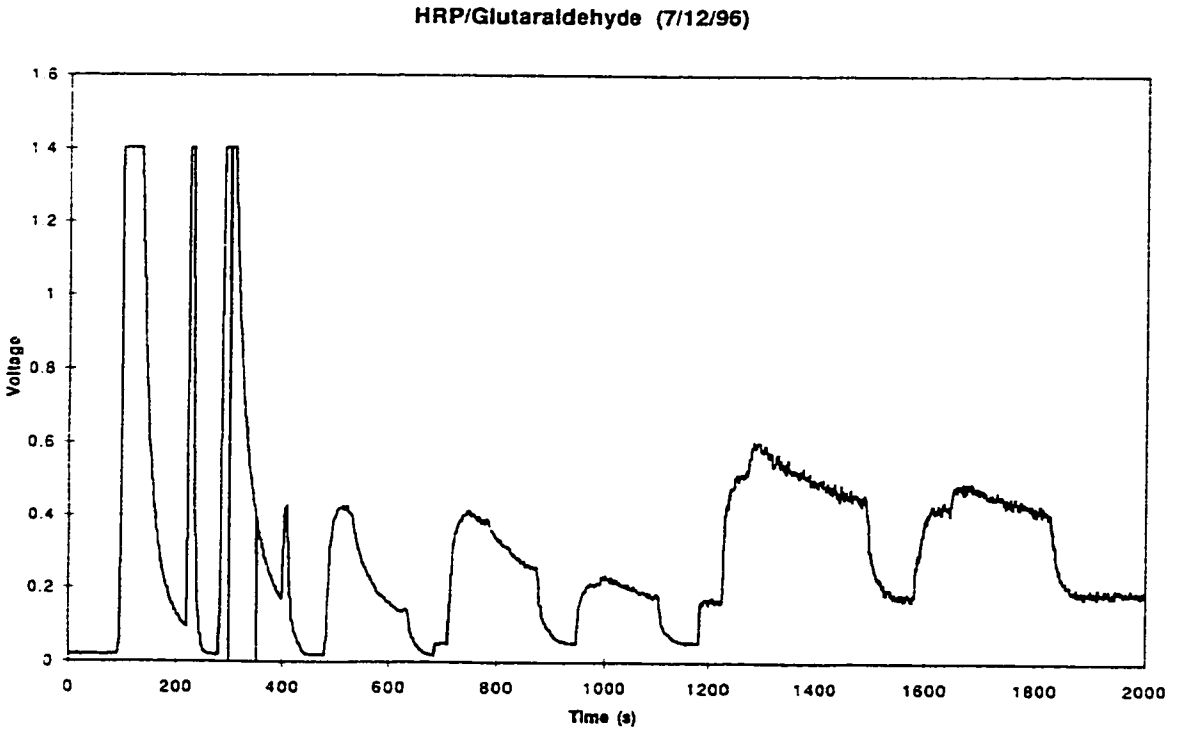

Figure 2.14 - Cycling study of HRP/glutaraldehyde tube – Cycles were performed similar to those described in Figure 2.12. The increase in signal at ~1250 seconds is due to an amplifier gain change for more sensitive light collection.

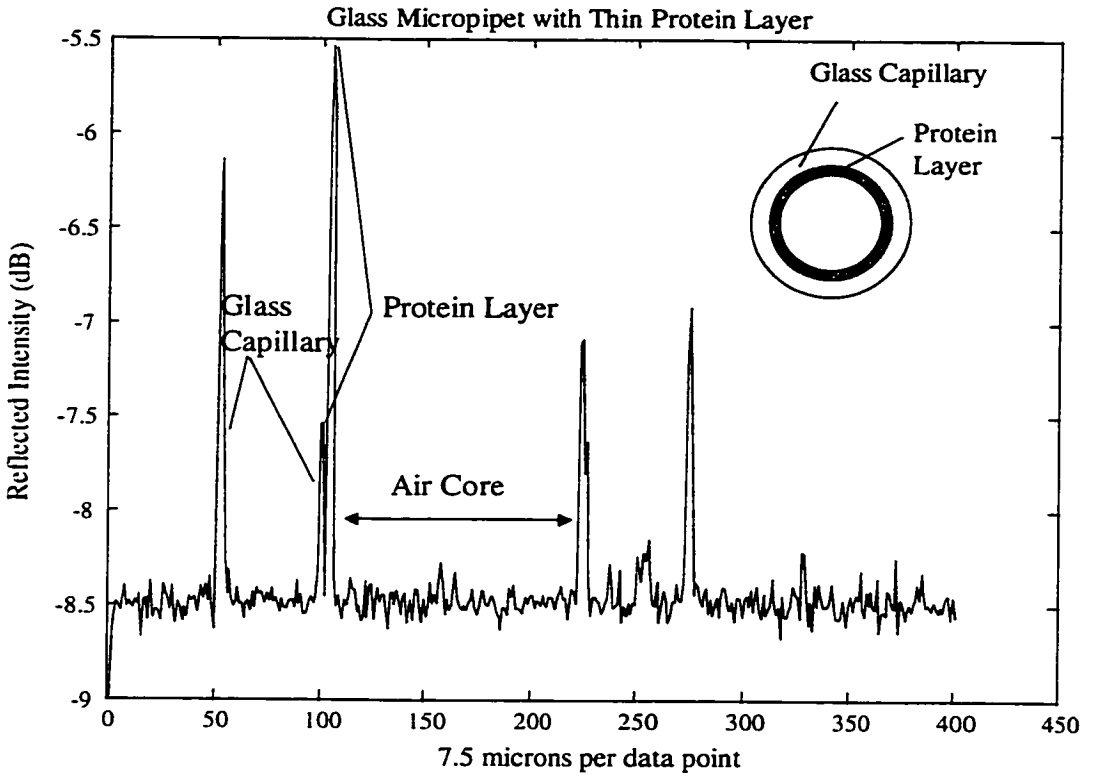

Figure 2.15 - Reflectometer Scan of a typical HRP/BSA protein layer

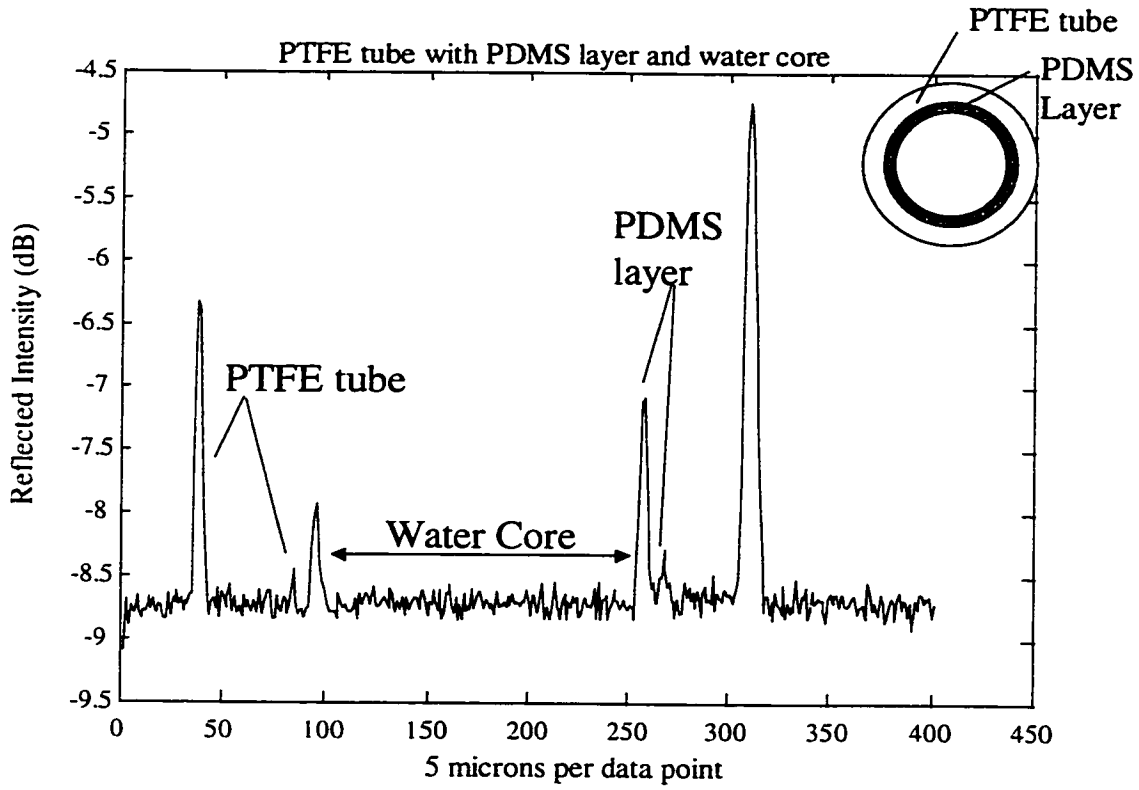

Figure 2.16 - Reflectometer Scan of a PDMS layer inside of a PTFE tube, analogous to the protein layers

Table 2.1 - Glutaraldehyde/HRP cross-linking optimization

	Buffer	Mass BSA (g)	Mass HRP (g)	Vol (µL) Buffer + Protein	Volume / Conc. (solute) Glutaraldehyde	Gel Time / Gel Color
1	PBS	0.05	-------	500	1000 µL / 5% (PBS)	No gel; yellow-orange solution
2	PPA	0.05	-------	250	500 µL / 5% (PPA)	4 min.; cloudy yellow
3	PBS	0.05	-------	250	500 µL / 5% (PPA)	7.5 min.; cloudy yellow
4	PPA	0.05	-------	250	500 µL / 5% (PBS)	30 min. on microcope slide; cloudy yellow
5	PPA	0.05	-------	250	10 µL / 50%	5 min.; cloudy brown
***6**	**PBS**	**0.05**	**-------**	**250**	**10 µL / 50%**	**5 min.; clear brown**
7	PPA	0.05	-------	250	20 µL / 50%	2.5 min.; cloudy brown
8	PBS	0.05	0.005	250	20 µL / 50%	20 min.; clear brown
9	PBS	0.05	0.005	250	50 µL / 50%	No gel after 25 min.
10	PBS	0.05	0.005	100	200 µL / 50%	No gel; yellow-brown solution
***11**	**PPA**	**0.05**	**0.005**	**250**	**10 µL / 50%**	**4 min.; clear brown**

* These trials produced the best experimental results.
PBS = pH 7.6 phosphate buffered saline
PPA = pH 5 phosphate/acetate buffer

Chapter 3 – Development of a dissolved oxygen sensor with a regenerated sampling interface

3.1 - Introduction

Determination of dissolved oxygen with a high level of accuracy and precision is relatively simple to accomplish with a disposable sensor or a sophisticated measurement system. When the measurement also requires a low-power measurement technique, relatively inexpensive equipment, and long-term, autonomous operation under harsh conditions, the problem becomes much more difficult, ruling out many methods that are commonly used.

We have developed a two-chamber sensing system for remotely measuring dissolved oxygen in marine environments. This sensing system is based on an electrochemical measurement similar to the Clark electrode, a widely used remote method for dissolved oxygen analysis. Unlike the classic Clark electrode, this sensor employs a coulometric measurement that completely reduces all of the oxygen molecules in the cell. The first chamber is an equilibration chamber where the electrolyte is allowed to equilibrate with the external environment. After equilibration, the electrolyte is transferred to a second chamber, an oxygen-impermeable tube housing the electrodes. A potential is applied to the cell and the resulting current is measured. The current is directly related to the concentration of oxygen molecules in the electrolyte solution.

Commercially available oxygen sensors are typically Clark electrodes that operate either at a constant potential or in a pulsed mode. These electrodes rely on a

continuous flux of oxygen across a polymer membrane, making the signal dependent on the rate of diffusion through the membrane. These sensors are adversely affected by membrane fouling as well as stirring in the bulk outside of the membrane. The two-chambered cell we have developed removes this kinetic dependence upon membrane transport to offer an improvement in long-term stability over commercially available oxygen electrodes. Clark electrodes are furthered hampered by a limited supply of potassium chloride reagent, which can degrade over time and with repeated measurements from the accumulation of OH^- in solution. The sensor reported here employs a renewable reagent to reduce the affects of reagent degradation.

The basic sensor design was used for the development of a prototype which could ultimately be deployed to measure dissolved oxygen in marine environments. The premise behind the development of this sensing system was to improve upon the Clark electrode to increase the precision and long-term stability of the system as required for marine deployment. The key approach to this system is to first cycle the sensor and then consume all of the oxygen within the cell. This technique removes the continuous kinetic parameters under which most Clark-type electrodes must operate. By renewing the electrolyte, the possibility of reagent degradation is also minimized.

3.2 - Amperometry and Controlled-Potential Coulometry

In amperometric-based measurements of oxygen, the current associated with the reduction of oxygen molecules at a noble metal electrode is measured. This noble metal electrode (gold or platinum) is an easily polarized electrode as compared to a

reference electrode such as a saturated calomel electrode or silver/silver chloride electrode. A measurement is conducted by applying a constant potential between the working electrode and the reference electrode. The resulting current is proportional to the oxygen concentration in the sample.

In the case of the sensor reported here, a current vs. time curve is obtained for each measurement. This curve is integrated to give the total charge transferred which is directly related to the amount of oxygen consumed in the measurement. This type of measurement is known as controlled-potential coulometry. The analyte concentration (A) is calculated as follows:

$$[A] = (C)\left(\frac{1}{F}\right)\left(\frac{mol(A)}{mol(e-)}\right)\left(\frac{1}{V}\right) \qquad (3.1)$$

where C is the integrated number of coulombs transferred, F is the Faraday constant (96500 Coulombs/mol e^-), and V is the volume of the measured sample. The controlled-potential coulometric measurement provides a direct measurement of the oxygen concentration in the sample.

3.3 - Gas Permeable Membranes

Membrane choice is very important to the behavior of electrochemical oxygen sensors. In most cases, the membranes chosen are thin Teflon™ resin membranes such as polytetrafluoroethylene (PTFE), tetrafluoroethylene-hexafluoropropylene-copolymer (FEP), and poly(tetrafluoroethylene-co-perfluoro(alkylvinyl ether)) (PFA)

in order of decreasing diffusion rates.[1] These resins are known to have good diffusion rates for gases such as O_2 and CO_2. Another more recently developed Teflon™ resin, Teflon AF, a copolymer of 2,2-bistrifluoromethyl-4,5-difluoro-1,2-dioxole and tetrafluoroethylene, has an extremely rapid gas diffusion rates, making it a good choice for sensors in which a rapid equilibration is desired. Teflon AF™ comes in more than one type depending upon the weight percentage of dioxole in the copolymer, which changes the polymer's characteristics, including gas diffusion. In addition to the fluoropolymer resins, porous silicones such as silastic are also applicable as membranes in oxygen sensors. Table 3.1 shows the relative diffusion rates for O_2 through each of the above-mentioned membrane media.

3.4 - Existing Oxygen Sensing Technologies

Existing dissolved oxygen sensors include both optical sensors and electrochemical sensors. Perhaps the most readily utilized of the two types are the electrochemical oxygen sensors, specifically the Clark electrode.

3.4.1 - Electrochemical Oxygen Sensors

The Clark electrode, a bipolar amperometric sensor, is an electrode containing a noble metal electrode (either platinum or gold) and a silver/silver chloride reference electrode. These two electrodes are housed in a casing filled with half-saturated potassium chloride solution. The end of the housing is covered with a semi-permeable membrane that is readily permeable to oxygen (Figure 3.1). This membrane is usually

---

1 K. Hong; University of Washington Ph.D. Dissertation; (1995), 60-107.

PTFE or FEP, both Teflon™ resins. The membrane serves to eliminate the diffusion of fouling species or interfering anions to the electrodes, increasing the stability and the lifetime of the sensor. Dissolved oxygen in the matrix diffuses across the membrane and is reduced at the Pt cathode. The electrochemical half reactions are as follows:

$$O_2 + 2H_2O + 2e^- \rightarrow [H_2O_2] + 2OH^- \quad (3.2)$$

$$[H_2O_2] + 2e^- \rightarrow 2OH^- \quad (3.3)$$

$$Ag + Cl^- \rightarrow AgCl + e^- \quad (3.4)$$

The reduction of oxygen at a Platinum electrode is usually observed as a single four-electron step. The separate polarographic step corresponding to the reduction of hydrogen peroxide can be observed only on a mercury cathode. The traditional type of Clark electrode involves applying a continuous potential between -600 and -900 mV vs. Ag/AgCl to the sensor and measuring the resulting current. This method of measurement results in a continuous flux of oxygen across the membrane, making the electrode very kinetics-dependent.[2]

Varations on this type of electrode have been developed in an attempt to increase the accuracy of the measurement. This effort has included sensors in which the potential is pulsed to make calibration of the electrode more linear.[3] Another addition, a commercially available oxygen sensor from YSI (Yellow Springs, OH) uses a microelectrode cathode array. With a cathode surface area 100 times smaller

---

2 J. Janata, Principles of Chemical Sensors, Plenum Press, (1989), 201-206.
3 D.L. Short, G.S.G. Shell; J. Phys. E: Sci. Instrum., Vol. 18, (1985), 79-87.

than their conventional electrode, the manufacturers claim the microelectrode consumes far less oxygen within the cell, making the measurement independent of stirring. This does not avoid the dependence upon oxygen flux across the membrane, which is still subject to membrane failure and fouling.

3.4.2 - Optical Oxygen Sensors

Another technique for measuring dissolved oxygen relies on the quenching of fluorescence or phosphorescence of various molecules in the presence of oxygen. This phenomenon produces an optical sensor for dissolved O_2. A recent review article describes the different types of fluorophors and the wide variety of applications of this type of oxygen sensing.[4]

Wolfbeis and co-workers described the construction of such an optrode to monitor the glucose oxidase enzymatic reaction that releases O_2 as an enzymatic product. The 'optrode' described involved immobilizing a ruthenium complex on the tip of a fiber optic and calibrating the quenching of luminescence in the presence of oxygen.[5] Recently MacGraith and co-workers demonstrated this type of sensor in which the ruthenium complex had been immobilized in a sol-gel matrix on the tip of a fiber optic. The sol-gel matrix improved the long-term stability of the measurement by reducing degradation of the ruthenium complex due to exposure.[6] The stability of the sensor in both gas and liquid phase measurements of O_2 was also described.

---

4 J.N. Demas, B.A. DeGraff, P.B. Coleman; Anal. Chem.; Vol. 71, No. 23, (1999), 793A-800A.
5 M.C. Moreno-Bondi, O.S. Wolfbeis, m.J.P. Leiner, B.P.H. Schaffer; Anal. Chem., Vol. 62, (1990), 2377-2380.
6 C. McDonagh, B.D. MacCraith, A.K. McEvoy; Anal. Chem., Vol. 70, (1998), 45-50.

Sanz-Medel and coworkers have completed work involving sol-gel immobilized luminescent O_2 sensing materials. This group describes the room temperature phosphorescence of a metal-chelate complex that is quenched in the presence of O_2.[7] The researchers also report on the phosphorescent signal in aqueous micellar media.[8,9] The inherent difficulties of this type of sensing include interferences from other molecules in the matrix, immobilization of the fluorophor, and detecting O_2 concentration changes at the sub-percent level.

3.5 - New oxygen sensor in dip-probe configuration

Initially, the sensor was a dip-probe type of geometry (Figure 3.2) in which a platinum wire and a silver wire were inserted into a Teflon tube filled with a 2.4 M solution of KCl. The idea was to build, essentially, a Clark electrode using a thick-walled polymer tube. Due to its thickness, it would have a slower transport rate than that of typical Clark electrodes. We postulated that the slower oxygen permeation rate of the tube would allow for the complete reduction of the oxygen inside of the cell before significant additional O_2 permeates the tubing walls from the surrounding matrix. This polymer tube would act as the membrane as well as an electrochemical cell. The KCl reagent could be renewed between measurements to prevent the effects of reagent degradation due to the formation of OH· during the reduction of oxygen. The initial complete sensing system (Figure 3.3) included the O_2 cell, a reagent

---

7 A. Sanz-Medel, J.M. Costa-Fernandez, M.E. Diaz-Garcia; Anal. Chim. Acta., Vol. 360 (1998), 17-26.
8 A. Sanz-Medel, M.E. Diaz-Garcia, M.R. Fernandez, W.L. Hinze; Mikrochim. Acta, Vol. 3 (1988), 269-282.
9 A. Sanz-Medel, Y.M. Liu, M.R. Fernandez, M.E. Diaz-Garcia; Mikrochim. Acta, Vol. 1, (1991), 53-64.

reservoir, and a solenoid pump. The pump delivered reagent in 50 µL pulses. The pump and electrodes were controlled with an Onset Tattletale datalogger.

The first dip-probe sensor used a 22 gauge PTFE tube (305 µm wall thickness). There seemed to be considerable diffusion across the tube walls when potential was applied as the current did not seem to come to an asymptotically low value when compared to the current generated in a nitrogen-bubbled system (Figure 3.4). This meant that oxygen was diffusing through the tube wall as the oxygen inside of the tube was reduced. A PTFE tube with a thicker wall (405 µm) was tried, but the results were similar. Smaller diameter FEP and PFA tubing (405 µm I.D., 230 µm wall) with slower gas diffusion rates were also tried. The results were similar to the results obtained with the PTFE tube sensors where it appeared that there was diffusion across the tube wall before all of the oxygen inside of the tube could be consumed (Figure 3.5). Because the current generated could not be associated with just the oxygen contained within the tube during the measurement, it was concluded that there was continuous flux of oxygen through the tube walls. The chamber housing the electrode cell evidently must be oxygen impermeable to ensure complete reduction of all O_2 in the cell.

3.6 - Two-Chamber O_2 Sensing System

In order to remove the factor of diffusion during the oxygen consumption measurement, a two-chamber sensor was constructed (Figures 3.6 and 3.7). Basically, it consisted of a large piece of PTFE tubing filled with 2.4 M KCl electrolyte as the

first chamber. The electrolyte in this tube is allowed to come to equilibrium with the environment. After reaching equilibrium, the electrolyte is transferred into a second, oxygen-impermeable chamber. In this case the second chamber is a small glass tube with a Pt wire and a Ag/AgCl wire inserted inside. The oxygen content is measured by applying the potential across the electrode and measuring the current as the oxygen inside the glass cell is reduced. For an effective zero oxygen measurement, the electrolyte was not renewed between cycles of the electrode. The measured current over time was plotted (Figure 3.8) and the integrated value of each current trace was calculated. The mean and standard deviation for the traces shown in Figure 3.8 is shown in Figure 3.9. However, there was a large amount of error (> 5% Std. Dev.) in the integrated value for the sensor in both oxygenated and anoxic environments.

The equilibration time between cycles was determined using a 0.025 cm I.D., 0.158 cm (1/16") O.D., 100 cm long PTFE equilibration coil with an internal volume of ~ 50 μL. The fluid in the tube was equilibrated for times a short as 1 minute or as long as 8 minutes in between ten-minute measurements. The error associated with each of the experiments seemed to level off beginning at 5 minutes equilibration time in between cycles(Figure 3.10). This coil was replaced with a thinner-wall, larger volume PTFE tube (0.076 cm I.D. x 0.158 cm O.D. x 145 cm long, volume = 660 μL) for the rest of the sensor development described here. This new, thinner-walled tube has an equilibration time of less than 15 minutes, so the cycles could be run continuously without a delay.

The amount of variance in the data was addressed by trying to reduce the axial diffusion pathways in the cell that were potentially contributing to the error in the measurements. This was done by placing one-way valves in line before and after the glass cell to minimize diffusion or fluid flow due to pumping from motion of the sensor. The variance in the data was still larger than was desired for the instrument in order to see dissolved O_2 concentration changes of less than 1%.

The next steps taken were to reduce the remaining electrical noise in the measurement. In all of the measurements to date, the potential applied across the electrodes, it was stepped to the full value of –0.7V with respect to the Ag/AgCl electrode. This produced a capacitive spike at the beginning of the current vs. time trace that was not easily measured and was difficult to integrate accurately. The first solution was to increase the data collection rate to 100 Hz in an effort to better track the initial current values of the cells. Increasing the data collection rate did not reduce the error in the repeated measurements. The next step was to gradually apply the potential to a final value of –0.7 V. Stepping of the potential gives a current trace, including a charging increase, that is both measurable and more readily integrated (Figure 3.11). It was also realized that if the cell had not been operated for several days, there appeared to be a conditioning phase of the electrodes in the first several cycles. After this conditioning, the measurements were quite stable and reproducible (< 5% standard deviation from the mean integrated curve). Figure 3.12 shows the integrated intensities for the oxygenated traces for a typical experiment, this one was conducted over 4 days.

3.7 - Verification of measured O_2 concentration with theoretical O_2 concentration

A theoretical calculation was conducted to confirm that the predicted amount of oxygen in the cell corresponds to the measurement with the sensor. Based upon the electrolyte concentration in the half-saturated KCl, the air-saturated oxygen concentration at ambient conditions was determined to be 1 x 10^{-4} mol O_2/L (at 20 °C).[10] This value is approximately half of the saturation value for O_2 in seawater, which is ~2 x 10^{-4}. The decrease in oxygen concentration in the higher concentration salt solution is due to the salting-out effect of O_2, first quantitatively documented by Setchenov in 1889.[11] The difference in concentration means that is a bias between the oxygen concentration measured by the sensor and the oxygen concentration in the surrounding matrix. However, if the bulk is in equilibrium with the sensor system, the concentration ratio will remain constant, so quantification of the external O_2 concentration is possible if the bias is known.

Equation 3.1 was modified for the oxygen measurement as follows. The theoretical number of Coulombs of charge was determined by multiplying the O_2 concentration by the glass cell volume (~ 70 µL), the Faraday constant, and the number of electrons required to reduce one O_2 molecule (Equation 3.2).

$$[O_2] = C\left(\frac{1}{96500}\right)\left(\frac{1 mol O_2}{4 mole^-}\right)\left(\frac{1}{V}\right) \qquad (3.5)$$

The calculated number of Coulombs was determined to be 2.7 x 10^{-3} C. The actual number of Coulombs measured with electrolyte equilibrated with a fresh-water

10 CRC Handbook, 71st edition, (1994).
11 J. Setchenov, Z. Phys. Chem., Stoechiom. Verwandtschaftsl.; 4, (1889), 117-125.

environment at ambient conditions was determined as 2.6×10^{-3} C, within 5% of the theoretical value. We were confident that the primary species undergoing reduction in the glass capillary cell was indeed dissolved oxygen.

3.8 - Conclusions

This chapter incorporates the design, construction, and testing of a sensing system for detecting dissolved oxygen. The two-chamber sensing system addresses some of the weaknesses of Clark oxygen sensors for long-term, continuous monitoring applications. These weaknesses include the kinetic dependence upon membrane diffusion, and reagent degradation. The two-chamber design was shown to be an improvement over a conventional Clark electrode, demonstrating less than 5% drift over a period of days. The system is still subject to membrane fouling that can affect the total integrated current. In addition, the electrodes seem to undergo a conditioning phase that is not fully understood or well characterized.

The next chapter describes the construction of a working, submersible prototype, long-term testing of the prototype compared to a standard reference method, deployment of the prototype into a fresh water environment, and modeling to better understand the bias that exists between the sensor readings and bulk concentration.

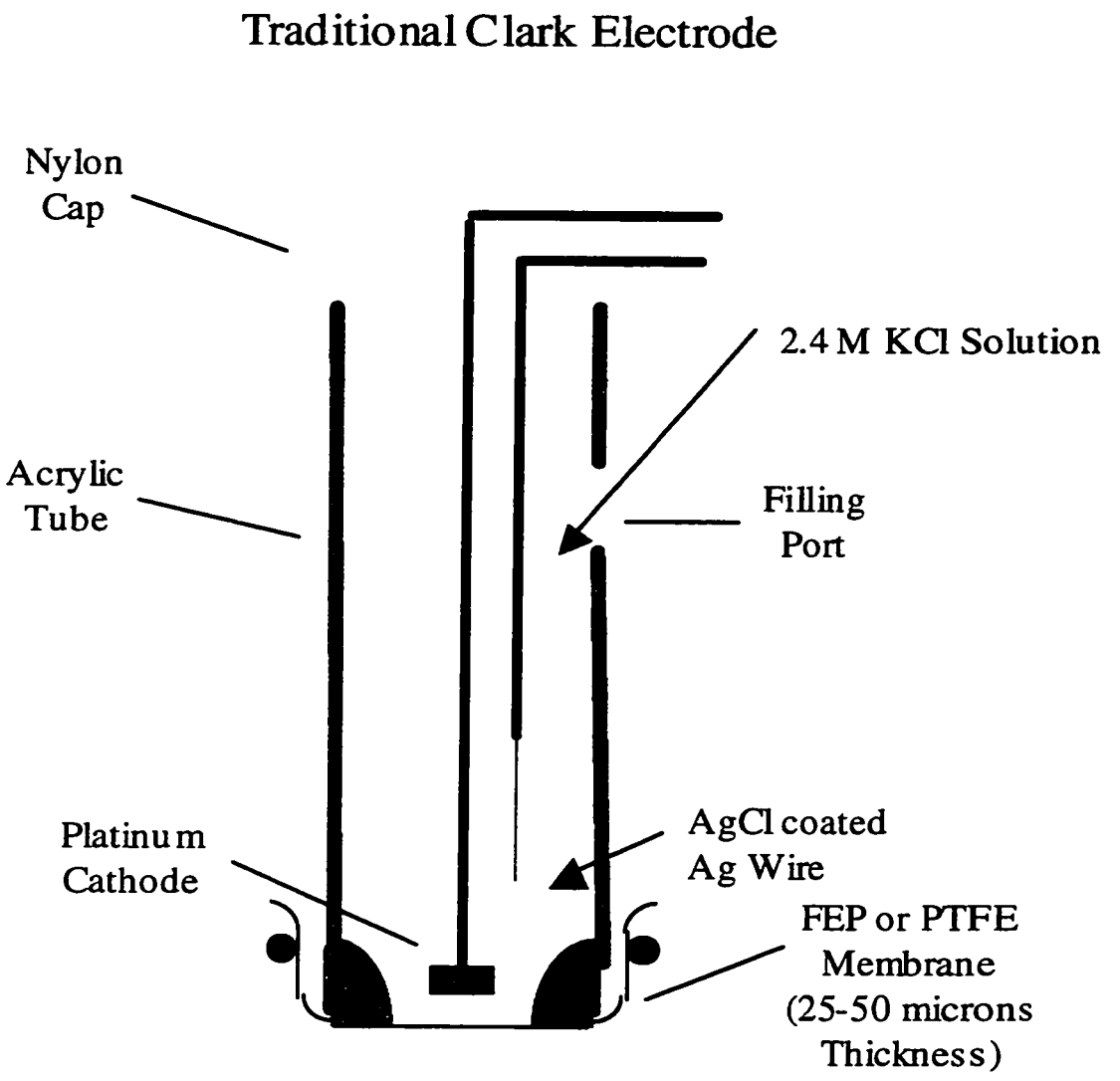

Figure 3.1 - Clark Electrode Schematic: ~0.5" plastic tube filled with half-saturated KCl electrolyte solution. A platinum cathode and a silver chloride coated silver wire reference electrode. It provides a continuous measurement of O_2 at a fixed potential of –0.7V with respect to the Ag/AgCl electrode. The current depends upon the concentration of oxygen in the sensor which is dependent upon the rate of oxygen diffusion through the membrane that changes depending on the stirring conditions outside of the membrane and membrane fouling.

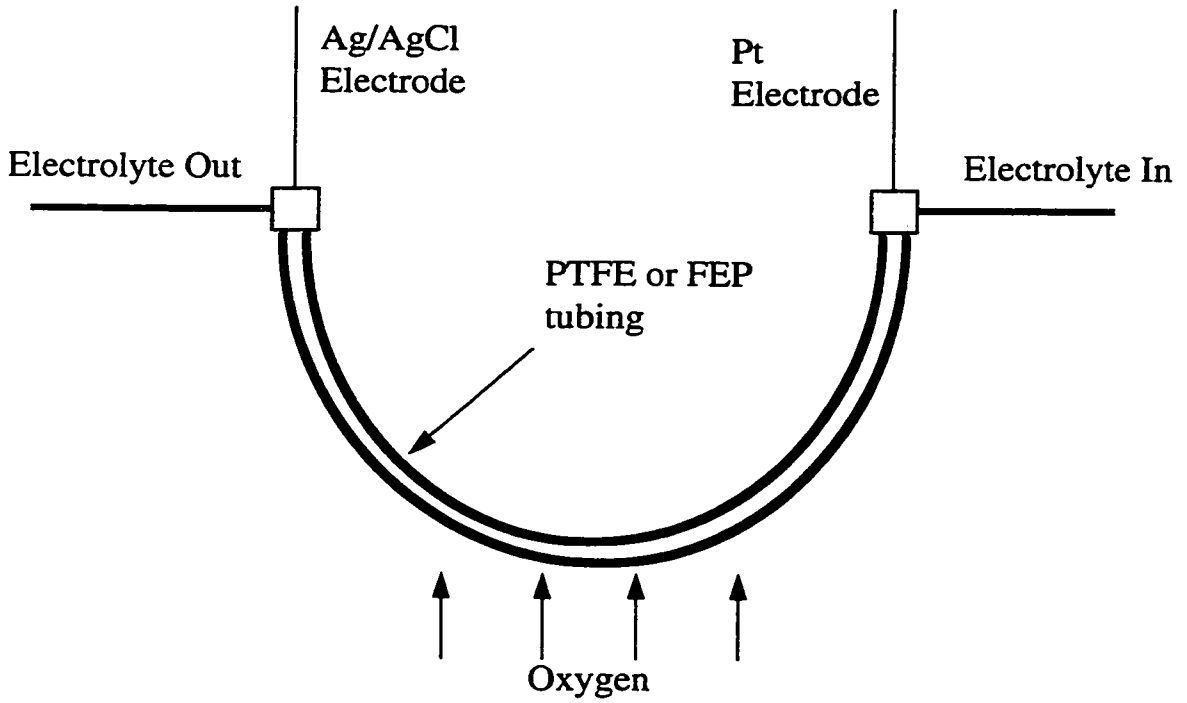

Figure 3.2 – Dip-Probe oxygen sensor design. This sensor was constructed from either PTFE of FEP Teflon™ tubing with a platinum wire cathode and a silver chloride coated silver wire anode. The tube wall, the membrane in this case, is much thicker than the traditional clark electrode and the diffusion path-lengths are shorter, so complete reduction of the O_2 in the tube is possible. This format also employed the renewable reagent concept by replacing the electrolyte in the tube after each measurement.

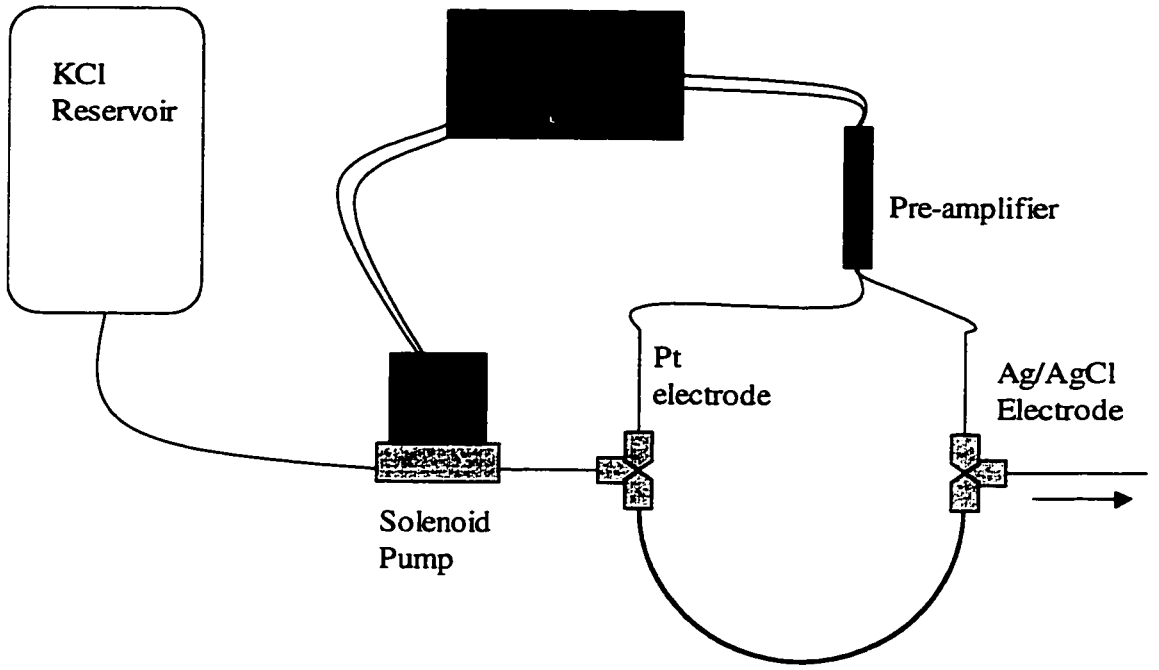

Figure 3.3 - Schematic of initial O2 sensing system with the cell depicted in Figure 3.2. The solenoide mini-pump delivers reagent in 50 μL pulses. A current to voltage converter and some conditioning electronics take the signal from the cell and put it into the Onset Tattletale datalogger/controller.

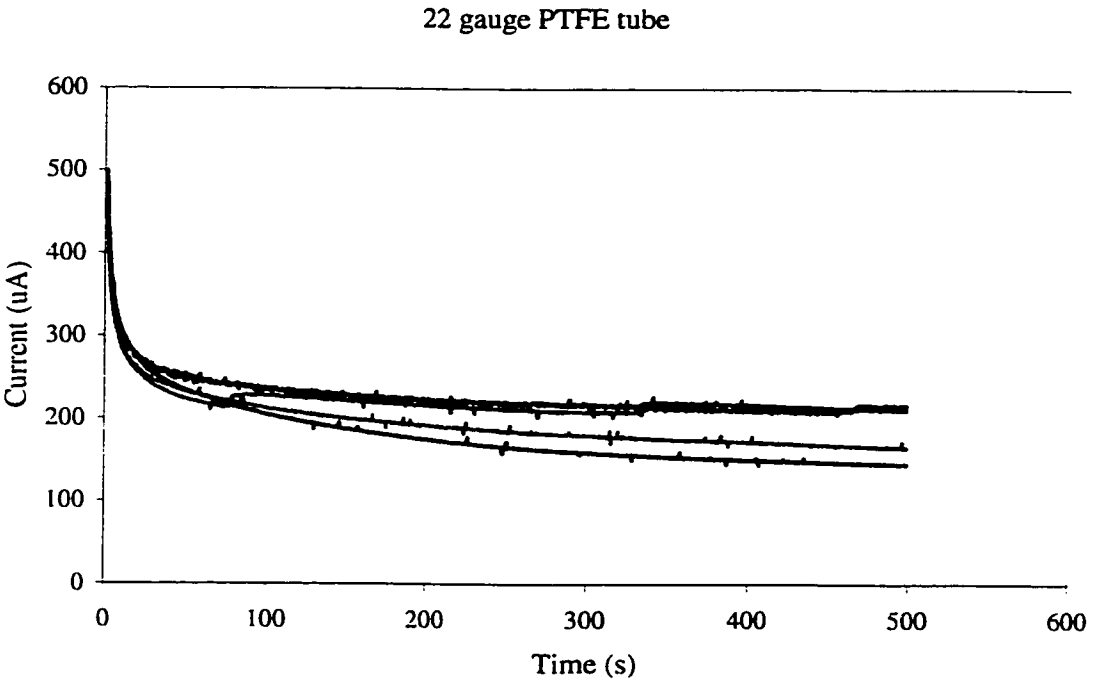

Figure 3.4 – Preliminary 22 gauge PTFE dip-probe data collected at 2 Hz, four scans. The current does not drop below 200 μA indicating that the O_2 diffusion through the membrane is occurring during the measurement.

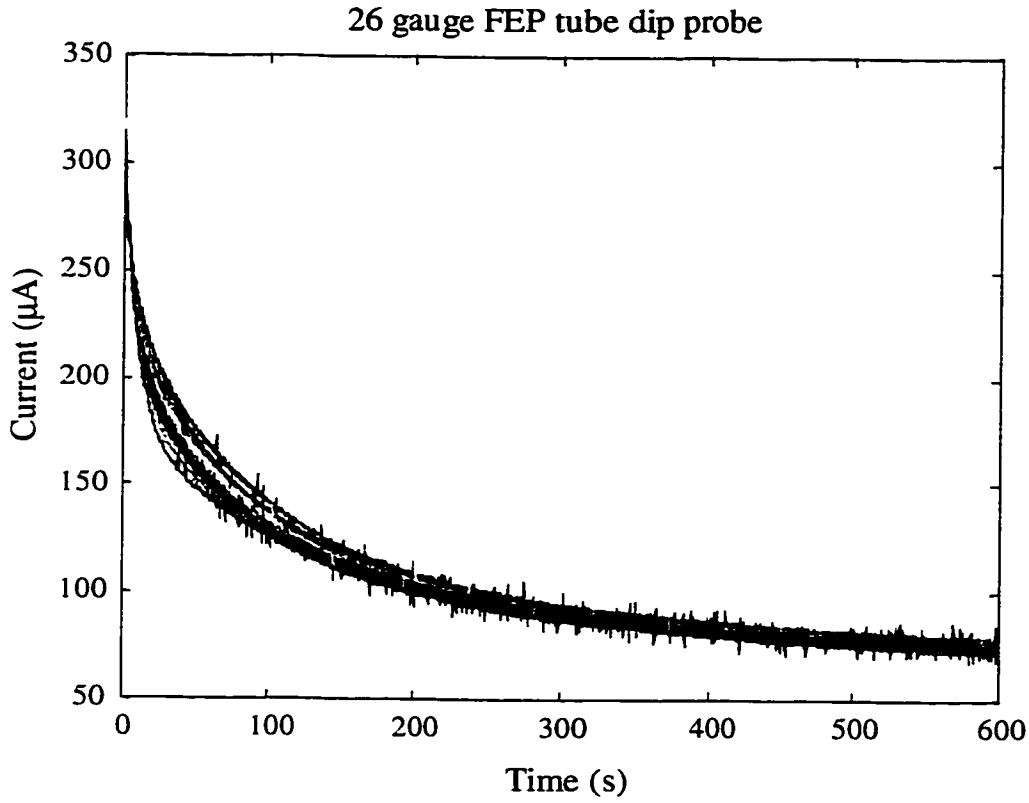

Figure 3.5 – 26 gauge FEP Teflon™ tube dip-probe results collected at 2Hz. The current reaches a lower value due to the shorter diffusion path-lengths and the slower permeation rate for FEP, but the signal is still relatively high.

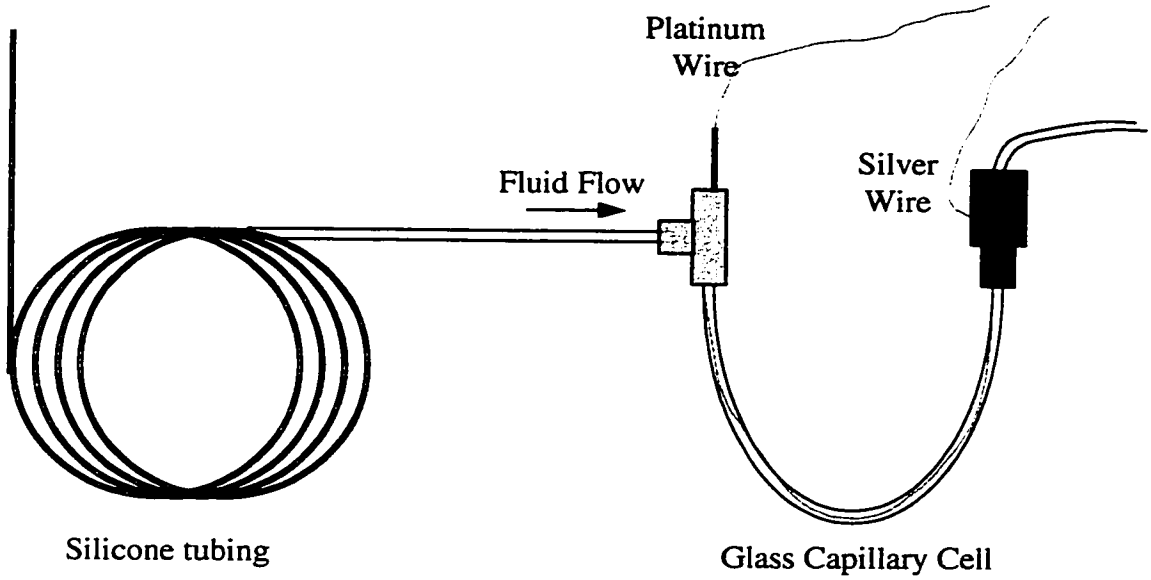

Figure 3.6 - Schematic of the two-chamber oxygen electrode. The membrane equilibration of the electrolyte is separated from the electrode measurement cell allowing for a membrane material with a rapid O_2 permeation rate to be used.

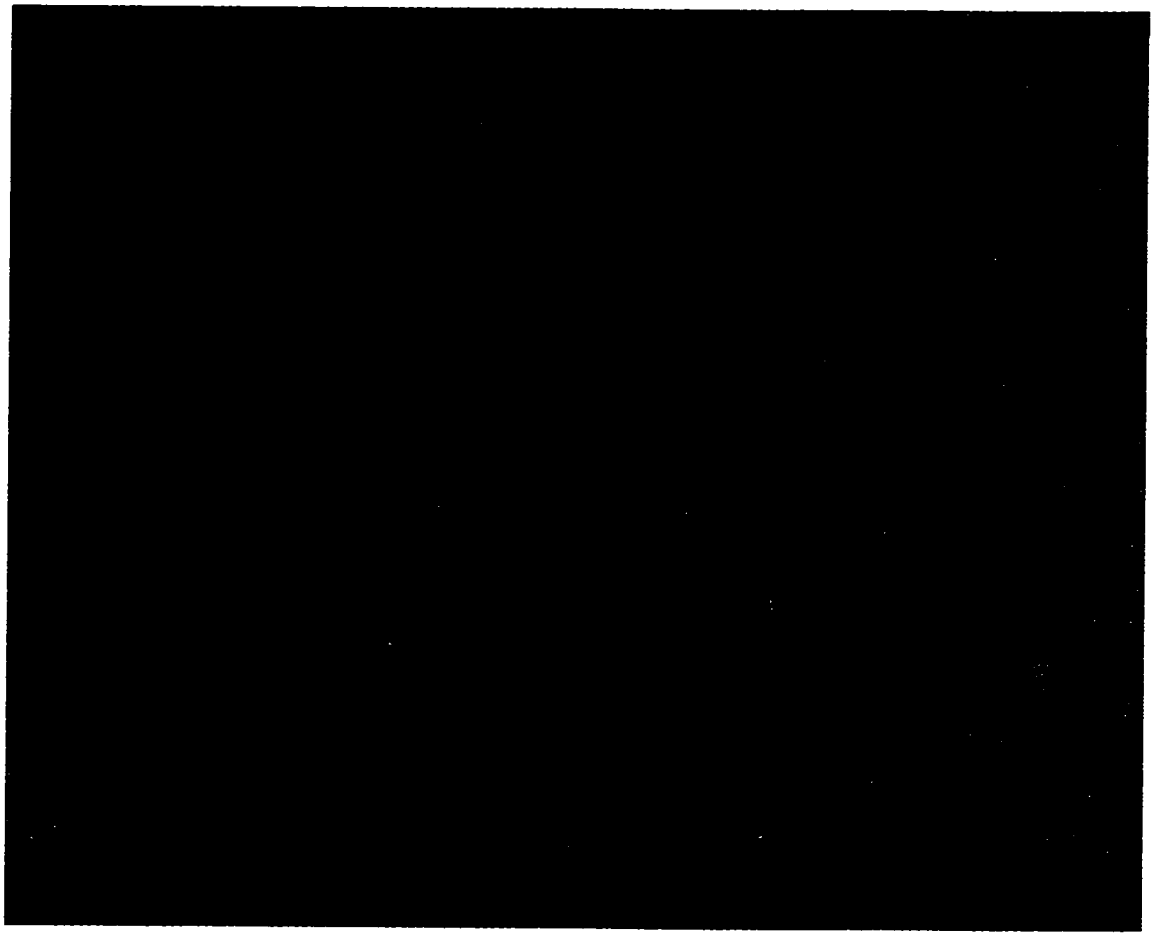

Figure 3.7 – Silicone equilibration coil (top) ~ 1 meter long, 1 mL volume. Oxygen measurement cell (bottom).

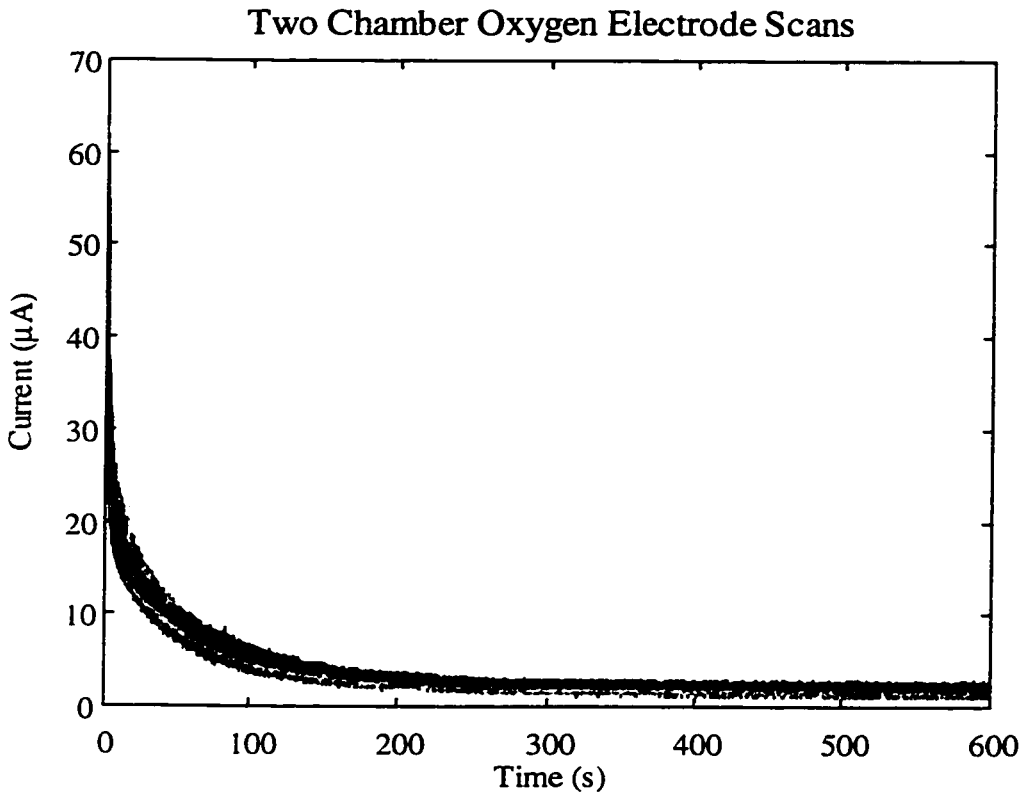

Figure 3.8 - Data from the two-chamber oxygen electrode. Note that the current trace reaches a low value compared to figures 3.4 and 3.5.

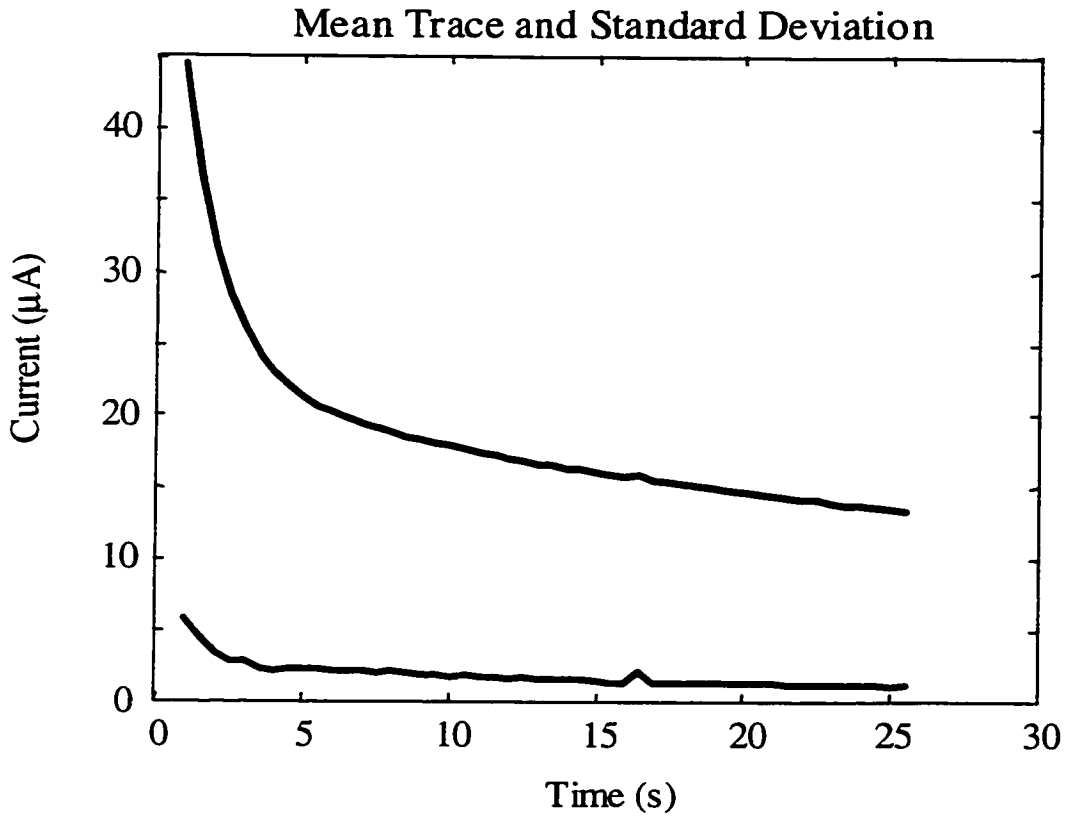

Figure 3.9 - Mean (blue) and standard deviation (red) traces for the initial part of the oxygen reduction current traces shown in Figure 3.8.

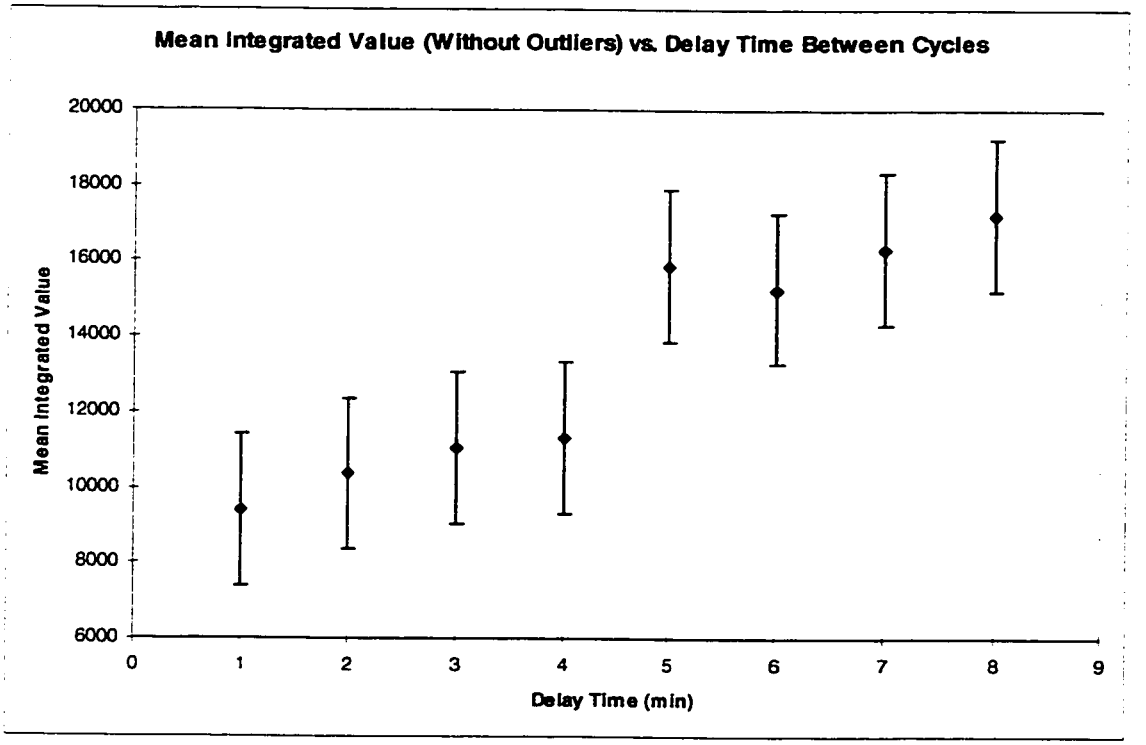

Figure 3.10 – The average integrated value compared with the delay between cycles for a 2-chamber sensor with a PTFE equilibration coil. The results of this study prompted the change of the coil to silicone with a larger volume (~ 1 mL), and the measurement time was increased to 15 minutes.

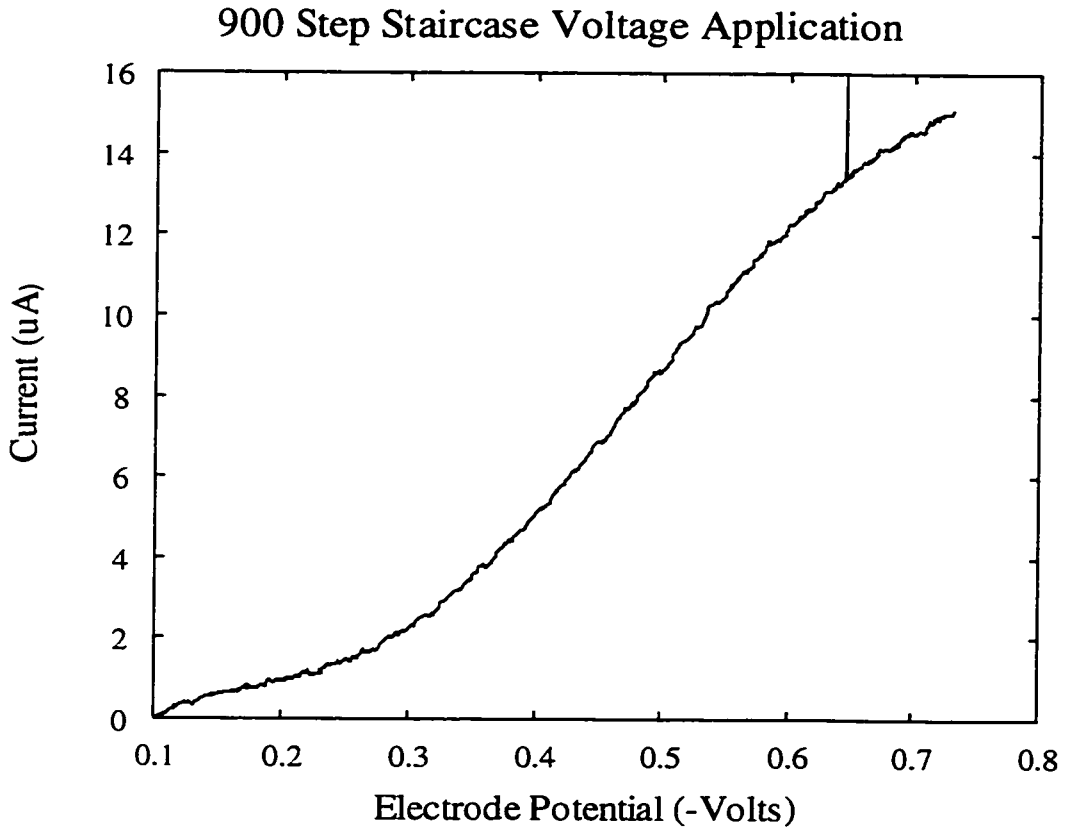

Figure 3.11 – To increase the precision of integration of current vs. time curves, a gradual staircase voltage application was used. This greatly improved the reproducibility of the integrated values.

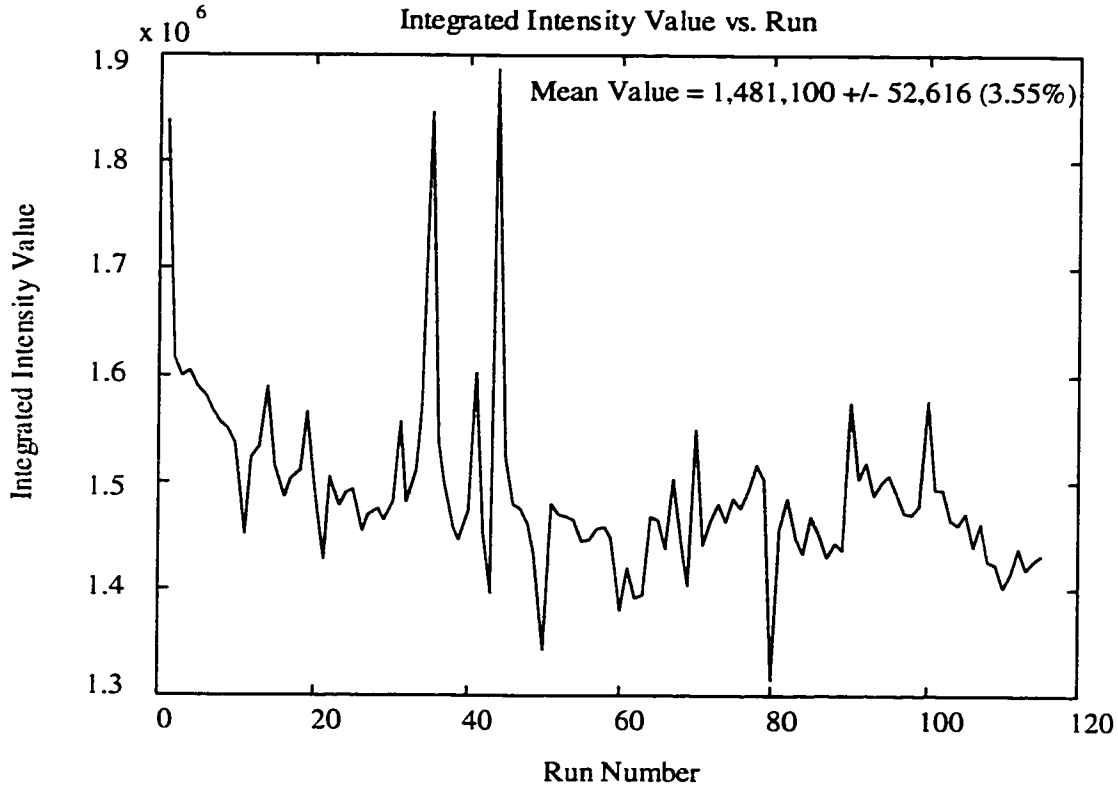

Figure 3.12 – Integrated traces for oxygenated runs for a four day test with 1 cycle per hour and periodic anoxic cycling. The outliers were removed from the data for the calculation of the mean, but are shown here.

Table 3.1 – Oxygen Permeation Rates of Membrane Materials

Membrane Material	Permeation Rate $[(cm^3)(mil)/(100\ in.^2)(24\ hr)(atm)]$[12]	Relative Rate
FEP (Zeus)	84	1
PTFE (Zeus)	420	5
PFA (Zeus)	880	10.5
Silicone (Cole-Parmer)	48,000	571
AF-2400 (Biogeneral)	99,000	1178

[12] Biogeneral Application Notes, 1999.

Chapter 4 – Submersible, Autonomous Oxygen-Sensing System

4.1 Introduction

The oxygen-sensing system reported in the previous chapter was incorporated into a submersible, autonomous prototype for deployment at depths up to 100 m. This system was developed for a long-term deployment due to the failure of Clark sensors after one to two months of marine deployment, even with anti-fouling measures. Some sensor failures are due to the thin membrane developing pinhole leaks, but many times the failure mode is not directly diagnosed by a visual inspection. Rather, the data begin to drift from other readings. The latter drift is likely due to reagent degradation in the small reagent volume from the build-up of O_2 reduction by-products. Recall from Chapter 3, the following reactions occur within the Clark cell:

$$O_2 + 2H_2O + 2e^- \rightarrow [H_2O_2] + 2OH^- \quad (4.1)$$

$$[H_2O_2] + 2e^- \rightarrow 2OH^- \quad (4.2)$$

$$Ag + Cl^- \rightarrow AgCl + e^- \quad (4.3)$$

Four OH^- molecules are formed for every O_2 molecule that is reduced at the Pt cathode. The sensor described in Chapter 3 is robust against both failure modes of the traditional Clark sensor, the equilibration membrane is much thicker and therefore more robust, and it employs a renewable reagent component that removes the possibility of reagent degradation from reaction product build-up.

This chapter describes prototype construction and testing, as well as model-based confirmation of its readings. The sensor's measurements were compared to the

reference samples taken, where dissolved O_2 was determined by the modified Winkler method. The prototype was deployed in fresh water, and stability tested for more than two months in temperature-controlled, artificial seawater.

4.2 Analytical Reference Method

The reference method in this work, and the standard laboratory method for the measurement of dissolved oxygen, is a modernized version of the Winkler method.[1] The Winkler method is very widely used in the determination of dissolved oxygen in seawater. Depending on the skill of the analyst, the Winkler method can be precise to at least 0.5%, with greater than 99% accuracy. The protocol for the modified Winkler method entails adding a solution of $MnSO_4$ to a known quantity of seawater, immediately followed by the addition of an alkaline NaOH/NaI solution.[2] Manganous hydroxide precipitates and reacts with dissolved oxygen in the water, forming a hydrated, tetravalent oxide of manganese.

$$Mn^{2+} + 2OH^- \rightarrow Mn(OH)_2 \qquad (4.4)$$

$$2Mn(OH)_2 + O_2 \rightarrow 2MnO(OH)_{2(s)} \qquad (4.5)$$

The solution is acidified and the manganese hydroxide dissolves. In the acid solution, the $MnO(OH)_2$ acts as an oxidizer and liberates free iodine from the iodide ions in solution.

$$Mn(OH)_2 + 2H^+ \rightarrow Mn^{2+} + 2H_2O \qquad (4.6)$$

---

1 L.S. Winkler, Ber. Dtsche. Chem. Ges., Vol. 21, (1888), 2843-2855.
2 J.H. Carpenter, Limnology and Oceanography, 10, (1965), 141-143.

$$MnO(OH)_{2(s)} + 4H^+ + 2I^- \rightarrow Mn^{2+} + I_2 + 3H_2O \qquad (4.7)$$

The liberated iodine, equivalent to the dissolved oxygen concentration, is then titrated with a standardized sodium thiosulfate solution to a clear endpoint with a starch indicator.

$$I_2 + 2S_2O_3^{2-} \rightarrow 2I^- + S_4O_6^{2-} \qquad (4.8)$$

4.3 Prototype Construction

The next phase of the project included development of a prototype to be immersed in a constant temperature, constant concentration water bath for testing and calibration. A new cell with modest revisions was prepared for the prototype. This cell had only one in-line check-valve (Upchurch Scientific – Oak Harbor, WA) on the outlet end and a solenoid valve on the inlet end. The solenoid valve was placed on the inlet end of the cell to eliminate temperature and motion-induced pumping into the cell, which caused erroneous results in initial tests. During the testing phase of the cell, the check-valve on the outlet was eliminated because its relatively large holdback volume (~ 150 µL) caused further variance in the data due to the axial diffusion of oxygen from that volume to the platinum electrode. The solenoid valve eliminated any flow from the waste outlet back into the cell.

The first pump used in the prototype was a solenoid minipump that delivered 50 µL per pulse (Lee Co) (Figure 4.1). These pumps have been employed in continuous flow analyzers designed for long-term, submerged deployment for

injecting standards into a sample stream.[3] Additionally, a solenoid pump was employed to renew the pH indicator for measuring pCO_2 in seawater *in situ*.[4] The solenoid pump is a unique fluid-delivery module; it is compact and consumes little power, and generates little heat.[5] But, this pump presents a few challenges to work properly and reproducibly. The major challenge with the Lee solenoid pump is the need for a continuous pressure-head on the pump. Additionally, the feed tubing entering the inlet side of the pump must be larger than that of the outlet side so that vacuum-induced bubbles are not generated.

A screw-driven syringe pump replaced the solenoid pump in the final version of the prototype. The primary reason that the solenoid pump was replaced for this configuration was the lack of accurate volumetric delivery. Variable pulse volume affected the overall reproducibility of the O_2 measurements, indicating that the pump was not flushing the cell out completely. Figure 4.2 shows the mean oxygenated and zero traces for the manual prototype test conducted with a syringe. A zero-oxygen experiment is a series of repeated measurements made without renewing the electrolyte in the cell, so all of the oxygen is reduced within the cell, and subsequent measurements are free of dissolved oxygen. The variance in the integrated oxygen data was calculated to be 1.35% while the variance associated with the integrated values for the zero traces is 0.08% of the total integrated oxygen value. Figure 4.2 also shows the mean oxygenated trace for a 10-cycle prototype solenoid pump (green).

---

3 H.W. Jannasch, K.S. Johnson, C.M. Sakamoto, Anal. Chem., 66, (1994), 3352-3361.
4 M.D. DeGrandpre, T.R. Hammar, S.P. Smith, F.L. Sayles, Limnol. Oceanogr., 40, (1995), 969-975.
5 D.A. Weeks, K.S. Johnson, Anal. Chem., 68, (1996), 2717-2719.

Note that the green trace is of less average amplitude and the integrated value is smaller. The variance associated with the mean is 4%, greater than the error associated with the syringe.

The syringe pump housed three 60 mL syringes and acted as both the pump and the reagent reservoir. A threaded rod connected to a motor drove the endplate that pushed the syringe plungers at an equal rate, sending a reproducible amount of fluid from the equilibration coil into the measurement cell. This volume was calibrated to be 440 μL in a 1 second pulse of the pump motor, sufficient to completely flush out the cell and all of the tubing between the coil and the cell. The coil volume was chosen so a representative sample from the equilibrated fluid in the coil is delivered into the cell.

The rest of the assemblage was put together out of commonly available parts. The KCl reagent reservoir was simply an IV solution bag and all of the fluid delivery tubing, with the exception of the equilibration coil, was 1/16" O.D. PEEK (polyetheretherketone) tubing, both of which are readily available commercially (Upchurch Scientific – Oak Harbor, WA). The fittings used were standard low-pressure fittings (Upchurch Scientific – Oak Harbor, WA) and the equilibration coil was ~0.4 m of commercially available Silastic™ tubing (I.D. 0.51 mm) providing a coil volume of ~800 μL.

The completed submersible prototype (Figure 4.3) was a brass syringe pump, and plexiglass pressure case (Figure 4.4) housing the O_2 cell, solenoid valve, pump motor, and signal conditioning electronics. The electrical connections were made

through water-proof connectors to the power supplies and Onset Tattletale datalogger. The mechanical rotating connection had its own waterproof seal. For this initial prototype, control of the datalogger was done through a Basic computer program running on a laptop computer via a serial connection.

The entire sensing system electronics consisted of an Onset Tattletale datalogger (Onset Computer Corporation, Pocasset, MA) with a customized prototype board. The datalogger was run via a BASIC computer program downloaded to the logger/controller via a serial interface. The Tattletale both operated the instrument and stored the data. The entire system was battery-powered with 8 AA alkaline batteries, but could also be powered by Li ion batteries.

Initial testing of the prototype was conducted with the equilibration coil immersed in a beaker of water to determine if the cell, pump and valve functioned normally. After these tests, we began testing under more realistic, laboratory conditions. For this, the complete submersible prototype was constructed with a second pressure case to house the Onset datalogger and the batteries for operation (Figure 4.5). This pressure case was connected to the instrument with waterproof cables and connectors. The operating program was modified to integrate the data and store it on the datalogger itself, which can be read when the system is retrieved.

4.4 Anti-Fouling

Growth of bacteria and algae on the surface of the sensor equilibration coil is problematic because these types of fouling layers can alter the local O_2 concentration

around the sensor. In the general case, a layer of aerobic bacteria would consume oxygen while an algal layer would produce oxygen. To minimize the growth of either type of organism, a mercury vapor lamp was incorporated into the sensing system. Most bacteria and algae do not survive under ultraviolet radiation. The lamp, ~ 6" in length, was housed in a quartz pressure case and inserted into one of the syringe slots in the pump (Figure 4.6). The silicone equilibration coil was wrapped around the quartz tube. The power supply for the lamp was housed in a separate pressure case to minimize the introduction of noise into the oxygen measurement (Figure 4.7). The lamp was turned on for one minute of each hour-long measurement cycle. This time period was found to be sufficient to prevent the growth of a fouling layer on the coil.

4.5 Prototype Laboratory Test

Controlled-environment tests were conducted in a large tank filled with 0.7 N NaCl to mimic the salinity of seawater. The seawater tank at was bubbled at 100 cm^3/min with humidified air drawn from outside of the building. The saline-filled tank was immersed in a controlled-temperature bath held at 20°C, and was allowed to come to equilibrium. The prototype was immersed into the tank and ran a series of zero-oxygen experiments as a diagnostic to determine that the system was functioning properly. Then the stability of the system was determined by running the system over a period of weeks to determine the drift in the measurements over time. The system was run alternately between renewed electrolyte and non-renewed electrolyte cycles. Figure 4.8 shows both types of cycles.

The spread in these data was used to determine the drift associated with the instrument. For example, the data represented in Figure 4.8 are from the completely submersible prototype over a two-day period. The variance associated with the mean integrated value of the aerated traces was ± 2.4%. Note that the integrated values of the submerged prototype are lower than those conducted in room air (see Chapter 3); this is due to a lower O_2 concentration in water. The variance associated with the data could be associated with slight temperature fluctuations as well as atmospheric pressure fluctuations, as the system was not a closed system. For example, the O_2 concentration can fluctuate 3%/°C in seawater based on calculations using the Benson model described in Section 4.7.

The integrated values from a 16-day test are shown in Figure 4.9, and indicate some drift in the apparent O_2 concentration over time. The mean integrated value does not accurately represent the upward trend in the data, and the variance around the mean of ± 2.8% does not represent the drift from an integrated value as low as 108 mol/L digital units to an integrated value as high as ~117 mol/L, a change of over 12% in value from the beginning of the experiment to the end of the experiment. Upon examining the barometric pressure changes from the same time period, a similar trend in the barometric pressure was noted. Additionally, the tank temperature fluctuated more than ± 1°C. These environmental changes can drastically effect dissolved oxygen concentrations. Therefore, it is important to make standard method measurements as well as temperature and pressure measurements.

To confirm the measurements taken by the experimental sensor, reference samples were taken from the saline tank on a regular basis. Samples were removed from the tank by siphoning solution from the tank into numbered glass-stoppered sampling bottles (~125 mL volume). The samples were treated with 1 mL of 3M $MnCl_2 \cdot 4H_2O$ and 1 mL of alkaline NaI solution. The bottles were sealed carefully so air bubbles were not captured within the volume, and shaken vigorously. A brownish precipitate formed and settled to the bottom. The rims of the bottles were filled with water to prevent air introduction into the samples, and the samples were stored at 4°C until analysis. In addition to water samples, the tank temperature and barometric pressure were recorded at the time of sampling and used in the data calculations.

When the samples were analyzed via the modified Winkler method (or Carpenter method) described above, the water in the rim was poured off and the stopper removed. One mL of 5M H_2SO_4 was added to the bottle, the bottle was recapped, and shaken vigorously. The precipitate dissolved, yielding a yellow-brown solution containing free I_2. The solution was titrated with standardized $Na_2S_2O_3 \cdot 5H_2O$ to a pale yellow. One milliliter of starch indicator was added to the sample, and the sample was titrated to a clear endpoint. The standard for this titration is a standard solution of KIO_3 which is treated with the same reagents and titrated using the same procedure as the samples. Blanks are performed by using replicate 1 mL KIO_3 aliquots and determining the difference between titrant volume between aliquots.

The dissolved oxygen content of the samples was calculated using the following formula:

$$DO = \frac{[R - R_{blk}]V_{IO_3} \bullet N_{IO_3} \bullet E}{[R_{std} - R_{blk}][V_b - V_{reg}]} - DO_{reg} \qquad (4.9)$$

where DO is the dissolved oxygen concentration of the sample (mL/L), R is the sample titration volume, R_{blk} is the blank correction factor, R_{std} is the volume required to titrate the standard to the endpoint, V_{IO3} is the volume of KIO_3 standard titrated, V_b is the sample bottle volume (mL), V_{reg} is the volume of sample displaced by reagents (mL), N_{IO3} is the concentration of the KIO_3 standard (equivalents/L), E is a constant (5,598 mL O_2/equivalent), and DO_{reg} is the correction for the oxygen added with reagents, which is defined as 0.018 mL/L by Carpenter.[2] In the case of the method we used, the volume and concentration of standard and reagent volumes were the same, so the formula can be reduced to:

$$DO = \frac{[R - R_{blk}]559.8}{[R_{std} - R_{blk}]V_b - 2} - 0.018 \qquad (4.10)$$

The reference sample dissolved oxygen concentrations were compared to the sensor readings. As explained above, a bias associated with the difference in salt concentration exists between the sensor readings and the reference samples taken from the tank. This bias is associated with the difference in oxygen saturation values for each solution. The oxygen saturation drops as the salt concentration increases, known as the salting-out effect.[6] The saturation value for O_2 in the 0.7N NaCl tank solution ($\sim 2 \bullet 10^{-4}$ mol/L) twice the concentration of O_2 in the 2.4M KCl solution ($\sim 1 \bullet 10^{-4}$ mol/L). The bias is constant over a range of temperature and barometric pressure

---

6 W. Lang, R. Zander; Ind. Eng. Chem. Fundam.; Vol. 25, No. 4, (1986), 775-782.

fluctuations, as shown in the data presented in sections 4.6 and 4.7. Therefore, if the sensor system is in equilibrium with its environment, its dissolved O_2 concentration can be related back to the dissolved O_2 concentration of the bulk, if the bias of the system is known with respect to the bulk.

4.6 Fresh-Water Deployment

The submersible system was deployed two meters below the surface off the dock of the University of Washington Marine Sciences Building into Portage Bay. The deployment lasted for six days, over which time the system ran once per hour. Reference samples were taken daily by lowering a Niskin bottle to the same depth as the measurement system. A Niskin bottle is a bottle with two spring-loaded end-caps. The bottle is dropped into the water with the caps open. Once the bottle reaches a specified depth, a weight, called a messenger, is sent down the line releasing the lines holding end-caps open. The end-caps close, trapping water inside. The samples were collected from the Niskin bottle, pre-treated and measured as discussed in Section 4.5.

The results from the first deployment indicate this is a promising technique (Figure 4.10). The general trend in the integrated value data is matched by the trend in the reference sample data. The fluctuations in the integrated values over a 24 hour period are due to decreased algae photosynthesis during non-daylight hours, causing a decrease in dissolved O_2 concentration, which reaches a minimum before sunrise. The O_2 concentration increases once again during daylight hours as photosynthesis increases. The general downward trend of both data sets is matched by the

atmospheric pressure trends during the same time period. The two data sets were plotted on separate y-axes to overlay the two to illustrate their similar trends. Atmospheric pressure does not greatly affect the oxygen solubility, but if the temperature had increased one degree over the time period of the test, with the well-mixed layer the sensing system was deployed in, the decrease in dissolved oxygen would decrease by 3% per °C. There is still a bias in the data that we could not accurately account for, so the sensor was returned to the laboratory for additional testing to accurately determine the bias.

4.7 Drift Test, Comparison with model concentration

A two-month test was conducted with the sensor immersed in the salt-water tank described in Section 4.5. Tank water samples were taken twice daily and the water temperature and atmospheric pressure were recorded at the same times. Figure 4.11 shows a plot of the sensor and reference sample data collected during this test. The y-axis on the left represents the O_2 concentration measured in the sensor, and the secondary y-axis on the right represents the O_2 concentration of the water in the tank as measured by the reference method. After calibration of the sensor response to the reference samples, one should be able to correlate the sensor response O_2 concentration to the dissolved O_2 concentration of the matrix in equilibrium with the sensor. One way to do this would be to calculate the average ratio of the reference method value to the sensor value. This value could be used as a constant multiplier to convert the sensor readings to bulk matrix O_2 concentrations. Figure 4.12 shows the

ratio values for the samples and the corresponding sensor reading for that time. The average of the ratio is 2.48 ± 0.12 (± 4.9%). The amount of deviation is larger than we would like for a 'constant'. In addition, unexplained outliers in both the sensor and sample data sets can figure prominently in the average. Two known changes occurred during the experiment that could cause a shift in the ratio. First, the equilibration coil was changed in the middle of the experiment. Second, the tank temperature changed drastically over the course of the experiment, due to a chiller failure, and the sensor system may not have been at equilibrium with the tank at that point.

In addition to comparing the sensor and reference values, the reference values were compared to a model of oxygen saturation. The Benson and Krause model is commonly used to calculate oxygen solubilities in seawater. This model approximates the dissolved O_2 concentration (C_O) by the following equation:

$$\ln C_O^* = A_0 + A_1 T_s + A_2 T_s^2 + A_3 T_s^2 + A_3 T_s^3 + A_4 T_s^4 + A_5 T_s^5 + S(B_0 + B_1 T_s + B_2 T_s^2 + B_3 T_s^3) + C_0 S^2 \quad (4.11)$$

where C_O^* is the approximate O_2 concentration, T_s is the scaled temperature calculated by equation 4.12, and S is the salinity of the solution. The solubility coefficients A_n, B_n, and C_n are defined over a range of temperatures and salinities.[7] The scaled temperature equation scales the temperature reading (t) to 0°C and 25°C as follows:

$$T_s = \ln\left[\frac{(298.15 - t)}{(273.15 + t)}\right] \quad (4.12)$$

7 H.E. Garcia, L.I. Gordon; Limnol. Oceanogr., 37(6), (1992), 1307-1312.

Figure 4.13 compares the theoretical Benson values to the actual titrated samples. The Benson model fits the samples very well. If anything, the samples are slightly oversaturated according to the Benson model, which is possible because the tank was bubbled. Evaporation was negligible because the tank was closed and the bubbled air was humidified.

Similarly, the sensor values were compared to the Benson model and also to the predicted O_2 concentration in KCl electrolyte based on the Bunsen coefficient[8], and to the Sherwood model.[9] The Bunsen coefficient is the oxygen solubility of pure O_2 in a given concentration salt solution at standard temperature and pressure. Using the data presented by Lang and Zander[8], the Bunsen coefficient for 2.4 M KCl was interpolated to:

$$\alpha = 0.01275 mLO_2/(mL \cdot atm). \tag{4.13}$$

The $[O_2]$ in air-saturated 2.4M KCl is obtained by converting to mol O_2/L KCl and multiplying by the O_2 content in air (21%), which yields a saturation value of 1.195 x 10^{-4} mol O_2/L. The Sherwood model predicts O_2 concentration in hypersaline water by the equation:

$$\begin{aligned} \ln C_O^* &= a_0 + \frac{a_1}{T} + a_2 \ln T + a_3 T + a_4 T^2 \\ &+ S(a_5 + a_6 T + a_7 T^2) + a_8 S^2 \end{aligned}, \tag{4.14}$$

where T is the temperature, S the salinity, and C_O^* is the estimated oxygen concentration. The solubility coefficients a_0 through a_8 are given by Sherwood et al.

---

8 W. Lang, R. Zander; Ind. Eng. Chem. Fundam.; Vol. 25, No. 4, (1986), 775-782.
9 J.E. Sherwood, F. Stagnitti, M.J. Kokkinn, Limnol. Oceanogr., 36(2), (1991), 235-250.

Figure 4.14 shows sensor data compared to the three models. The sensor data are presented in blue, the Sherwood model prediction is in red, the Benson model in green, and the Bunsen model in black. By far, the Sherwood model best estimates the measured oxygen concentration in the sensor electrolyte. The comparison with the Sherwood model suggests that the electrolyte inside of the sensor system is under-saturated, which would indicate that the electrolyte was not at equilibrium with the tank. The ratio of the modeled Benson numbers for the samples to the modeled Sherwood numbers for the sensor was calculated. The average ratio was 2.11±0.014 for the model over the course of the experiment. This number is lower than the ratio of 2.48 ± 0.12 that was determined experimentally.

4.8 Conclusions

We successfully constructed, tested, deployed, and modeled a prototypical submersible device based upon the two-stage electrochemical oxygen sensor presented in Chapter 3. The sensor worked well a controlled, artificial environment as well as in a biofouling natural environment. Additionally, we were able to approximate the oxygen concentrations both in the external conditions and within the sensor. Under equilibrium, the apparent oxygen concentration is ~2.5 times less within the sensor than in the seawater matrix that surrounds the system, but this ratio will have to be determined for individual conditions to maximize the accuracy of the oxygen numbers reported by the sensing system. The drifts in the sensor are still not understood well enough to confidently deploy the sensing system for a long time.

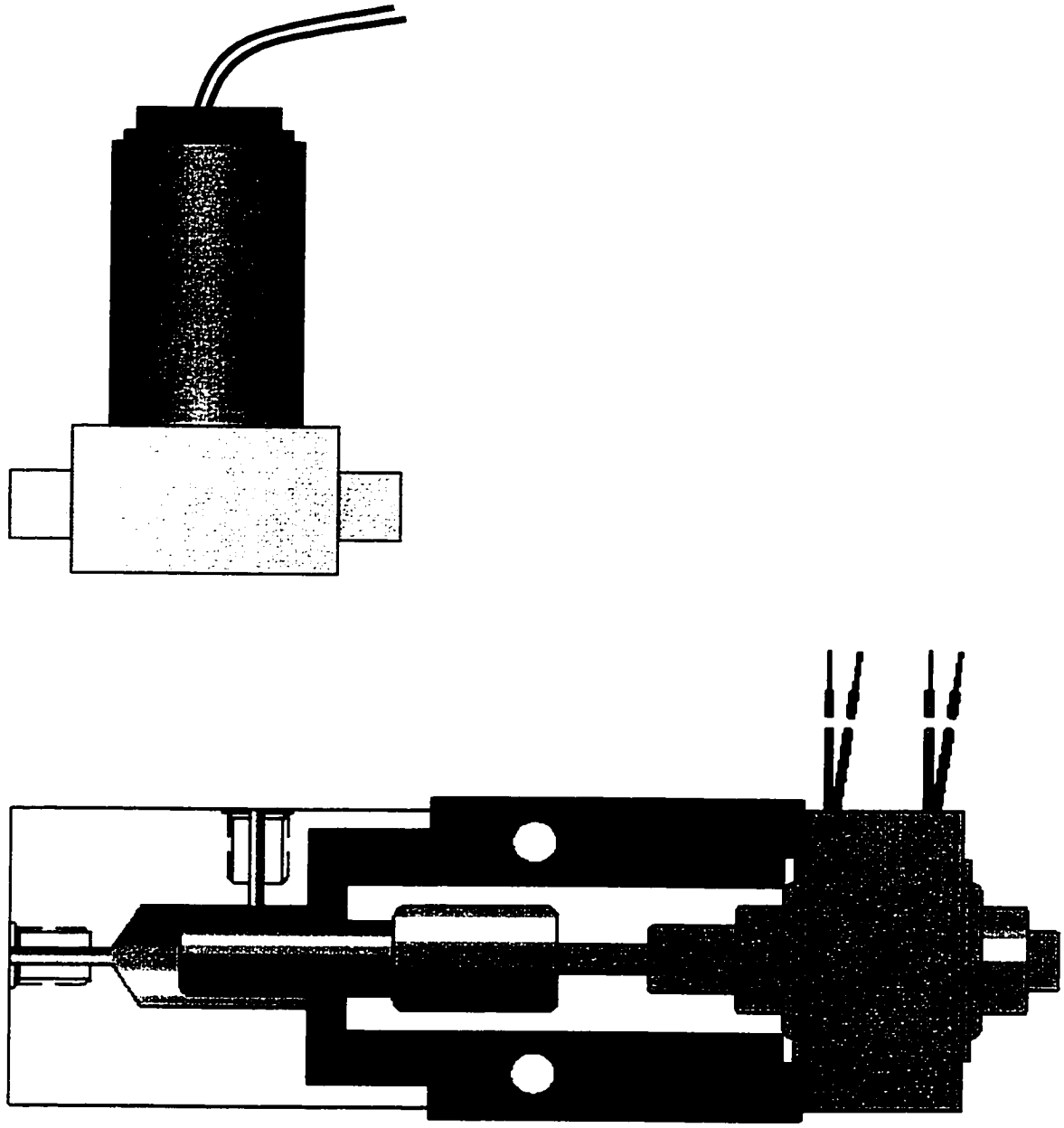

Figure 4.1 - Schematic of Lee Co. solenoid minipump, with ¼-28 flat-bottom PEEK fittings. The entire unit is ~2" high, 1 ½" wide.

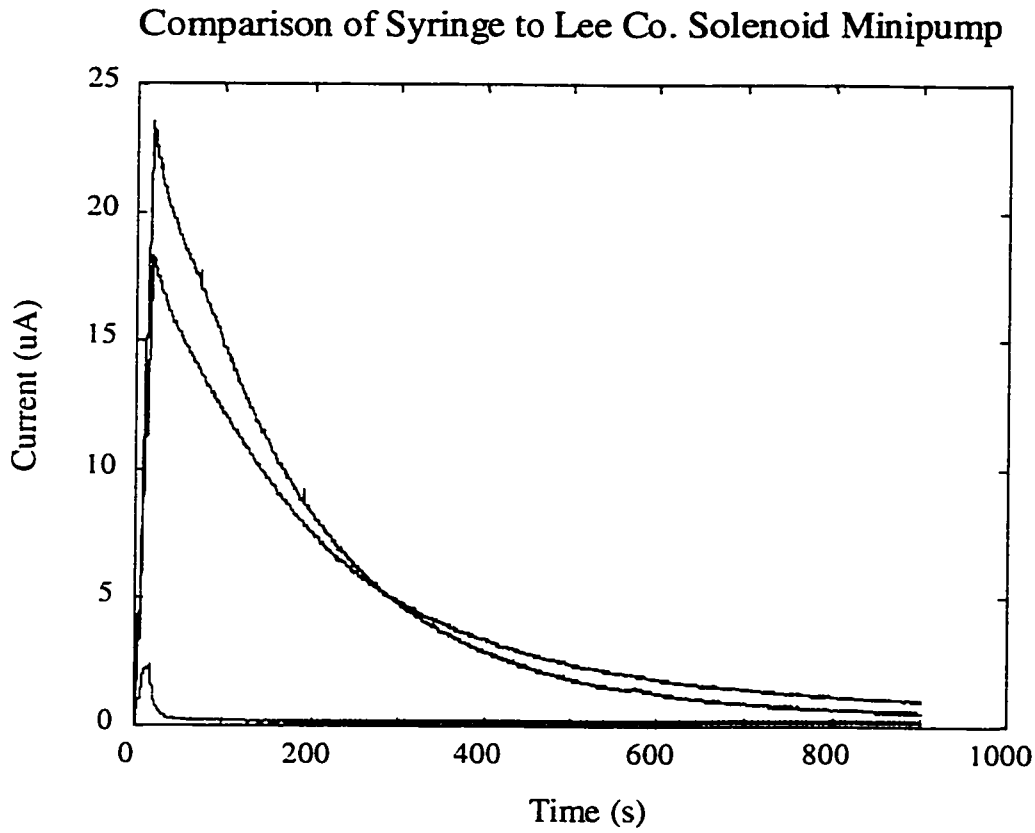

Figure 4.2 - A comparison of the mean oxygenated traces for the prototypes with syringe and solenoid pumps. The syringe pump (blue), has a higher average amplitude than the solenoid pump (green). The mean zero oxygen trace from the syringe test is in red.

Figure 4.3 - Submersible prototype O_2 sensor without battery or operating electronics.

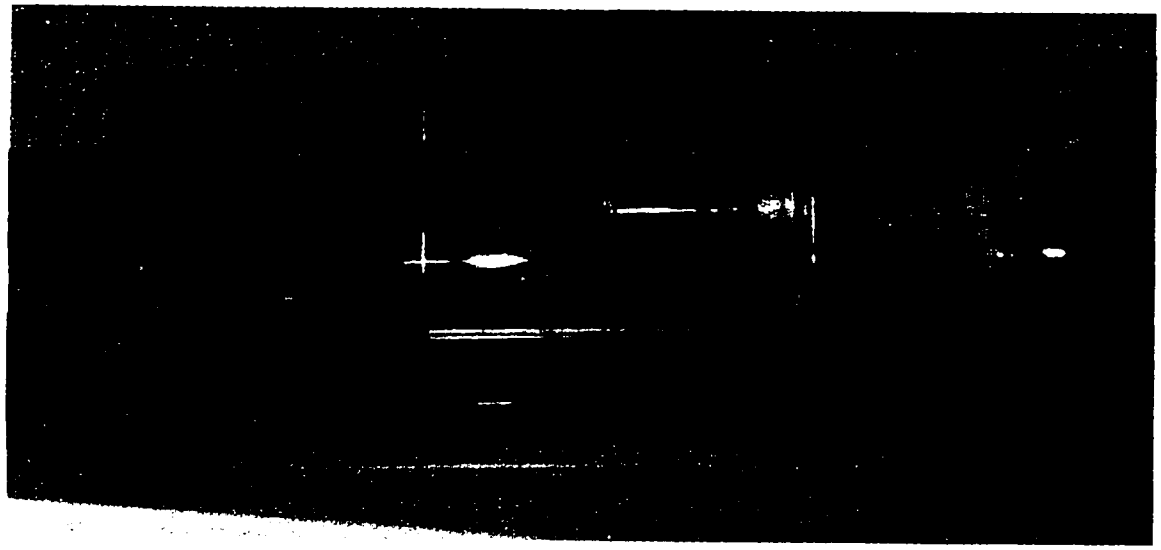

Figure 4.4 - Plexiglass pressure case housing cell, conditioning electronics, and pump motor with mechanical and fluidics feed-throughs.

Figure 4.5 – Completed submersible prototype electronics and battery housing.

Figure 4.6 - Antifouling Hg lamp with the silicone equilibration tube wrapped around it.

Figure 4.7 - Complete submersible prototype system

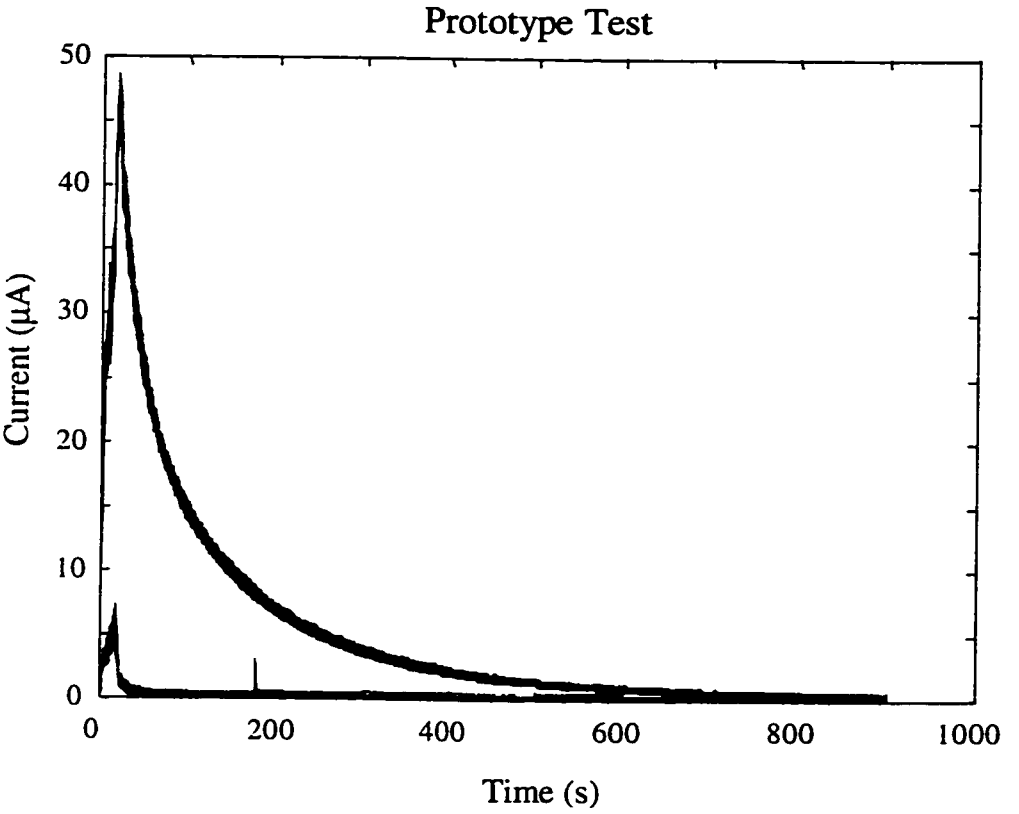

Figure 4.8 - Prototype System Data – Blue traces from the oxygenated runs (30 traces, renewed electrolyte), red traces from the zero runs (73 traces, electrolyte not renewed).

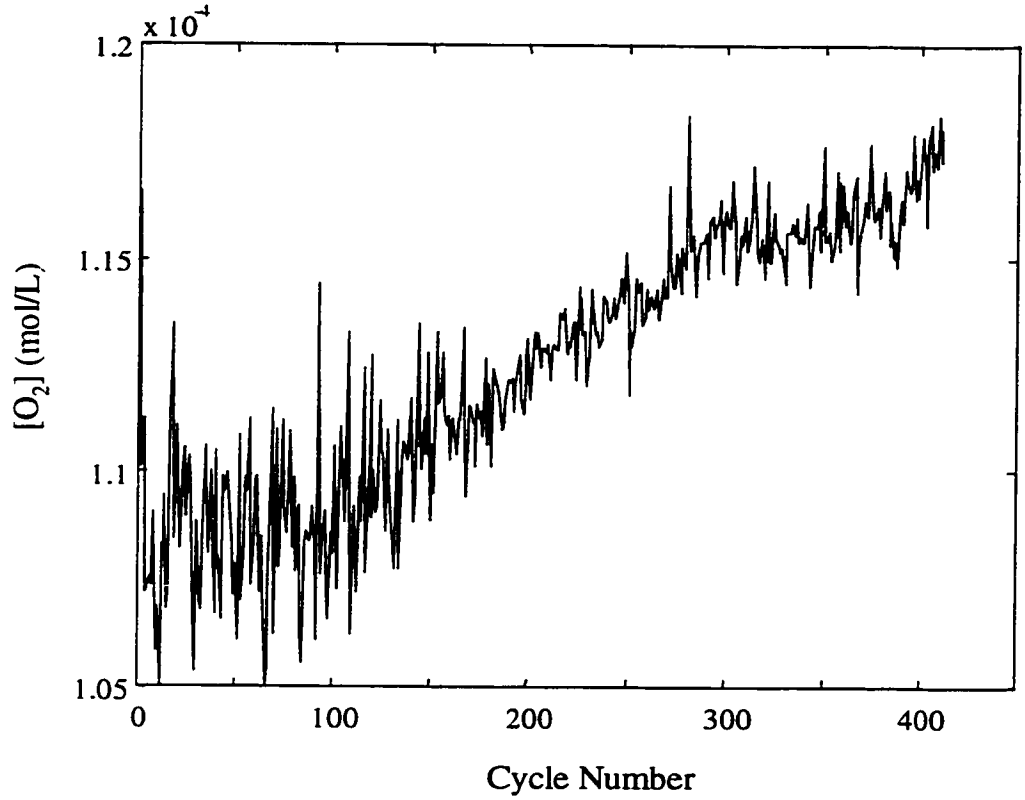

Figure 4.9 - Integrated values from a 16 day test in the saline tank. The drift associated with these values is 2.8% around the mean value.

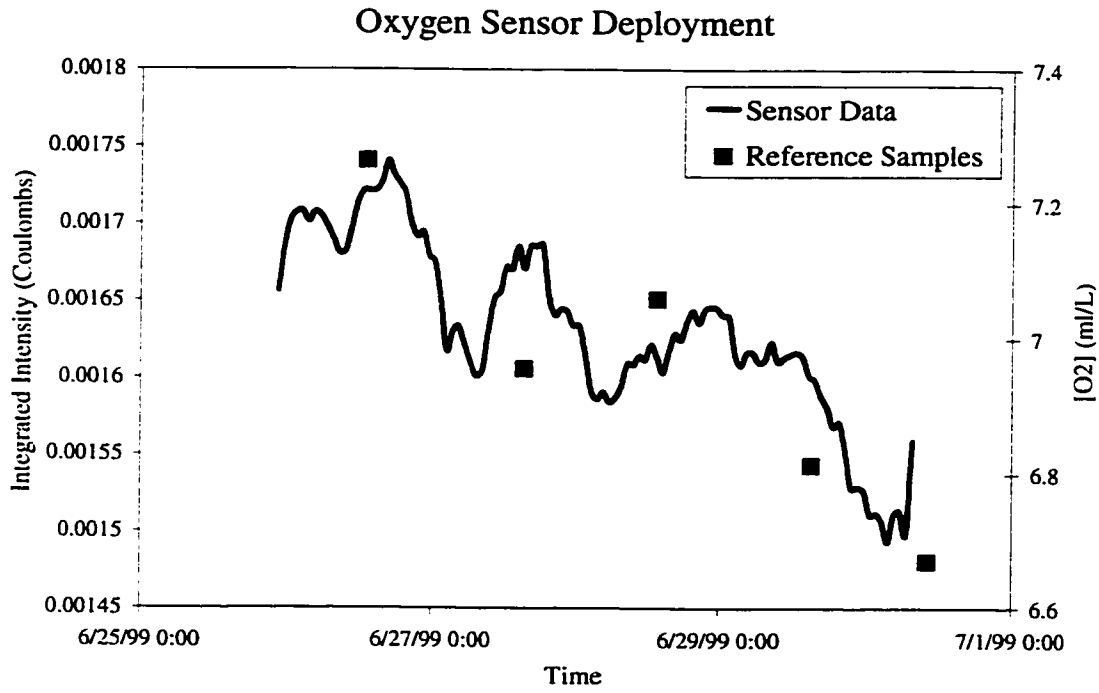

Figure 4.10 - Integrated values from the lake deployment (blue line) compared to the Winkler titration values (pink squares). Note the different y-axes, but that the trend is the same.

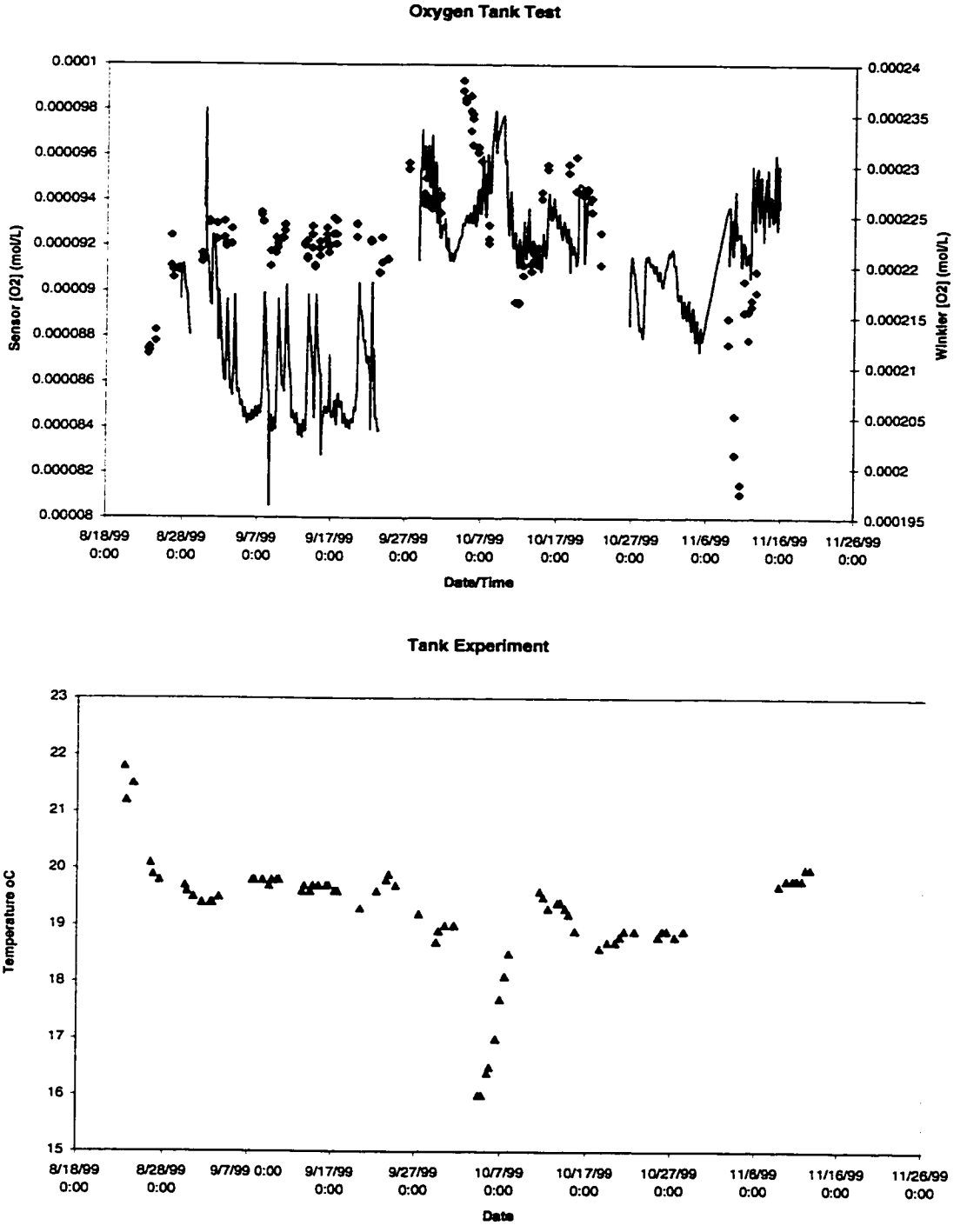

Figure 4.11 – The top plot shows data from extended tank experiment. Sensor data (blue) and reference samples (red). The bottom plot show the tank temperature conditions during the experiment.

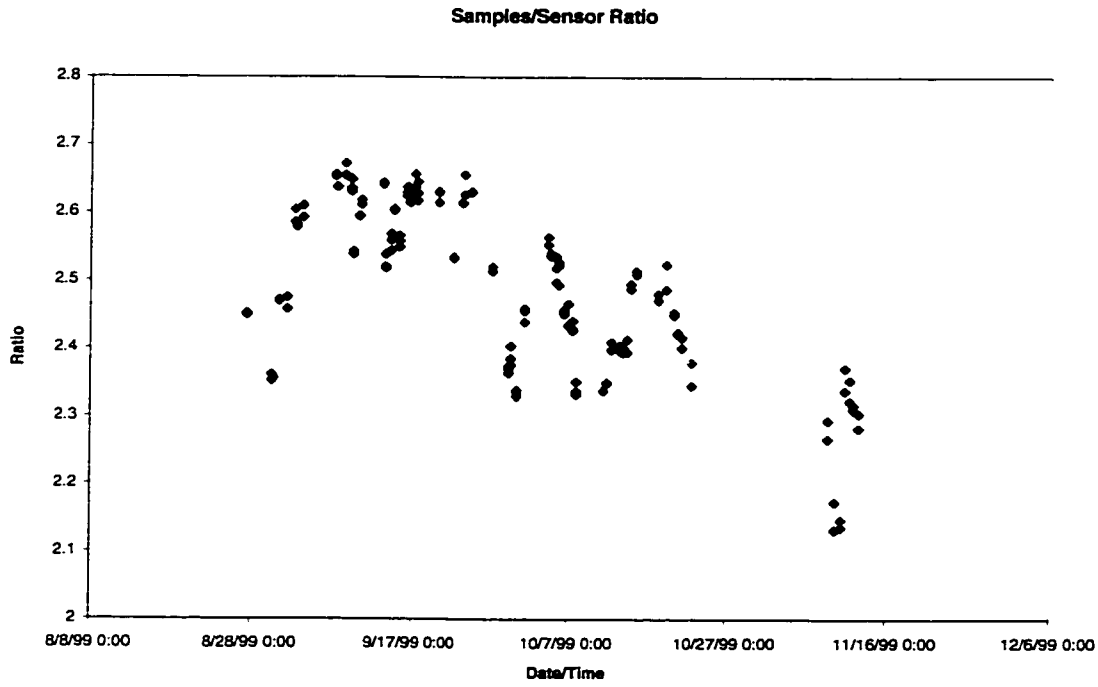

Figure 4.12 - Plot of Samples [O2] to Sensor[O2] ratio

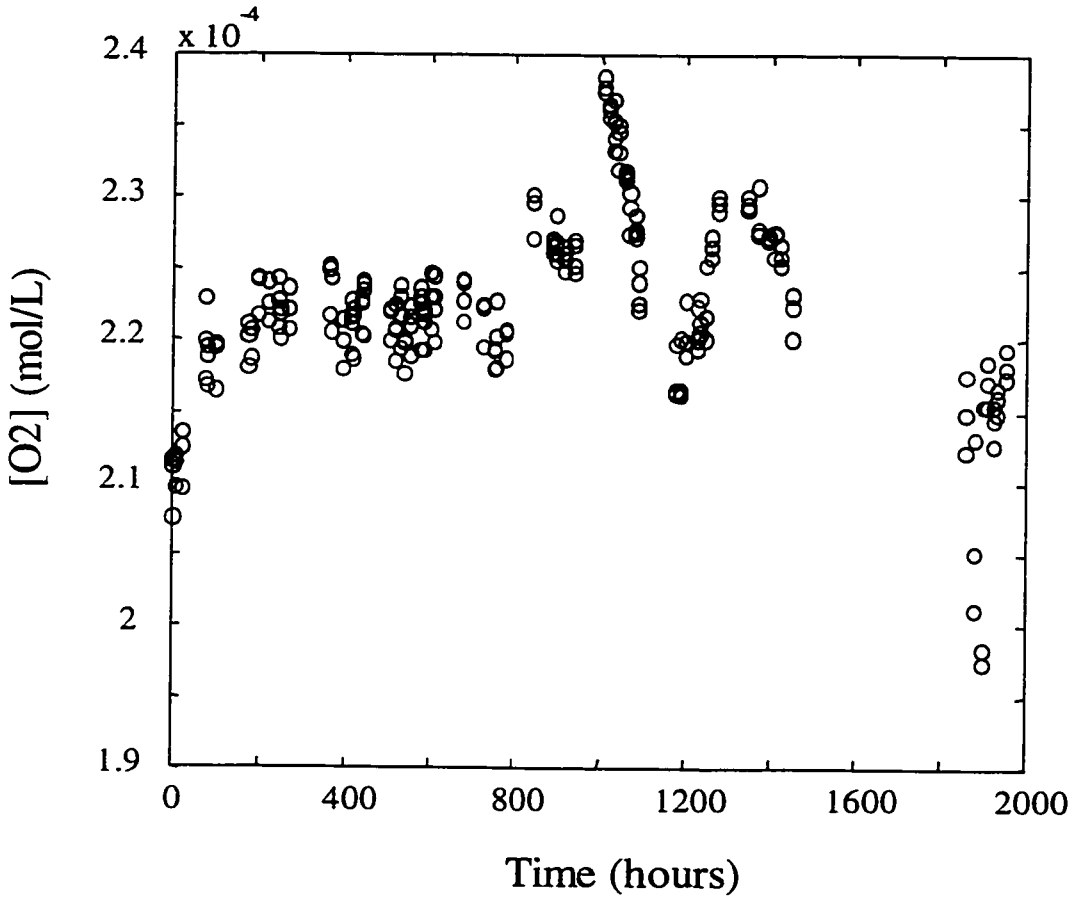

Figure 4.13 - Tank samples (blue) compared to the Benson model for O_2 concentration (red)

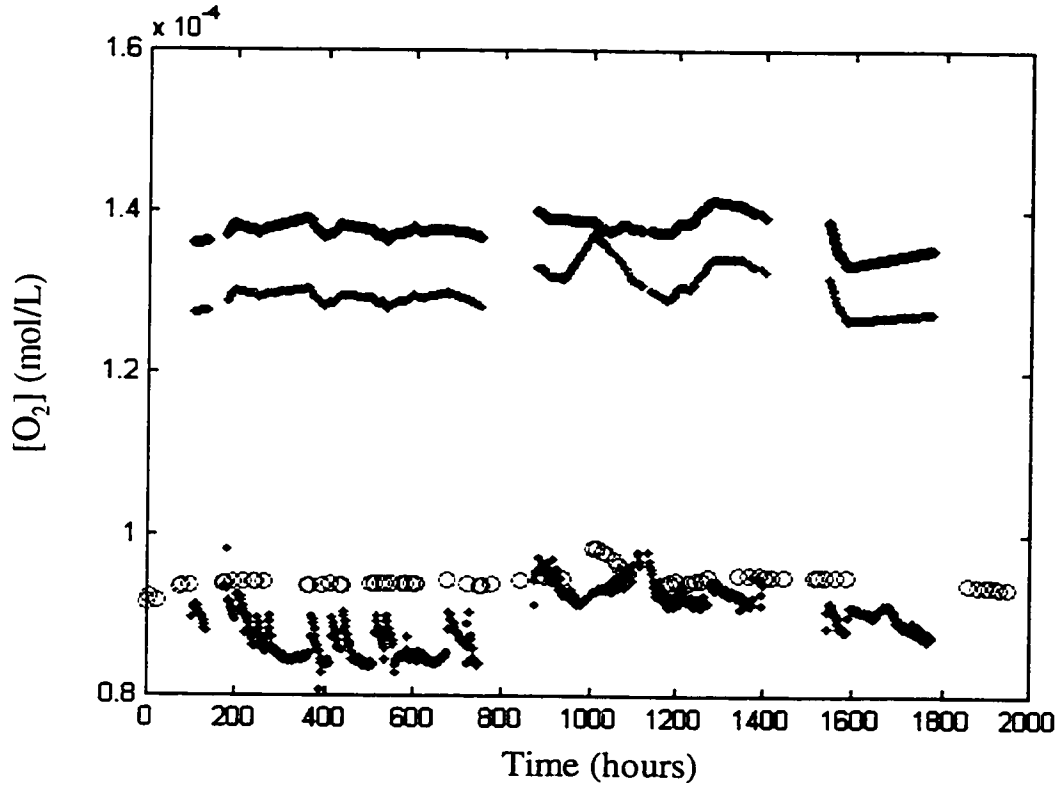

Figure 4.14 - Comparison of the real sensor data (blue) to three different model calculations. Bunsen (black), Benson (green) and Sherwood(red).

Chapter 5 - Liquid Core Waveguide Sensing Systems

5.1 Introduction

This chapter describes a liquid core waveguide (LCW) chemical sensing system (Figure 5.1). The waveguide acts as a long-path UV/Vis absorbance cell where the liquid core is the reagent as well as the sampling interface. The cladding can act as a semi-permeable membrane. The core material can be renewed between measurements. The systems described here were used to detect HCl vapor and CO_2 in a gas mixture.

The Burgess research group has recently completed a lot of work involving renewable-reagent chemical sensing systems.[1,2,3] The most recognized of these systems is the FlowProbe™. The rationale behind renewable-reagent chemical sensors is to eliminate degradation that can occur over time in sensors employing immobilized reagent chemistries. The FlowProbe™ incorporates membrane sampling, reagent flow, and multi-channel chemical detection in a miniaturized format. The detection mechanism of the probe is based upon absorption of light by a product that is formed from the analyte(s) passing through the sampling membrane and reacting with a reagent stream. The sensing medium (reagent) is regenerated *in situ* by flushing the reacted product out of the sensor head and replacing it with fresh reagent solution for each analysis. A wide range of reagent chemistries can be

---

1 R. Berman, G. Christian, L. Burgess; Anal. Chem., (1990), 2066-2071.
2 Z. Lin, L. Burgess; Anal. Chem., (1994)2544-2551.
3 L.K. Moore, D.J. Veltkamp, J.L. Cortina, Z. Lin, L.W. Burgess; Sensors & Actuators B, Vol. 38-39, (1997), 130-135.

employed for monitoring different analytes with this type sensing system. However, the fixed pathlength of the FlowProbe can limit the sensitivity of the sensing system.

The liquid core waveguide is another renewable reagent sensing system developed by Burgess and co-workers (Figure 5.1). This system has variable pathlength, unlike the FlowProbe™ mentioned above. Liquid core waveguides, fiber optics with liquid cores, operate under the same principles as solid-core optical fibers. Fiber optics propagate light by total internal reflection (Figure 5.2). Total reflection of light occurs when light traveling through a medium with refractive index n_1 meets an interface of lower refractive index n_2 at an angle greater than the critical angle (ϕ_c), defined as:

$$\sin \phi_c = \frac{n_2}{n_1}. \qquad (5.1)$$

This means that in the case of the liquid core waveguide, the liquid core material must have a higher refractive index than the surrounding cladding, presenting unique challenges for the use of these devices for chemical sensing.

During the course of waveguide optimization, the numerical aperture (NA) of a liquid core waveguide is an important parameter determining how much light the waveguide can accept. The numerical aperture is defined as:

$$NA = n_0 \sin \theta_a = \sqrt{(n_1^2 - n_2^2)} \qquad (5.2)$$

where θ_a is the acceptance angle of the fiber, or the maximum angle at which light launched into the fiber can propagate. The terms n_0, n_1, n_2 are the refractive indices of the outside medium (usually air), core, and cladding materials, respectively.

The liquid core waveguide, when used as a long-path absorbance cell, can be subject to a phenomenon known as anomalous dispersion. Material dispersion is the change in refractive index of a material with increasing wavelength. Anomalous dispersion is defined as 'an anomaly in the normal variation of refractive index versus wavelength, commonly observed near an absorption band'.[4] Refractive index is proportional to the real part of the complex dielectric, and absorbance is proportional to the imaginary part of the complex dielectric, so in the presence of a strong absorbance band, the refractive index will shift anomalously low at wavelengths less than the center of the band, and anomalously high at wavelengths greater that the center wavelength of the band (Figure 5.3).

The liquid core waveguide consists of a tube acting as the cladding of the waveguide, and a liquid material inside the tube acting as the waveguide core. The first liquid core waveguides were hollow quartz fibers (R.I. = 1.458) filled with tetrachloroethylene (R.I. = 1.505) reported by Stone.[5,6] Later, liquid core fibers were applied as detector cells in spectroscopic measurements.[7,8,9] The use of waveguiding techniques is very effective for elongating the optical pathlength through a sample. In the case of an absorptive measurement, Beer's Law states that the absorbance of a sample is related to the sample's concentration (c) and the pathlength (b) by the sample's molar absorptivity (ε), or

---

4 Harcourt Academic Press Dictionary of Science and Technology (2001).
5 J. Stone, IEEE J. of Quantum Electronics, QE-8, (1972), 386-388.
6 J. Stone, Appl. Phys. Lett., Vol. 20, (1972), 239-240.
7 L. Wei, K. Fujiwara, K. Fuwa, Anal. Chem., Vol. 55, (1983), 951-955.
8 P.K. Dasgupta, Anal. Chem., Vol. 56, (1984), 1401-1403.
9 K. Fuwa, W. Lei, K. Fujiwara, Anal. Chem., Vol. 56, (1984), 1640-1644.

$$A = \varepsilon \cdot b \cdot c \qquad (5.3)$$

If b, is increased, the concentration detection limit will decrease.

More recently, liquid core waveguide cells constructed from polymer claddings have been reported. In 1990, Tsunoda and co-workers reported a capillary waveguide cell using FEP Teflon.[10] The FEP material has a refractive index of 1.338, so the core material must have a higher refractive index to meet the conditions for total internal reflection. This means that aqueous core materials would require a refractive index modifier (i.e. ethylene glycol) to raise the refractive index of the core above that of the cladding. Modification of the liquid core could negatively affect the chemistry of the core if the core is also used as the reagent for a chemical measurement.

Development of the liquid core waveguide in the Burgess group demonstrated the applicability of these waveguides as sensors in which the polymer cladding also acted as a semi-permeable membrane for analyte transport.[11] This work also demonstrated the use of Teflon AF™ as a cladding material cast on the inside of porous polypropylene. Teflon AF™ is a unique material in that it has a refractive index less than that of water, allowing for the use of unmodified aqueous systems as core materials. Additionally, Teflon AF™ has extremely rapid gas permeation rates for small molecules such as O_2, CO_2 and small hydrocarbons. Recently, Teflon AF-2400 tubing (n = 1.29) has become commercially available. Several papers have been

10 K. Tsunoda, A. Nomura, J. Yamada, S. Nishi, Appl. Spec., Vol. 44, (1990), 163.
11 K. Hong, L.W. Burgess, SPIE, Vol. 2293, (1994), 71-79.

published describing its use as a long-path absorbance cell and as a method for enhancing Raman spectroscopy.[12,13,14]

5.2 – Preliminary Waveguide System

Some initial work has been completed using liquid core waveguides. Several LCWs have been assembled using various polymer materials. The geometry of these sensors is similar to that shown in Figure 5.1. The fiber optics used to couple the light to and from the LCW were 200/220/245 glass on glass polyimide jacketed fibers (FiberGuide). The waveguide material was 26 gauge (~ 750 μm I.D.) PTFE (n = 1.35) tubing. The source and collection fibers were inserted directly into the PTFE tube through low-pressure tee connectors (Upchurch Scientific). Dimethyl sulfoxide (DMSO) was the initial core material (n = 1.48). The refractive indices of the core materials were determined using the Milton-Roy ABBE-3L refractometer. The core material was pumped through the waveguide manually with a syringe.

The waveguide was illuminated using a blue LED light source pulsed at 10kHz with a 1% duty cycle with 2 A of current.[15] Pulsing the LED increases the emission from the InGaN component of the diode, increasing the emission at 380nm. This near-UV emission was ideal for analysis of p-nitroaniline with its absorbance band peaking at 383nm. Figure 5.4 shows the driving circuit for the LED and Figure 5.5 shows the pulsed blue LED spectrum. The transmitted intensity was detected on an

---

12 R.D. Waterbury, W. Yao, R.H. Byrne, Anal. Chim. Acta., Vol. 357, (1997), 99-102.
13 R. Altkorn, I. Koev, R.P. Van Duyne, M. Litorja, Applied Optics, Vol. 36, (1997), 8992.
14 B.J. Marquardt, P.G. Vahey, R.E. Synovec, L.W. Burgess; Anal. Chem., *71*(21), (1999), 4808-4814.
15 T. Araki, H. Misawa; Rev. Sci. Instrum., Vol. 66, No. 12, (1995), 5469-5472.

American Holographic MD5 CL dual-input diode array spectrometer. The spectrometer imaged the transmitted waveguide intensity in the 340-630nm range on one input while imaging the source on the other input simultaneously. A measurable, but not optimal signal was obtained, indicating low light transmission due to inefficient illumination/detection and/or the formation of bubbles within the waveguide (Figure 5.6). A 50:50 ethylene glycol:water mixture was also tried as a core material resulting, in poor light transmission as well.

5.3 – HCl vapor detection

A subsequent liquid core waveguide was assembled in a similar geometry using Teflon AF-2400 tubing (n = 1.29) with an outer diameter of 0.038" (~1 mm) and an internal diameter of 0.035" (~0.88 mm) (Biogeneral). The input/ouput fibers were 800 μm core fibers designed to match the waveguide I.D. as closely as possible for efficient coupling of light. Initially this waveguide was filled with water as the core material. For a larger bandwith source, a Hg source (Zeiss) was used and the waveguide output was imaged on a dual-channel diode array spectrophotometer (American Holographic). The fiber and fluid connections to the waveguide were made through a jar lid so concentrated HCl could be injected into the headspace of the sealed jar. This assembly had good light throughput (Figure 5.7).

For detecting HCl acid vapor, I chose bromthymol blue, an acid/base indicator with a color change near neutral. Bromthymol blue (BTB) changes from blue to yellow in the presence of acid between pH = 6.0 and 7.5. The base form of BTB

absorbs at λ_{max} 615nm, and the acid form absorbs at λ_{max} 392 nm. Due to the long pathlength of the waveguide (~20 cm), and the high molar absorptivity (46,000/(cm M) for the basic form at its λ_{max}) of the indicator, the concentration needs to be low. The first concentration tried was 2.1 x 10^{-6} M. The core solution was also weakly buffered to pH 7.7 to keep the BTB in its basic form until exposure to HCl. The core solution was injected into the waveguide, and 30μL of concentrated HCl was injected into the headspace of the 1-liter jar while spectra were collected continuously. The core material was regenerated after 200 s. Figure 5.8 shows the results of this experiment, and Figure 5.9 shows the change in absorbance of the base form. Note that the absorbance is still relatively large (larger than A = 1), and the absorbance spectra also contain a lot of light-source structure.

5.4 – LCW Detection of CO_2

We constructed a waveguide system for CO_2 detection utilizing the same core reagent chemistry as the HCl waveguide system. This system used the Equitech spectrometer's xenon flash lamp (Figure 5.10) and CCD detector for illumination and detection via 400 μm core UV fibers. The xenon lamp was chosen for its broad, intense emission from 200 nm to 800 nm, making it a good diagnostic of the waveguide transmission characteristics. The CCD detection provided for better wavelength resolution and greater sensitivity over the American Holographic. The initial waveguide used was Teflon™ AF-2400 tubing (82 cm long, 50 μm I.D., 400 μm O.D.). This tube was inserted in an 1/8" stainless steel tube for gas flow around

the outside of the waveguide (Figure 5.11). The waveguide was connected on each end to a waveguide sampling cell (Figure 5.12). The cells provided a sealed flow channel for flushing, with a quartz window for coupling light in and out of the waveguide. The incident light was collimated and focused into the waveguide with a microcope objective, and the transmitted light was collected with similar optics. Gas flow was metered and mixed with a rotometer. Fluids were coupled into the waveguide through the cells mentioned above, standard 1/16" O.D. tubing and syringes.

The core reagent material was 2 μmol/L BTB buffered with pH=7.6 phosphate buffer so the predominant species in the core was the base form of the indicator. CO_2 rapidly permeates the Teflon™ AF tubing walls into the core solution. The CO_2 dissolves into the core, where it reacts with water to form carbonic acid and its dissociation products. The base form of the bromthymol blue indicator accepts a proton in the acidic solution changing color. The degree of color change indicates the CO_2 concentration. DeGrandpre and co-workers have shown that the pCO_2 can be for solved explicitly using the carbonic acid and indicator equilibria.[16]

The preliminary experiments compared the change in the BTB base indicator with CO_2 concentration within the gas mixture. The LCW core was filled with water while the gas flow cell was flushed with N_2. The core was filled with reagent and the gas mixture was changed. Figure 5.13 shows the change in absorbance of the blue basic-form of BTB when the waveguide was exposed to a CO_2:N_2 mixture (100

16 M.D. DeGrandpre, M.M. Baehr, T.R. Hammar; Anal. Chem., Vol. 71, (1999), 1152-1159.

mL/min each). In addition, cycling studies were done by maintaining a continuous flow of N_2 at 100 mL/min through the gas flow chamber, and turning on the CO_2 flow at 100 mL/min after the waveguide had been flushed with fresh reagent. Figure 5.14 shows a plot of the base-form BTB absorbance band over the course of the experiment. The absorbance increases when the reagent is renewed in the LCW core, then it drops off dramatically when CO_2 is introduced into the gas mixture at 100 mL/min.

A similar waveguide was constructed using thick-wall Teflon™ AF-2400 tubing (Biogeneral). The new waveguide was 80 cm in length, 100 μm I.D., and 1 mm O.D. The new tubing was made to stricter tolerances to guide light more efficiently. The new waveguide was incorporated into the gas flow cell in place of the LCW mentioned above. The same permeation studies with concentration were conducted to determine the permeation rate for the thick-walled material. Figure 5.15 shows the decrease in absorbance of the base-form of the indicator, similar to Figure 5.13. The sharp decrease occurs about 20 seconds later with the thick-wall tube. Figure 5.16 compares these decreases at the λ_{max} for the basic form of the indicator (620 nm).

The waveguide system was far from optimal at this point. The transmitted intensity through the waveguide dropped off significantly below ~400 nm, preventing the collection of accurate data for the acid form of the indicator (λ_{max} = 392nm). However, we were able to show a significant change in signal between a nitrogen gas flow and a CO_2 gas flow, indicating the possibility for sensitive CO_2 detection. With a

waveguide optimized for transmission from the near-UV to ~800nm, the change in the second absorbance band of the indicator can be used in the data analysis.

5.5 – Waveguide Optimization

The waveguide system was converted to continuous flow by connecting an HPLC pump to the system for core regeneration, and an injection valve for the injection of samples or additional reagents into the sample stream. Formation of bubbles at the optical interfaces is prevented by putting the system under continuous flow.

To decrease attenuation in the near-UV by optical components, the microscope objectives were replaced with fused silica f/2 singlet lenses. In addition, the quartz windows in the waveguide sampling cell were replaced with sapphire windows. Additionally, the waveguide was shortened to minimize scattering losses. Teflon™ AF has a large number of 'microvoids' that can act as scattering centers. The attenuation at shorter wavelengths (compared to the xenon lamp spectrum shown in Figure 5.10) is attributed Rayleigh scattering at the core-cladding interface, which increases by $1/\lambda^4$. Decreasing the waveguide length to 42 cm compared to the 80 cm waveguide described above increased the transmitted intensity markedly due to fewer scattering centers (Figure 5.17). The optimal waveguide length was determined to be 20 cm or less for maximum transmission with a 250 ms integration.

In addition to reducing the overall waveguide length, other means can be taken to optimize the transmitted intensity through the waveguide by removing excess gases.

One such mean is to flush the waveguide out with a small aliquot of isopropanol to remove any small bubbles that accumulate on the inside walls. Another means of removing excess gases from the waveguide is to evacuate the gas flow cell around the waveguide, which we have shown can decrease the attenuation through a water-core Teflon™ AF-2400 clad waveguide (Figure 5.18). The vacuum was applied after the first few scans. The scans were referenced to the first scan and the change in absorbance calculated. The data show a decrease in absorbance (an increase in transmission) through the waveguide, especially at longer wavelengths. This is consistent with the reduction of scatterers such as bubbles.

Repeated injections of isopropanol were conducted to determine if the injections were reproducible, and weather or not evacuating the gas flow tube helped this reproducibility. The isopropanol injections appeared to fluctuate with or without evacuation of the gas flow cell. The fluctuations were likely due to the pump.

Studies were conducted to determine the long-term stability of the flow system. The transmitted intensity through the waveguide showed periodic fluctuations that probably were caused by changes in the syringe pump's pressure readings, because their period and amplitude varied with the pump speed (Figure 5.19). A pulse dampener was placed inline between the pump and the injection valve to remove effect of pump pressure fluctuations, making the fluctuations undetectable in the waveguide transmission.

The final optimization to the system was masking the illumination end of the waveguide with an opaque, scattering epoxy coating to eliminate transmission through

the cladding. The waveguide was short enough to support some propagation of the incident light from the pulsed xenon source through the cladding which was collected by the collection optics and visible to the operator. Masking the illumination end of the waveguide eliminated this propagation. The isopropanol injections were repeated with the optimized system, showing improved reproducibility.

5.6 – Refractive index studies

We conducted studies on the transmission effects of injecting solutions with different refractive indices and/or absorbance from the core solution. Besides isopropanol, ethylene glycol/water mixtures and sucrose solutions were injected into the waveguide to observe the transmission effects. The ethylene glycol/water mixtures ranged from 5% to 90% with refractive indices ranging from ~1.34 to ~1.43. The sucrose solutions ranged from 5% to 45% with refractive indices ranging from 1.34 to 1.41. The numerical aperture of the LCW with the above refractive indices will range from 0.32 to 0.62.

The data showed that as an injected plug of a higher refractive index moves into the waveguide, the absorbance rapidly increases and then decreases sharply as the plug moves into the waveguide. The same transient increase is seen as the plug exits the waveguide. Both sharp transitions are likely due to the change in numerical aperture of the waveguide. Figure 5.20 demonstrates this for a 38% sucrose solution. Note that the absorbance is negative for the time during which the sucrose solution is

traveling completely through the waveguide. This increase in transmitted intensity is due to the increased numerical aperture of the waveguide.

5.7 – CO_2 detection with optimized waveguide

New CO_2 detection experiments were repeated with the optimized continuous-flow waveguide system by injecting bromthymol blue into the water carrier. First, the baseline response of the waveguide was determined by injecting basic bromthymol blue into the waveguide after equilibration with nitrogen. Then the waveguide's response to CO_2 in the gas flow cell was observed, followed by different CO_2/N_2 mixtures.

Figure 5.21 shows a comparison of the absorption spectra of BTB in the waveguide when N_2 or CO_2 were passed through the flow cell. Note that the acid form of the indicator's absorbance (λ_{max} = 420 nm) increases in the presence of CO_2 while the base form's absorbance decreases. The data at the shorter wavelengths are noisier due to the lower transmitted intensities at these wavelengths caused by greater scattering by microvoids. Figure 5.22 shows the base form's absorption spectrum for different CO_2/N_2 gas mixtures. Each mixture had the same total flow rate, and the core flow rate and bromthymol blue injection volume also remained constant. As expected, the absorbance of the base form of the indicator decreased with increasing CO_2 in the gas mixture.

5.8 – LCW as a long-path absorbance detector

The continuous flow liquid core waveguide has also been applied as a continuous flow, long-path absorbance detector. Chapter 6 will present its application for the detection of extracted polar organic molecules utilizing both UV/Vis spectroscopy and Raman spectroscopy for detection of two extractants. The sensing system is the same configuration as the system mentioned above, except that the waveguide cladding is not used as the sampling mechanism. When the waveguide cladding does not have to serve as the semi-permeable membrane, more options are available for waveguide cladding materials, including specially doped silica materials.

5.9 – Conclusions

This chapter has described the further development of a liquid core waveguide utilizing the newly available Teflon™ AF-2400 tubing. We demonstrated detection of CO_2 in a gas mixture with both the gas and waveguide under flowing conditions with a small transient reagent injection to detect the analyte. By utilizing injections of reagent rather than continuous reagent flow the system can be referenced after each injection allowing for better correction of drift. The system reported here, based upon the data presented would have a CO_2 detection limit of 1.5% CO_2 with little interference from other gases due to the reagent chemistry employed.

We also optimized the Teflon AF waveguide transmission characteristics by varying the waveguide length, degassing the system, and masking the cladding interface. Together, these techniques provided for a robust waveguide system. The

limitations of the Teflon AF™ waveguides are related to the material's high number of scattering 'microvoids', which limit effective transmission of light of wavelengths below 400 nm. Development of new low refractive index tubular materials will aid in future waveguide developments for long-path detection.

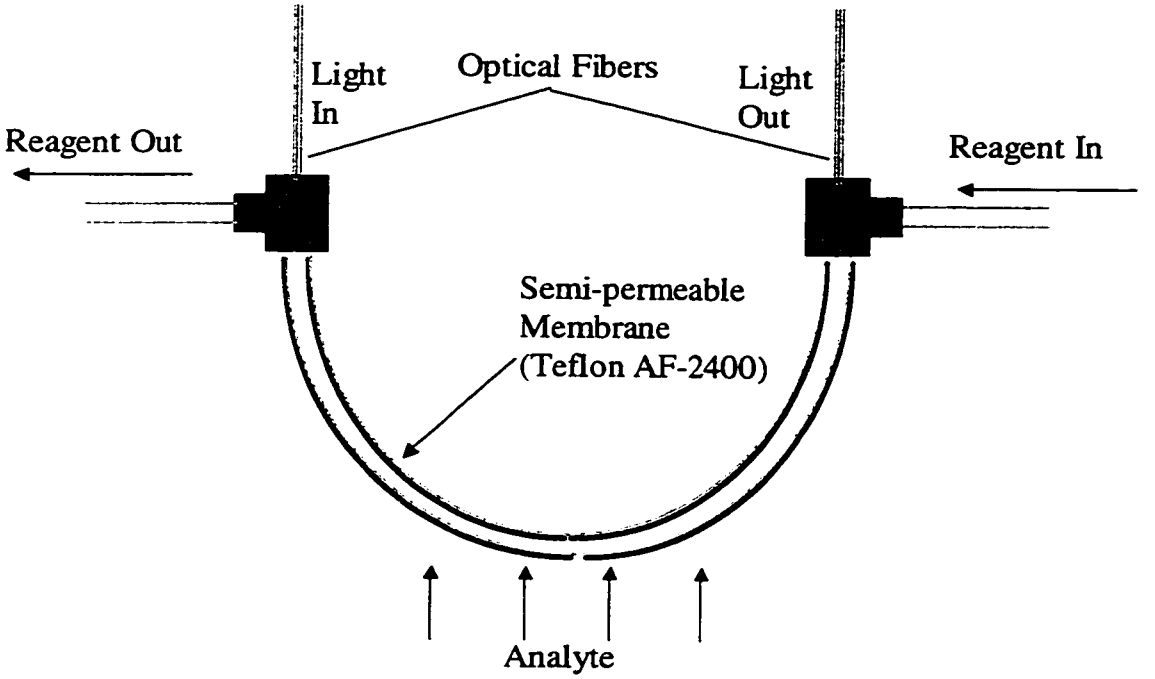

Figure 5.1 – Schematic of a Liquid Core Waveguide (LCW) in which the cladding is used as a semi-permeable membrane for analyte. The reagent core has a higher refractive index than the cladding, so light entering the waveguide is totally internally reflected and collected with a collection fiber optic.

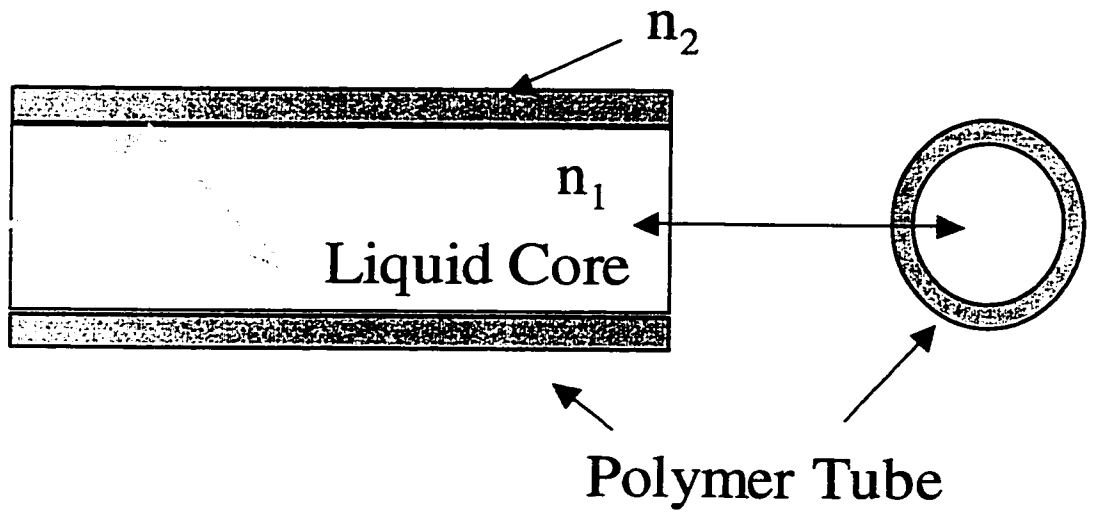

Figure 5.2 – Total internal reflection occurs inside of a polymer tube when the refractive index of the material filling the tube is greater than the refractive index of the polymer material.

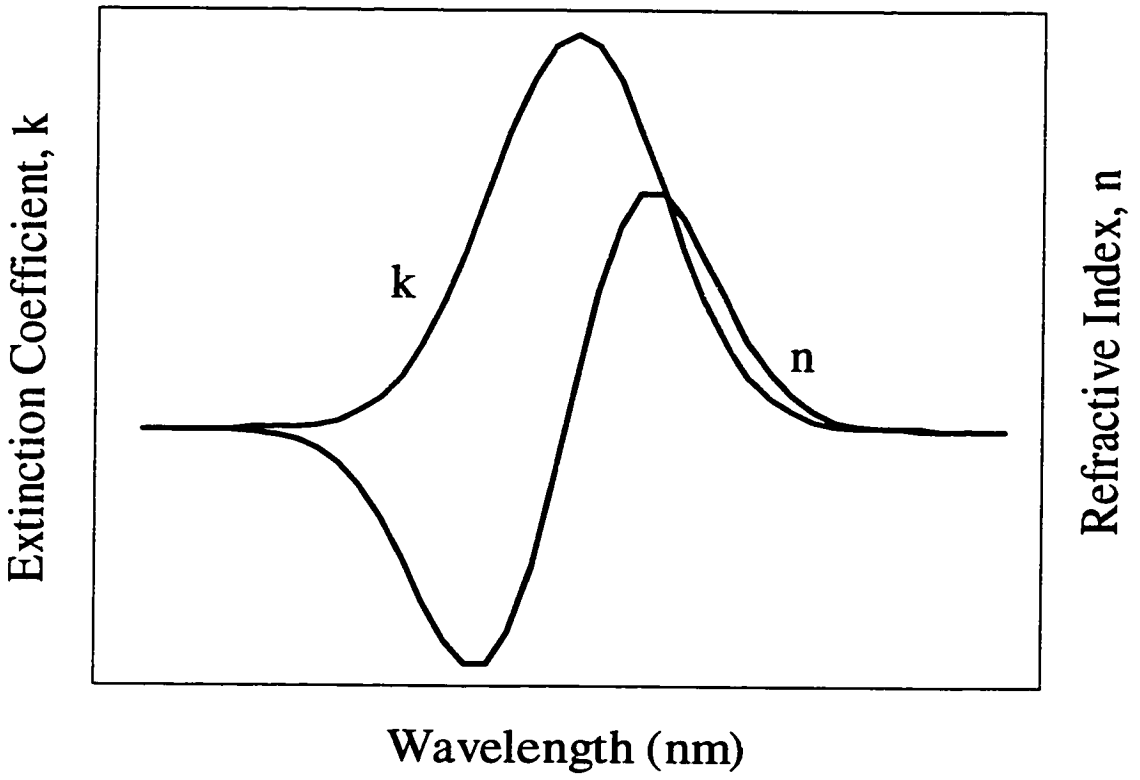

Figure 5.3 – Anomalous dispersion occurs around a strong absorbance band in which the refractive index n is anomalously low to the short wavelength side of the absorbance band and anomalously high at the long wavelength side of the absorbance band.

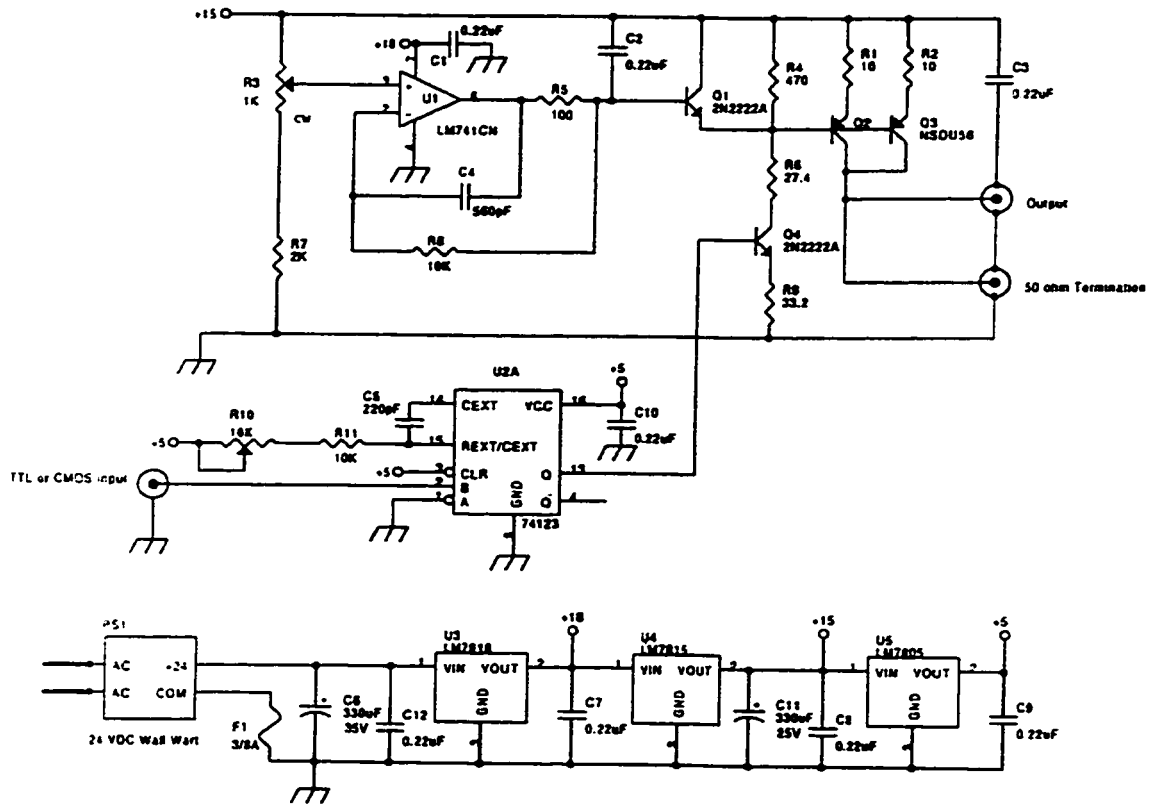

Figure 5.4 - Pulsed LED driving circuit designed and constructed by the UW Chemistry Department electronics shop.

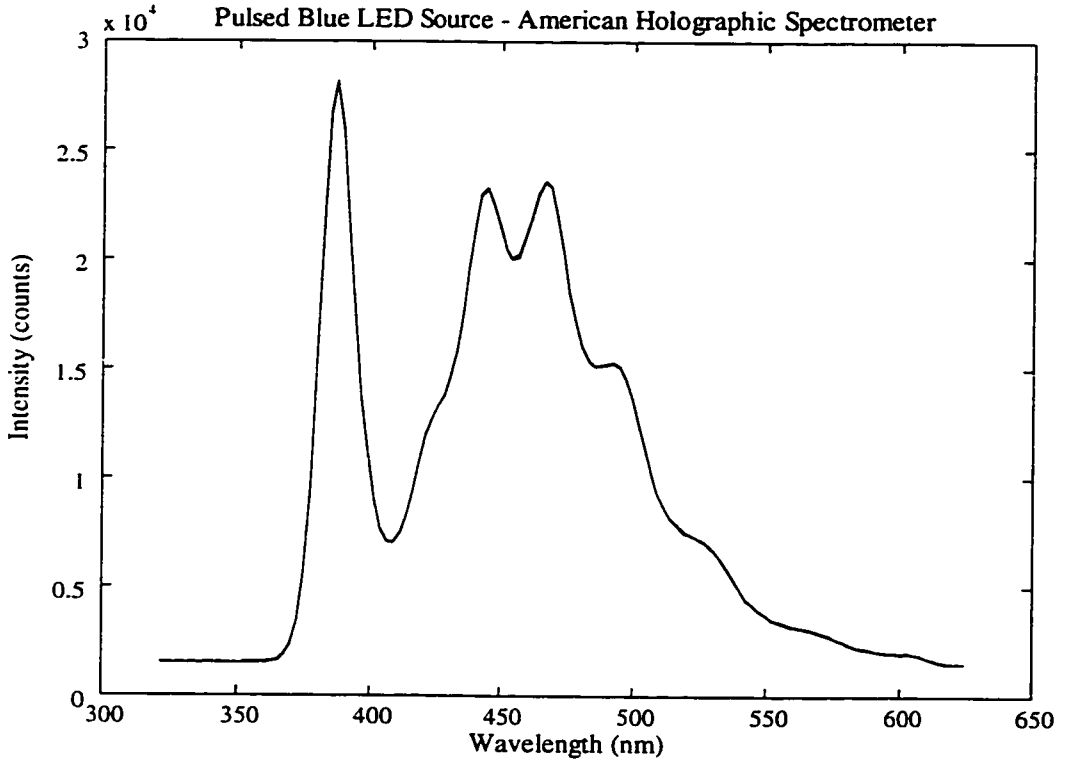

Figure 5.5 - Emission spectrum from a pulsed blue LED source (10 kHz, 1% duty cycle), imaged on the American Holographic Spectrometer (10 ms integration)

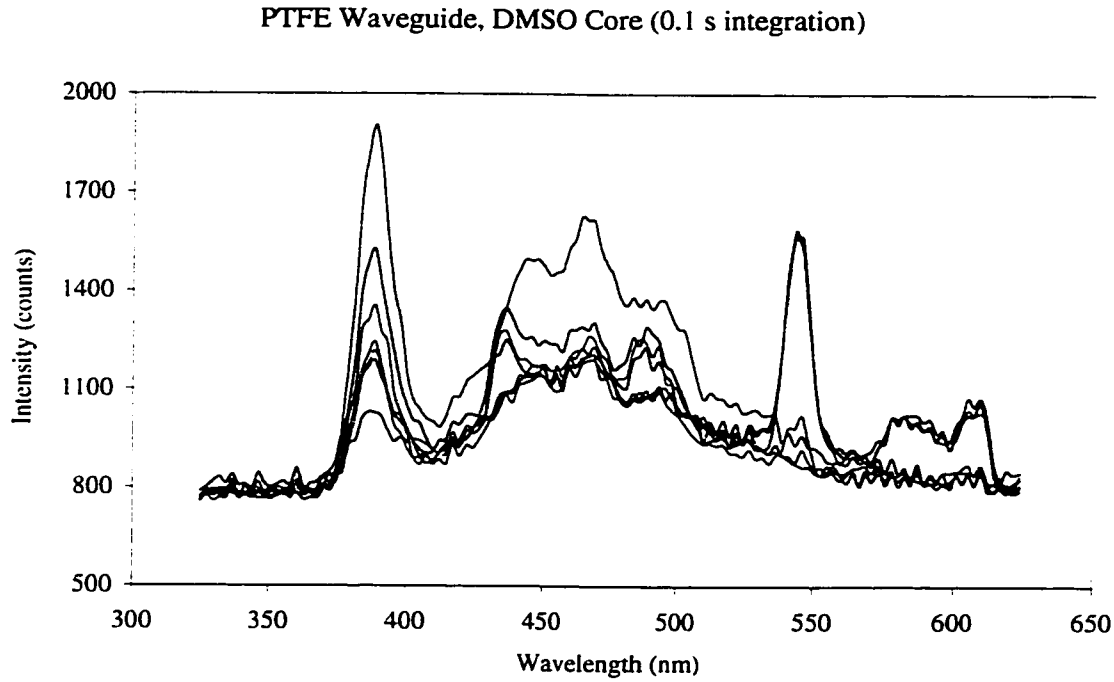

Figure 5.6 – Individual light transmission scans of a mercury light source through the waveguide. A ten centimeter, 22 gauge PTFE tube waveguide with a DMSO core. The high variability in the data indicates a poorly optimized waveguide.

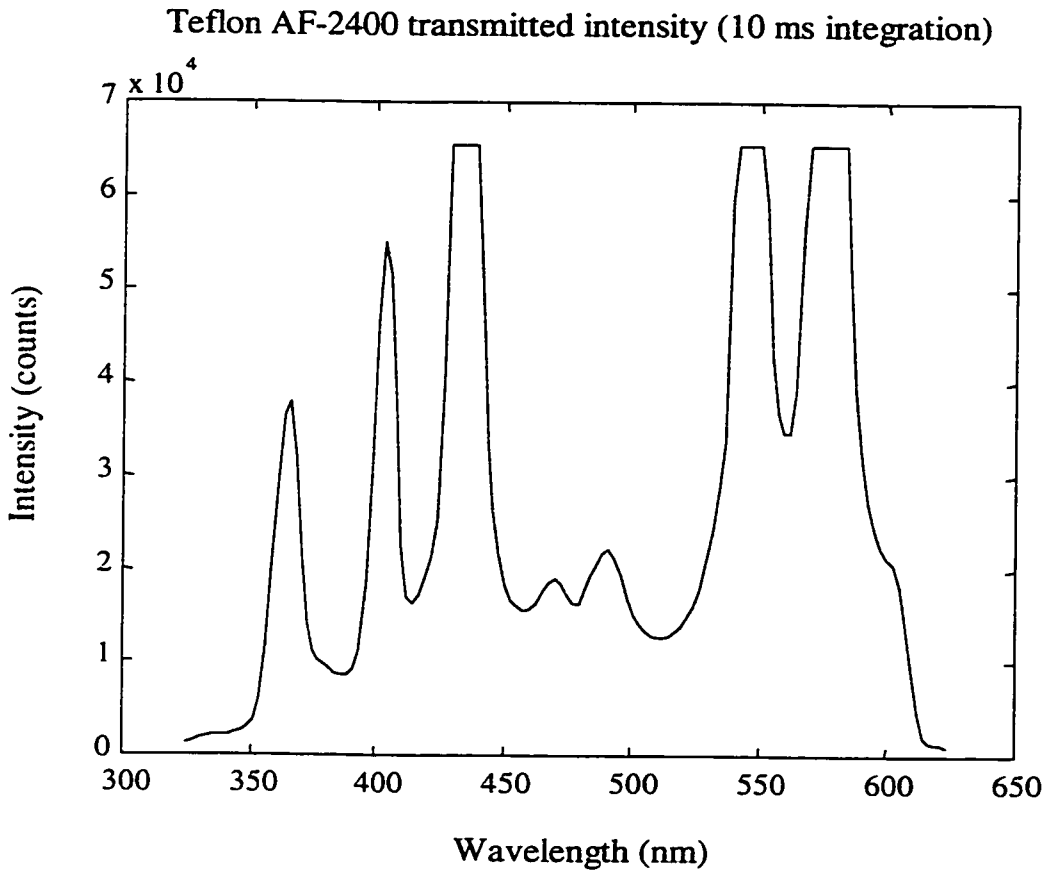

Figure 5.7 - Transmitted mercury light source intensity through the first water-core Teflon AF-2400 tube waveguide. Same source and collection conditions as the waveguide structure in the previous Figure.

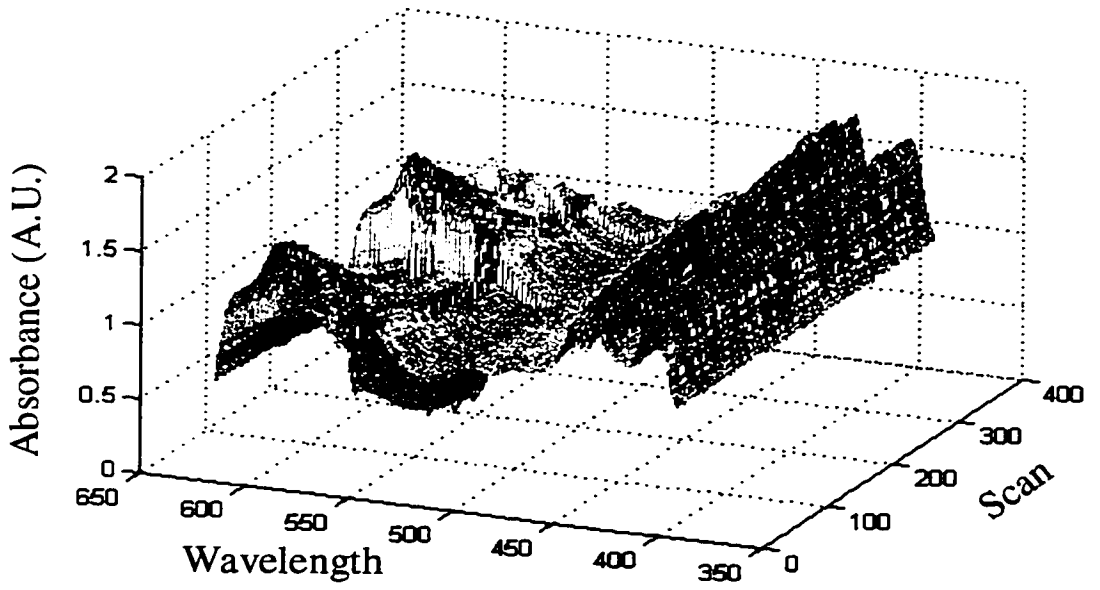

Figure 5.8 - HCl acid vapor response in the Teflon AF-2400 waveguide filled with buffered 2 μM/L bromthymol blue solution. The basic form of the indicator λ_{max} = 610 nm. Note the decrease in the basic forms absorbance as HCl vapor diffuses into the core. The sharp increase in the basic form absorbance at 200 seconds is due to the introduction of fresh core reagent solution. The structure in the absorbance spectra is due to the xenon light source. Figure 5.8 shows a cross section of the basic λ_{max} absorbance with time.

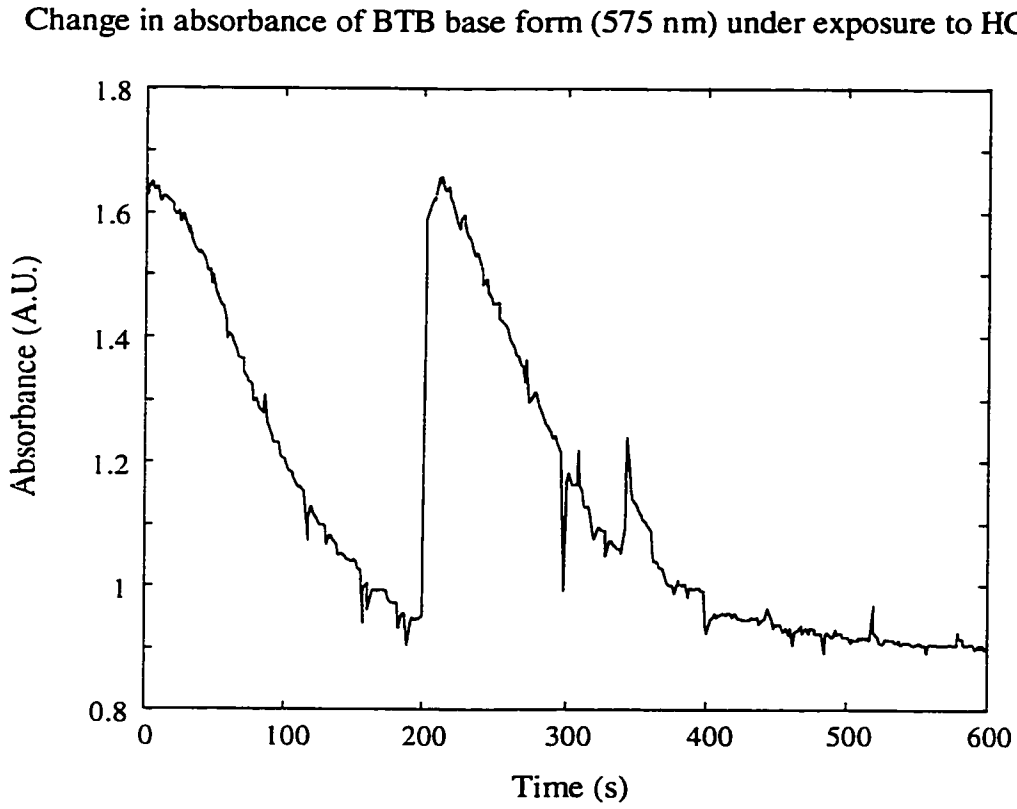

Figure 5.9 - Absorbance of BTB blue form (600 nm) as HCl vapor diffuses through the LCW membrane and reacts with the BTB. This is a cross-section of the data presented in Figure 5.7.

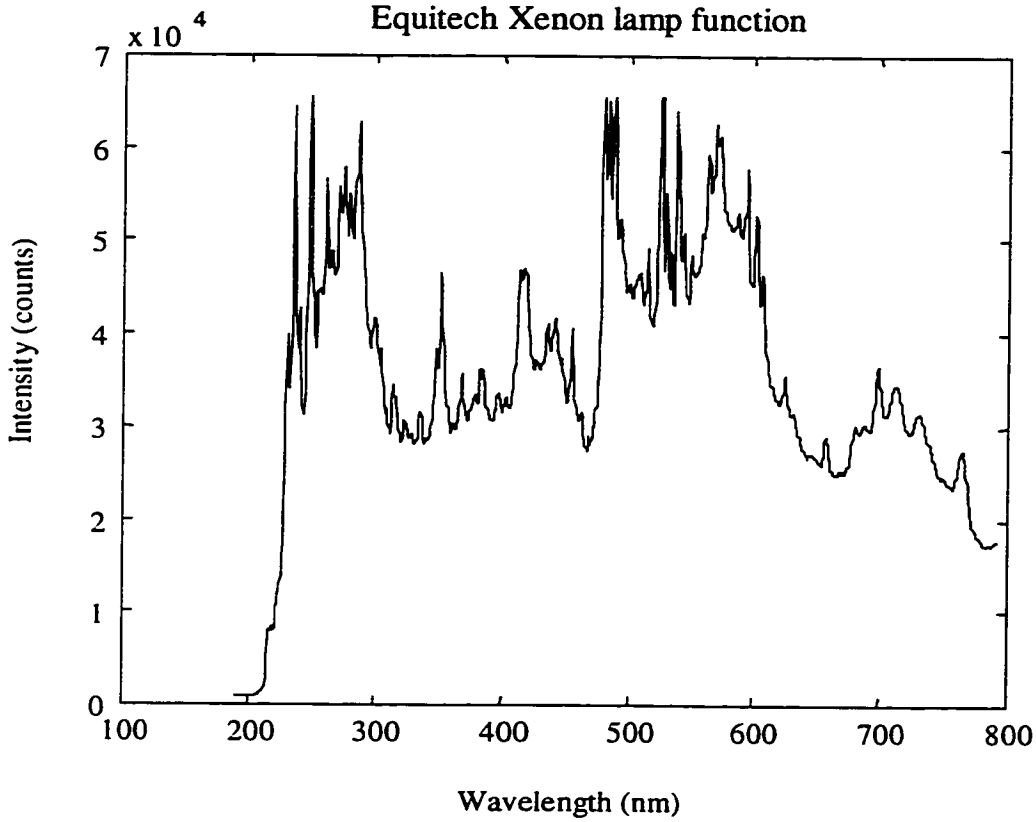

Figure 5.10 - Equitech flash lamp imaged on the Equitech CCD detector. One 2 ms lamp pulse imaged on the CCD detector with a 10 ms integration time through the same patch cord UV transparent fibers from the LCW optical train.

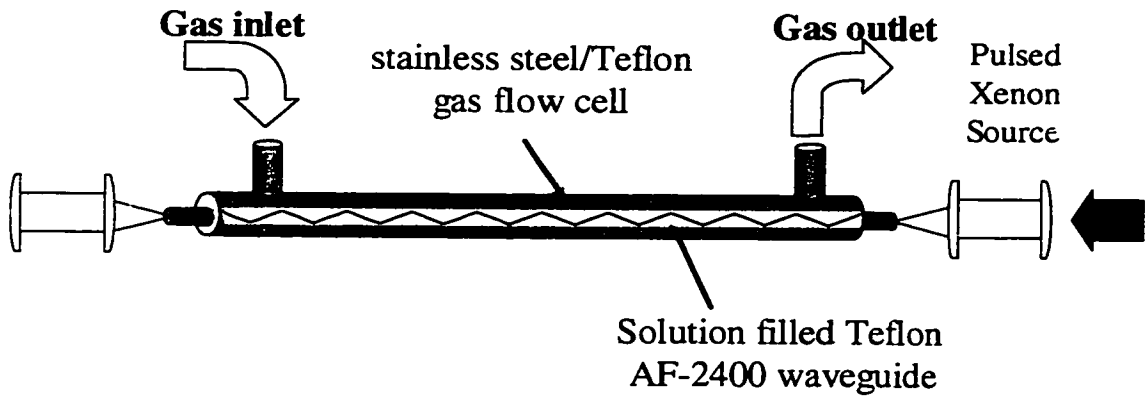

Figure 5.11 - Gas measurement with the liquid core waveguide are conducted with the waveguide that acts as a semi-permeable membrane housed in a non-permeable flow cell (i.e. stainless steel or PEEK). Gas diffuses into the LCW core and is detected either directly or indirectly by reacting with the liquid core reagent changing the waveguides optical transmission characteristics.

Liquid Core Waveguide Sampling Cell

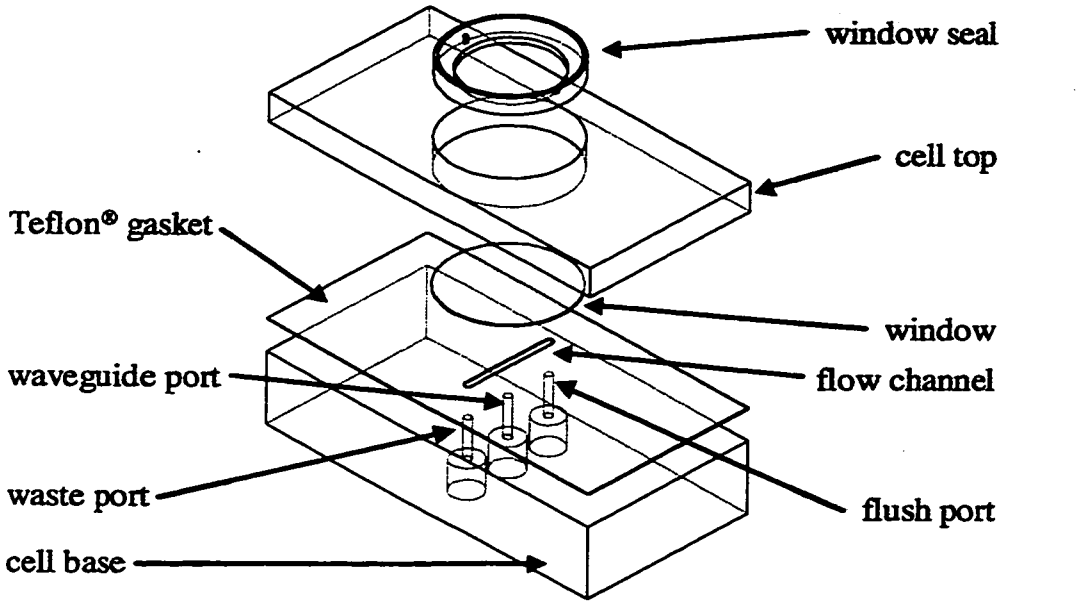

Figure 5.12 - Schematic of the liquid core waveguide optical interface. Fluids are delivered to the waveguide through the ports on the back of the cell that are ¼ 28 thread flat bottom to accept commercially available low-pressure flat-bottom fittings. The flow channel is a laser-cut Teflon thin film gasket. The base, top of the cell, and window seal are fabricated from PEEK. The window is a 1" sapphire window.

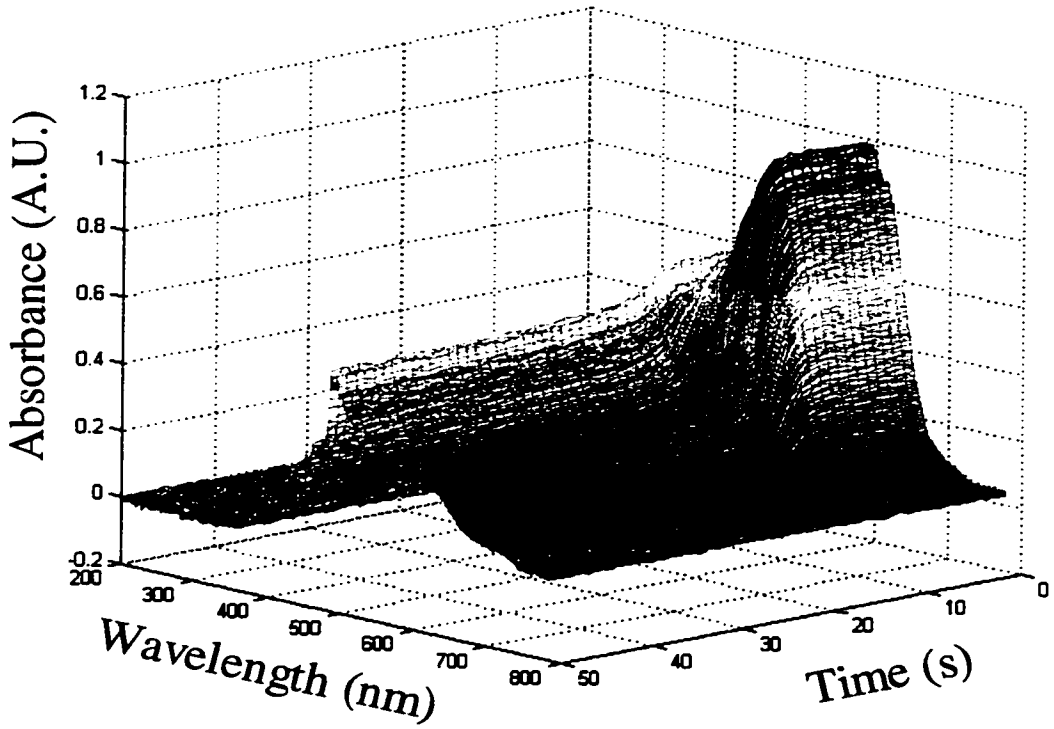

Figure 5.13 - CO_2 permeation data for a 80cm x 150μm I.D. x 400μm O.D. Teflon AF-2400 tube waveguide. A pulsed Xenon source and Equitech spectrophotometer were used for illumination and collection. Buffered bromthymol blue core [BTB] = 2mmol. Flow CO_2/N_2 (50:50) at 200 ml/min from 0 seconds until equilibrium is reached (~ 20 seconds). As CO_2 diffuses across the tubing wall, it reacts with the aqueous core and is converted to carbonic acid. This acid reacts with the bromthymol blue indicator. The basic form of the indicator gives the major absorbance (620 nm) noted here, decreasing as CO_2 concentrations in the core increase.

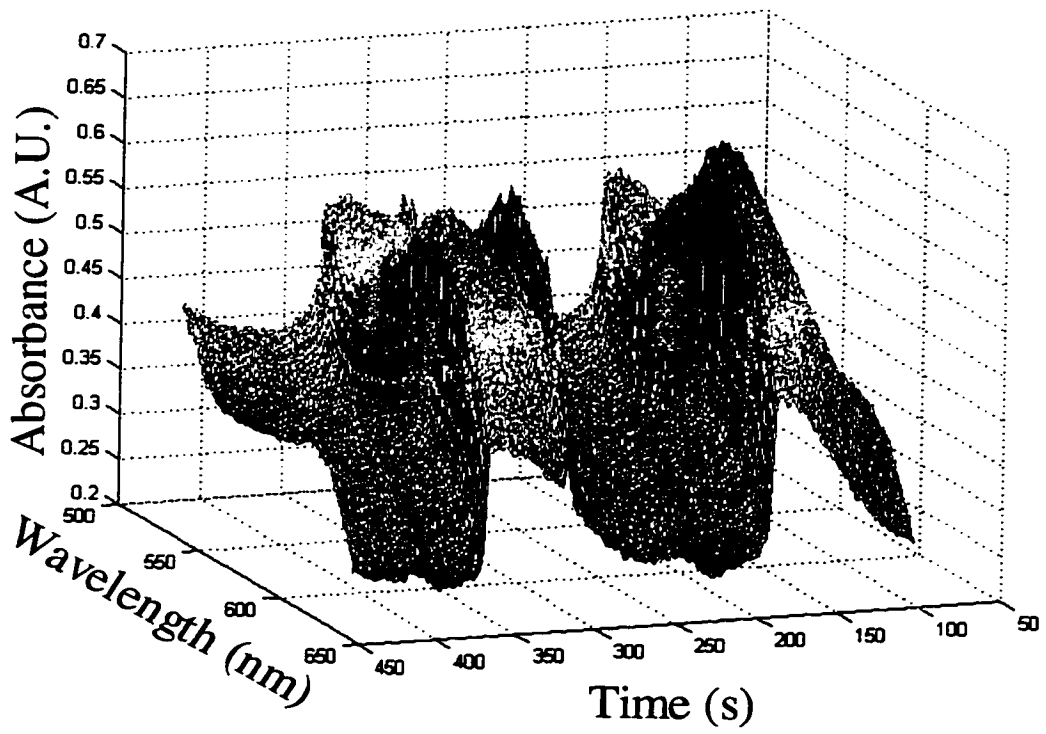

Figure 5.14 - CO_2 cycling study - Cycling study: 80cm x 50μm I.D. x 400μm O.D. waveguide. Equitech pulsed Xenon source and spectrophotometer N_2 gas flow 100 mL/min throughout. Flowed the core solution. Stopped flow. Flowed CO_2 gas at 100 mL/min (note sharp decrease in absorbance). Flowed fresh reagent into the waveguide core.

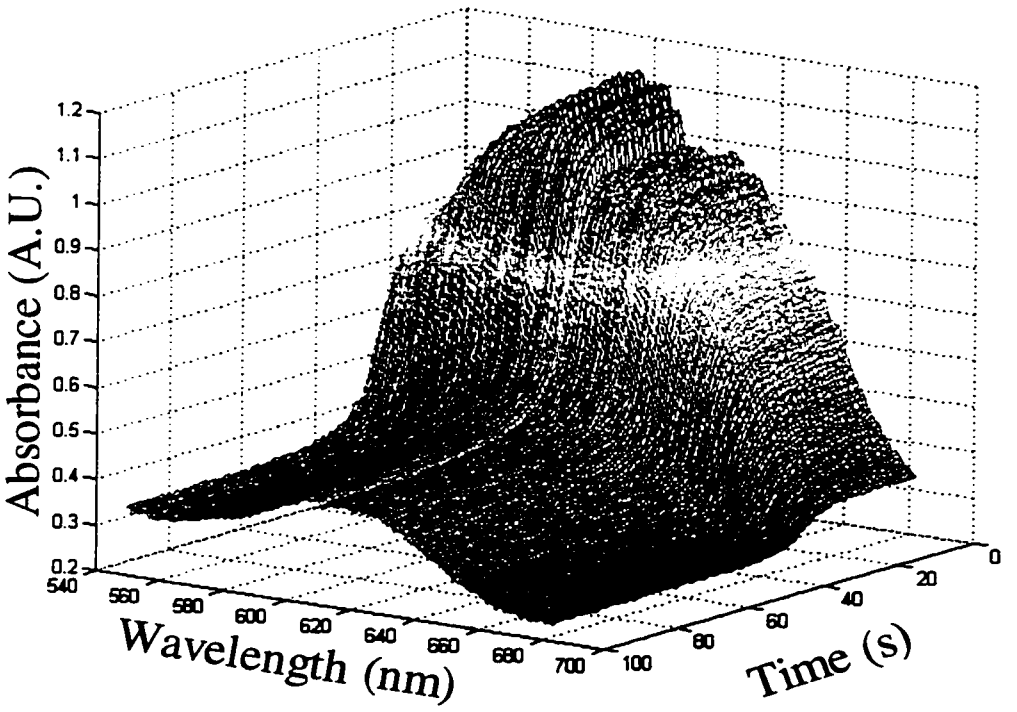

Figure 5.15 - CO_2 permeation, thick wall 80cm x 100μm I.D. x 990μm O.D. Teflon AF-2400 tube. Pulsed Xenon source and Equitech Spectrophotometer. Buffered bromthymol blue core [BTB] = 2μmol. Flow CO_2/N_2 (50:50) at 200 ml/min for duration of the experiment.

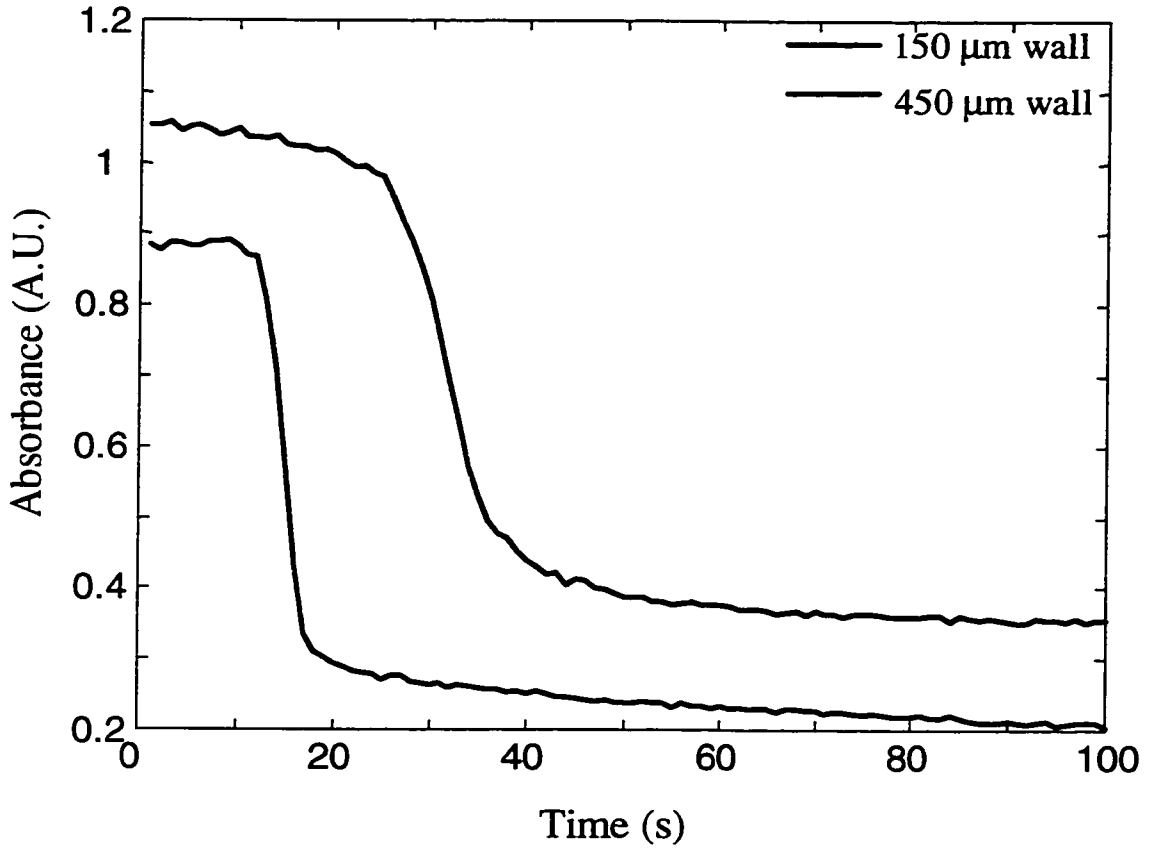

Figure 5.16 - CO_2 permeation rates combined with the buffered bromthymol blue reaction rates, varying Teflon AF wall thicknesses Absorbance at λ_{max} (620 nm) of the basic form of the bromthymol blue indicator vs. time. If the difference in wall thickness were the overriding factor in this experiment, the time would be 9 times greater as opposed to 2 times greater as shown here. We speculate that the difference in the two plots is the reaction time for CO_2 with the BTB core.

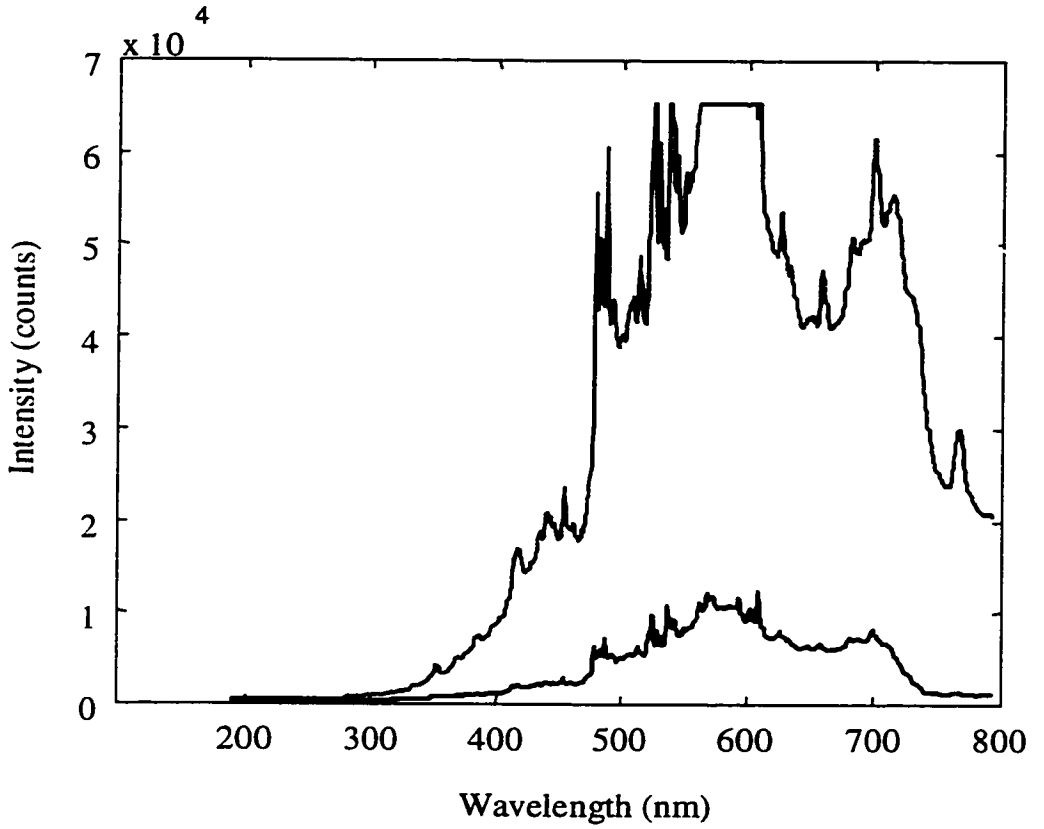

Figure 5.17 - Transmitted xenon lamp intensity through a 42 cm waveguide (red) vs. a 80 cm waveguide (blue) 1000 ms integrations. There is a huge increase in transmitted signal by reducing the waveguide length. This is due to the decrease in the number of scattering centers.

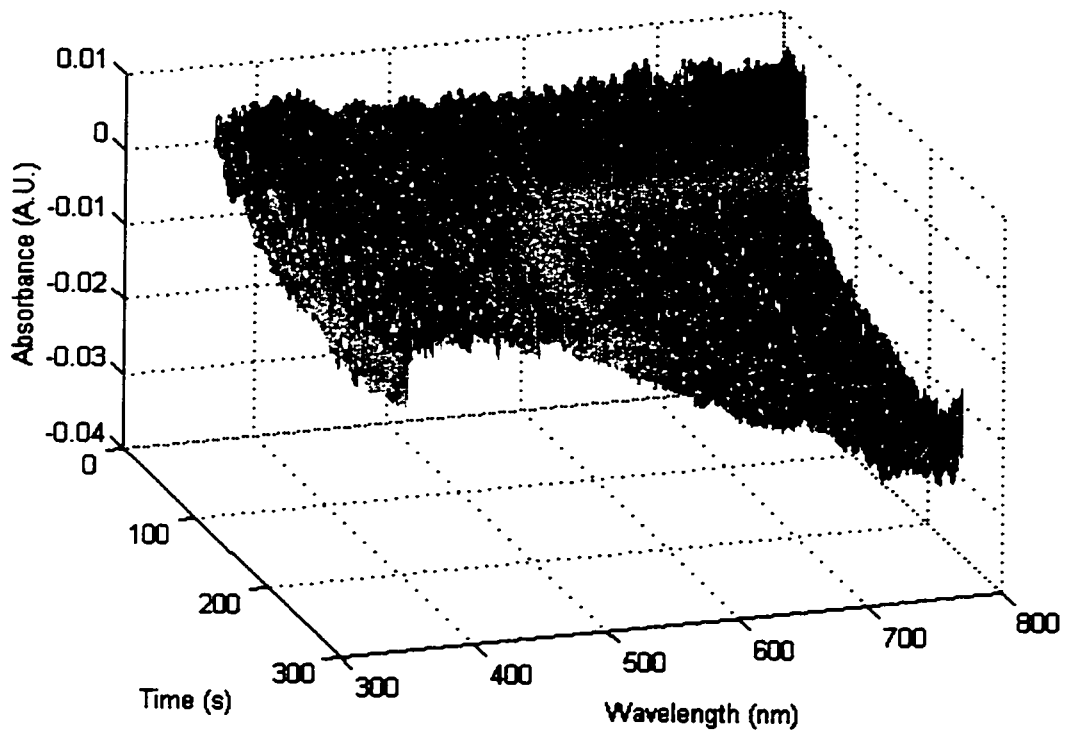

Figure 5.18 - Change in absorbance through a water-filled waveguide with evacuation of the external gas flow tube. Spectra were collected for ~20 seconds before the vacuum was applied. Note the decrease in absorbance (decrease in attenuation) is more pronounced at longer wavelengths indicating that the scattering centers are decreasing in size, decreasing the scatter at longer wavelengths.

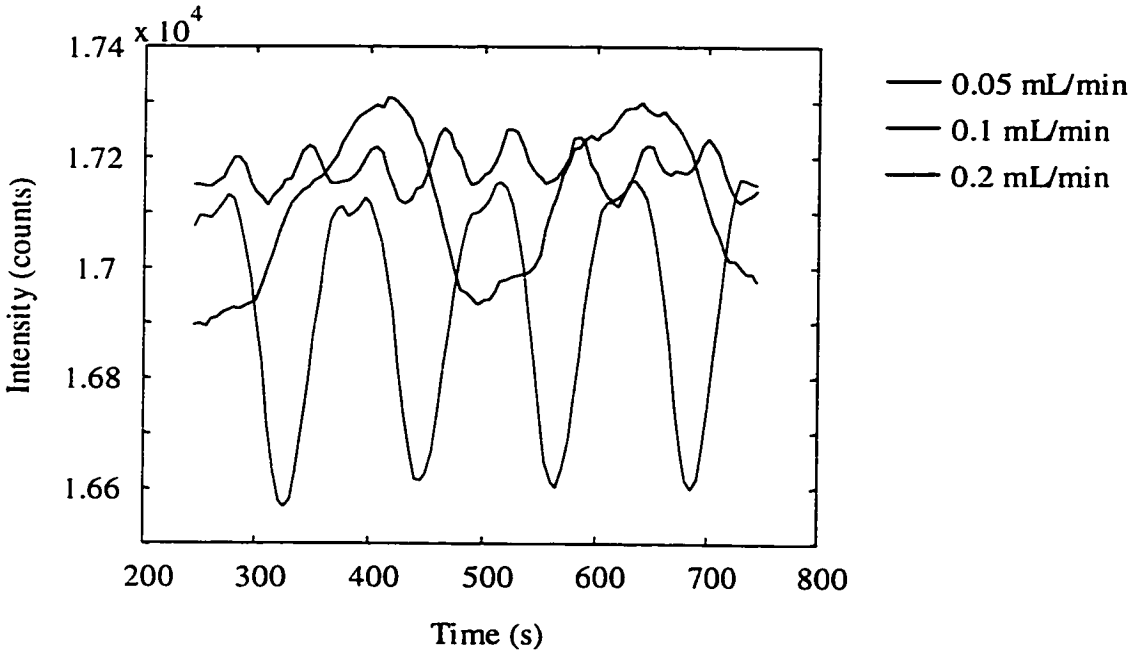

Figure 5.19 - Intensity fluctuations through the waveguide with pump flow rate. The amplitude of the fluctuations decrease at 0.2 mL/min flow rate on the pump which is the low end of the pump's optimal flow rate range. However, the waveguide system does not handle flow rates this large.

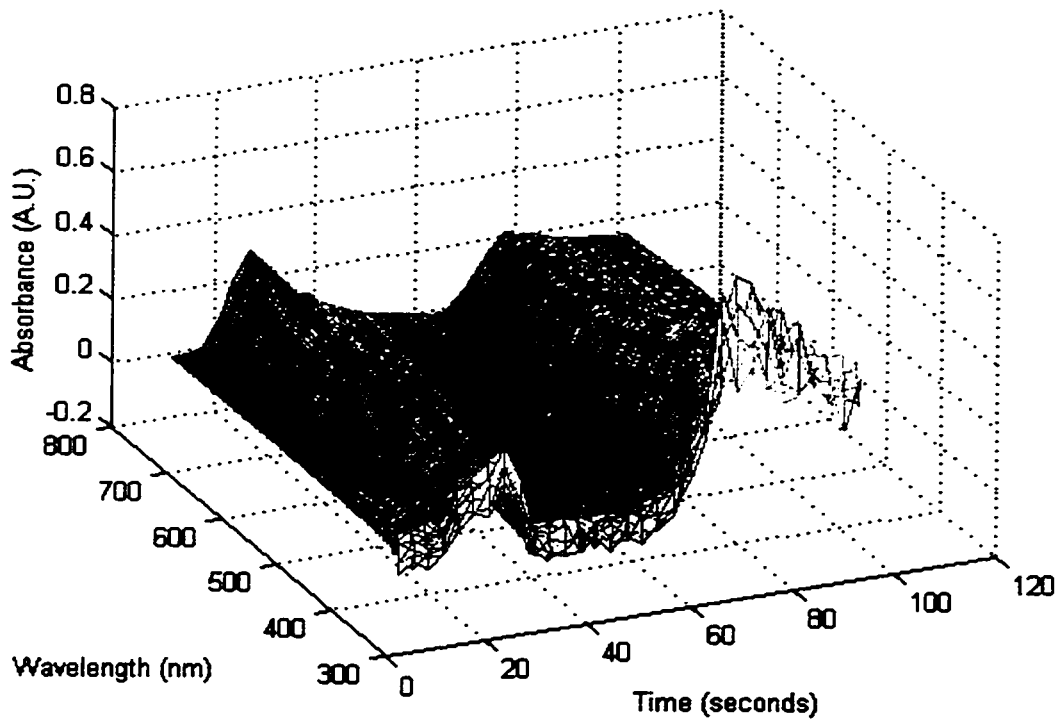

Figure 5.20 - Flow of a 20 μL injection of 38% sucrose through a 10 cm waveguide at 50 μL/min flow (water). As the front end of the injection enters the waveguide (time = 30 s) the waveguide transmission is attenuated (absorbance increases). As the plug fills the waveguide, (time = 40 s to 60 s) the transmission increases (negative absorbance referenced to water) due to the higher numerical aperture of the waveguide. Another attenuation is observed as the injected plug leaves the waveguide. This effect was observed for all of the refractive index standards, and increased as refractive index increased.

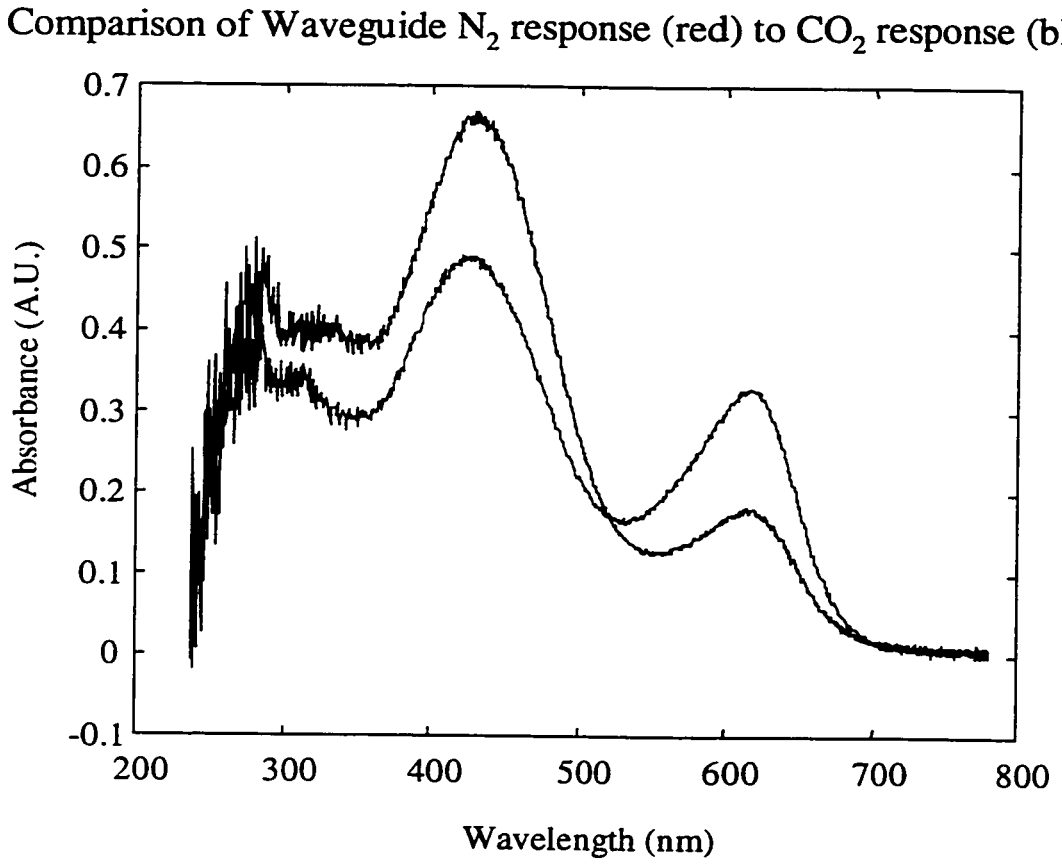

Figure 5.21 - CO_2 detection with optimized LCW system compared to the N_2 response with the same system. CO_2 (blue) and N_2 (red) flowed through the gas flow tube at 50 mL/min, a 20 µL injection of the bromthymol blue solution with a water carrier flowing at 50 µL/min.

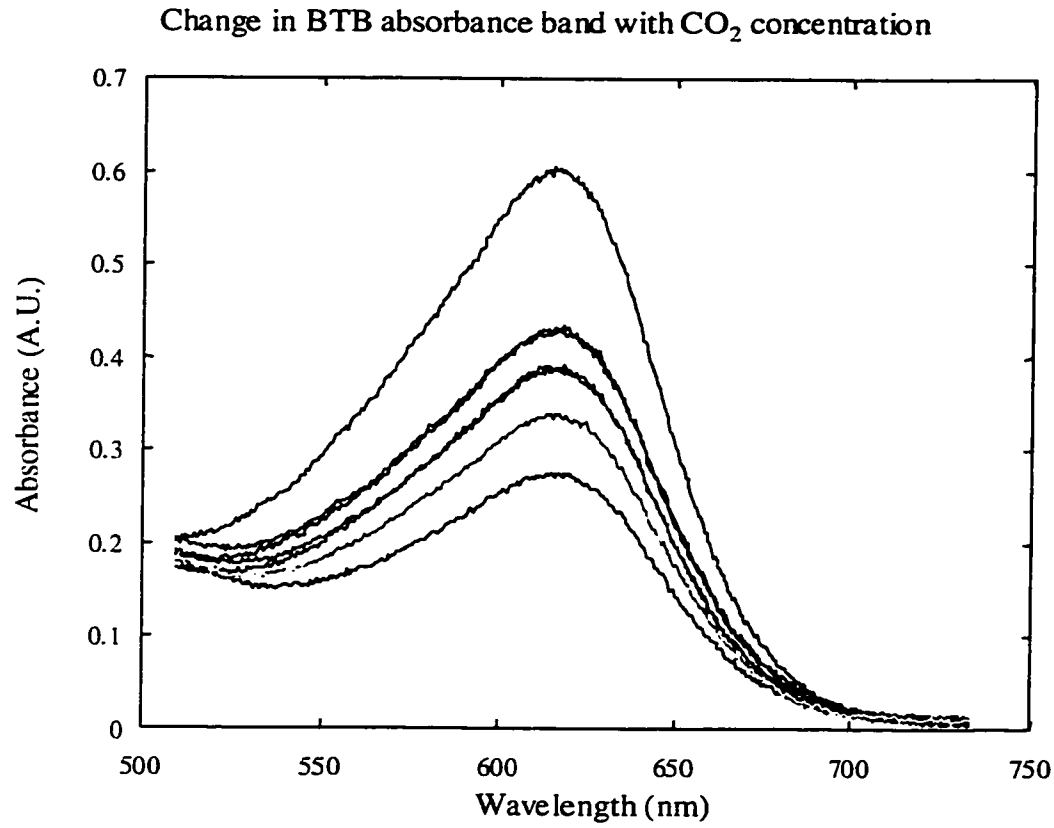

Figure 5.22 - Different CO_2/N_2 mixtures, decrease in base BTB absorbance band with increasing CO_2. Blue – 20% CO2 in N2, Green – 40%, Red – 50%, Magenta – 60%, Black – 80%. The water waveguide core solution was flowing continuously at 50 µL/min with 20 µL injections of buffered BTB solution.

Chapter 6 - Supported Liquid Membranes as a Sensor Interface

6.1 Introduction

Supported liquid membranes (SLMs) are becoming a common separation method. Literature on the subject dates back to the mid-1980s. In general, supported liquid polymer membranes are high moleular weight liquid polymers filled into the pores of porous microfiltration or ultrafiltration film. These membranes have been shown to be capable of removing low molecular weight, polar, non-ionic, organic species from dilute aqueous matrices. This extraction can be achieved even in the presence of high inorganic salt concentrations (i.e. high osmotic pressures).

The literature describes the use of SLM interfaces for the separation of metal ions from bulk matrices.[1,2,3] These liquid membrane interfaces have also been applied for the separation of organic materials.[4,5] Of particular use is the separation of miscible organics from aqueous matrices.[6,7] However, to this date, there has been no significant demonstration of these membranes as sampling interfaces for chemical sensing systems.

The key to using supported liquid membranes as sampling interfaces is the reagent chemistry to strip the analyte out of the SLM on the sensor side of the

---

1 A.B. de Haan, P.V. Bartels, J. De Graauw, J. of Membr. Sci., Vol. 45, (1989), 281-297.
2 N.K. Djane, K. Ndung'u, F. Malcus, G. Johansson, L. Mathiasson, Fres. J. Anal. Chem., Vol. 358, (1997), 822-827.
3 J. Buffle, K.J. Wilkinson, M. Tercier, N. Parthasarathy, Annali di Chimica, Vol. 87, (1997), 67.
4 M. Knutsson, L. Mathiasson, J.A. Jonsson; Chromatographia, Vol. 42, (1996), 165.
5 P. Wieczorek, J.A. Jonsson, L. Mathiasson; Anal. Chim. Acta, Vol. 346, (1997), 191-197.
6 S.V. Ho, U.S. Patents 5,507,949 & 5,512,180.
7 S.V. Ho, P.W. Sheridan, E. Krupetsky, J. of Membr. Sci., Vol. 112, (1996), 13-27.

membrane. The reagent must act as a sink to prevent diffusion back into the SLM and drive the diffusion of analyte towards the sensor. The sampling interface is regenerated each time the reagent is renewed. The reagent could do any of the following: a pH change, a reaction, complexation, biodegradation or pervaporation.

6.2 – SLM as a sampling interface for the FlowProbe™

A supported liquid membrane has been explored for use as a sensor interface on the FlowProbe™. The membrane system explored employs a porous polypropylene (Celgard 2400) membrane support impregnated with polypropylene glycol having a mean molecular weight of 4000. The analyte measured was a solution of p-nitroaniline in saline buffer. This amphiphilic membrane system transports polar, non-ionic, organic species. The experiments were conducted using a FlowProbe™ sensor head (Figure 6.1) with the SLM as the membrane interface to the probe head. Figure 6.2 shows the basic system setup for the supported liquid membrane experiments employing the FlowProbe™.

Extraction of p-nitroaniline was studied because it was of interest to an industrial sponsor who had developed an assay that cleaved p-nitroaniline during the assay, which could be determined colorimetrically. Extraction using an SLM was interesting because of the SLM capability to selectively transport the analyte and not other species that may be in solution, but rather only the polar, non-ionic organic molecules of a given molecular weight. This is helpful if the sample contains complex species such as those found in extracts of plants.

The absorbance was measured using a blue LED light source with a peak emission at 450nm, but it also has an emission peak at 383nm when run at much higher currents than specified, or when pulsed at 10 kHz with a 1% duty cycle.[8] The maximum absorbance of p-nitroaniline occurs at 380 nm near the 383nm peak of the LED. See chapter 5 and figures 5.4 and 5.5 for more information on this light source. The American Holographic spectrometer was used for these experiments as well. It was operated with a LabView VI for data collection and conversion.

6.2.1 – FlowProbe™ Extraction Studies

The membranes were prepared by punching out a piece of the Celgard to fit the end of the probe. These pieces were impregnated with polypropylene glycol (PPG) by placing a drop on the membrane and allowing it to penetrate the Celgard, making sure both sides were well coated with the liquid. Wetting of the membrane was determined visually as the porous support changed from opaque white to translucent when sufficiently wetted with the PPG material. After wetting, the excess PPG was wiped off the membrane.

The SLM was placed on the probe head and the probe was immersed into a solution of p-nitroaniline in saline buffer. The stripping reagent on the inside of the probe head was 0.01N HCl. The acidprotonated the p-nitroaniline, creating a sink and preventing diffusion back across the membrane, ensuring a constant flux of p-nitroaniline into the probe head (Figure 6.3). The absorbance of p-nitroaniline was measured over time while the probe head was in contact with the p-nitroaniline/saline

---

8 T. Araki, H. Misawa; Rev. Sci. Instrum., Vol. 66, No. 12, (1995), 5469-5472.

solution. Para-nitroaniline diffusion was observed in the presence of possible interferents (Figure 6.4).

6.2.2 – Bench-top Regeneration of the Supported Liquid Membrane

A qualitative regeneration of the celgard membrane system was investigated on the bench-top. A small piece of Celgard was impregnated with PPG. The PPG was removed using isopropanol. This removal was verified visually as the membrane had returned to its original white, opaque state. The membrane was then impregnated with a solution of 50:50 isopropanol and polypropylene glycol. Impregnating the membrane using a solution will be necessary for regeneration of the membrane *in situ* because the PPG-4000 material is too viscous to flow through the probe head. After evaporation of the isopropanol, the membrane appeared to remain wet with the PPG material, as it appeared translucent.

A small piece of Celgard was also impregnated with an emulsion of PPG in water as an alternative to the isopropanol/PPG solution. The membrane was also wet with PPG after the emulsion was poured off, although not as uniformly. The result of this experiment suggested that the liquid membranes can be regenerated *in situ* by flowing isopropanol through the probe head to strip out the existing liquid membrane, followed by a mixture of isopropanol and polypropylene glycol to rewet the Celgard membrane.

6.2.3 – In Situ Regeneration of the Supported Liquid Membrane

The *in situ* removal and redeposition of the polypropylene glycol provided inconclusive results. The probe head was flushed with isopropanol to strip the

polypropylene glycol from the Celgard. The probe was flushed with HCl reagent and immersed in the p-nitroaniline solution as before. Judging from the increase in absorbance at 383 nm, some p-nitroaniline had apparently diffused across the membrane, indicating incomplete stripping of the membrane. The probe then was immersed in isopropanol while it was flushed with isopropanol to strip any remaining PPG from the Celgard, and the PNA experiment was repeated. Para-nitroaniline absorbance was still present. The probe head was taken apart and inspected visually. It appeared that the membrane was not stripped out completely, as it still appeared translucent.

6.3 – Commercial SLM modules as sampling interfaces to the Liquid Core Waveguide

A new experimental set-up was constructed for further development of supported liquid membranes as sampling interfaces. The membranes are commercially available modules that were placed in line with the liquid core waveguide for long-path absorbance detection of extracted molecules (Figure 6.5). The SLM modules (SeleXtrac™), are commercially manufactured by Spectrum Laboratories, Inc. (Rancho Dominguez, CA). There are currently two liquid membrane types available in the SeleXtrac™ modules, S-type and P-type. The P-type used here has faster transport rates for polar organics such as phenol and p-nitroaniline, while s-type membrane is used for less-polar hydrophobic species such as benzene and toluene. The waveguide was a ~12 cm Teflon AF-2400 tube (100 μm I.D. x 1000 μm O.D., 0.98 μL). The pulsed xenon source and CCD detector of the

Equitech controlled with Equitech's software package were used for illumination and data collection. Core reagent delivery was automated using a Waters HPLC pump. Feed solutions containing organics and salts were delivered using syringes or a piston pump for continuous circulation of the feed.

Custom-fabricated, single hollow fiber membrane modules were used for these studies. The commercially available product of the same dimensions contains 6 hollow fibers, or six times the surface area for analyte extraction. The volume of the feed side of the fiber was measured volumetrically to be ~2.5 mL while the volume of the strip side was measured to be 30 μL. The membrane surface area was 2 cm^2. The modules were tested for integrity using commercial food coloring that is water-soluble and will not diffuse through an intact SLM membrane structure.

6.4 Phenol Extraction Study

Extraction and detection of phenol is useful for both industrial and environmental monitoring. The phenol readily diffuses into the p-type supported liquid membrane. The strip solution for phenol is 0.1N NaOH. The basic solution causes the phenol to dissociate, preventing diffusion back through the membrane. Figure 6.6 shows a schematic of the phenol/SLM chemistry.

Phenol has two UV absorbance bands at λ_{max1} = 220 nm and λ_{max2} = 270 nm. In basic solution, these bands shift to longer wavelengths so λ_{max1} = 240 nm and λ_{max2} = 290 nm as determined on a Hewlett-Packard UV/Vis instrument with 1 cm quartz cuvettes. Even in basic solution, these bands fall at the shorter wavelength limit for

detection with a Teflon AF waveguide due to the waveguide's high scattering losses at wavelengths less than 350 nm. The 240 nm absorbance band is not detectable in the LCW.

The instrumental responses to phenol and the sodium salt of phenol were determined by injecting known concentrations into the waveguide with a water carrier and a 0.1N NaOH carrier. The injected concentrations ranged from 5 μM to 5 mM. Figure 6.7 shows extractions of phenol from an aqueous stream flowing at 3 mL/min into both a stop flow 0.1 N NaOH and a flowing 0.1 N NaOH carrier. Note the pre-concentration effect of the stop-flow measurement compared to the continuous-flow measurement. Three concentrations of phenol were extracted, and detectable phenol was observed with feed concentrations as low as 5 μM. The concentration in the waveguide itself would be much lower due to the flowing conditions. The limit of detection is always going to be higher in the Teflon AF waveguide than for species that absorb at longer wavelengths due to the increased sensitivity of the apparatus above 400 nm.

6.5 p-Nitroaniline Extraction Study

We decided to use the p-nitroaniline chemistry again. The purpose of this experiment was to determine whether we could monitor the p-nitroaniline concentration of a feed solution if we monitor the strip side concentration using a liquid-core waveguide. The protonated p-nitroaniline absorbs at ~390 nm which is more easily detected by the Teflon AF waveguide system. As in the phenol extraction

study, the UV/Vis waveguide response was characterized by injecting different concentrations of p-nitroaniline and protonated p-nitroaniline into the waveguide.

6.5.1 – UV/Vis detection

The extraction was set up with ~10 mL of feed solution of a given concentration of p-nitroaniline, which was flowed in a fast-loop configuration at 2.5mL/min. The strip solution was 0.1N HCl flowing through the strip-side of the membrane module at 0.05mL/min. The feed flowed until the transmitted intensity at 392nm (λ_{max} for p-nitroaniline) began to decrease, then the feed side was flushed with deionized water. For actual extractions, the feed would flow until the extraction of analyte was complete.

Figure 6.8 shows the p-nitroaniline extraction data. The first plot shows one extraction, while the second plot shows the results of extractions of with several different PNA solution concentrations. The spectra were collected every three seconds as the waveguide core HCl strip solution was flowing. The blue traces are extractions of a 200 μM p-nitroaniline. The first extraction has a much larger absorbance because it was flowed on the feed side of the membrane for a longer period of time. The green traces are extractions of 100 μM p-nitroaniline. The red and magenta traces represent 40 μM and 20 μM p-nitroaniline, respectively.

Calibration was performed by 20 μL injections of various concentrations of p-nitroaniline (diluted in 0.1N HCl) into 0.1N HCl carrier solution. A linear calibration curve was constructed for absorbance at (λ_{max} = 392nm) vs. concentration. The coefficient for this relationship, a function of molar absorptivity and pathlength, was

determined to be 2.65 x 10^5 M^{-1}. The concentration traces were calculated based upon this calibration.

Note that the concentration of the strip solution is much smaller than that of the feed. With the LCW (pathlength ~ 13 cm) we have exceptional sensitivity for the highly colored p-nitroaniline chloride salt. I think we can improve upon these results by better matching the volume of the strip side of the membrane to the waveguide.

6.5.2 – Raman Detection

The same p-nitroaniline reaction was studied with the Raman waveguide detection cell. The differences in the system set-up include the waveguide's dimensions and the illumination/detection mechanism. The waveguide used in this study was a 0.002" I.D. (50 μm), 0.039" O.D. (1000 μm) 50 cm long Teflon™ AF-2400 tube (Biogeneral). The outflow from the injection loop or the SeleXtrac module was coupled to the waveguide inlet. The outlet of the waveguide was connected to the waveguide detection cell. The waveguide was illuminated and the Raman scatterind detected through a Kaiser Optical Systems Raman microscope.

The detection limit for p-nitroaniline is much higher for Raman than for UV/Vis. Raman scatter is a relatively weak phenomenon, but it provides structural information that UV/Vis absorbance does not. A Raman spectrum of p-nitroaniline is shown in Figure 6.9. PNA has a strong band near 1300 cm^{-1}. Different concentrations of p-nitroaniline were injected into the Raman waveguide to determine the minimum concentration that could be detected which was close to 15 μM PNA. Figure 6.10 shows the detection of the protonated PNA adduct with the Raman waveguide over the

course of the extraction. The feed concentration was 70 mg/L p-nitroaniline. The SeleXtrac membrane modules are also useful for imparting additional selectivity to the Raman LCW detection cell.

6.6 – Conclusions

The supported liquid membrane is a practical sensing system sampling interface. We have demonstrated its applicability to both the FlowProbe™ chemical sensing system as well as the liquid core waveguide sensing system with both UV/Vis absorbance and Raman detection. We have also demonstrated how renewing the reagent in this case regenerates the sampling interface, as the reagent is key to creating a continuous flux through the SLM. Additionally, we have demonstrated the feasibility of stripping out the liquid membrane material and replacing it *in situ*, thereby completely replacing the membrane interface.

Supported Liquid Membranes act to selectively extract classes of molecules from a sample. With a stripping solution on the other side, a continuous flux across the membrane can be achieved. The liquid polymer and stripping solution can be tailored for efficient extraction of analytes. Some limitations of the SLMs as sampling interface are physical fouling of the membrane support and small holes that cause leaks. In either case, the entire structure will have to be removed and replaced, negating any benefit over a regular semi-permeable membrane.

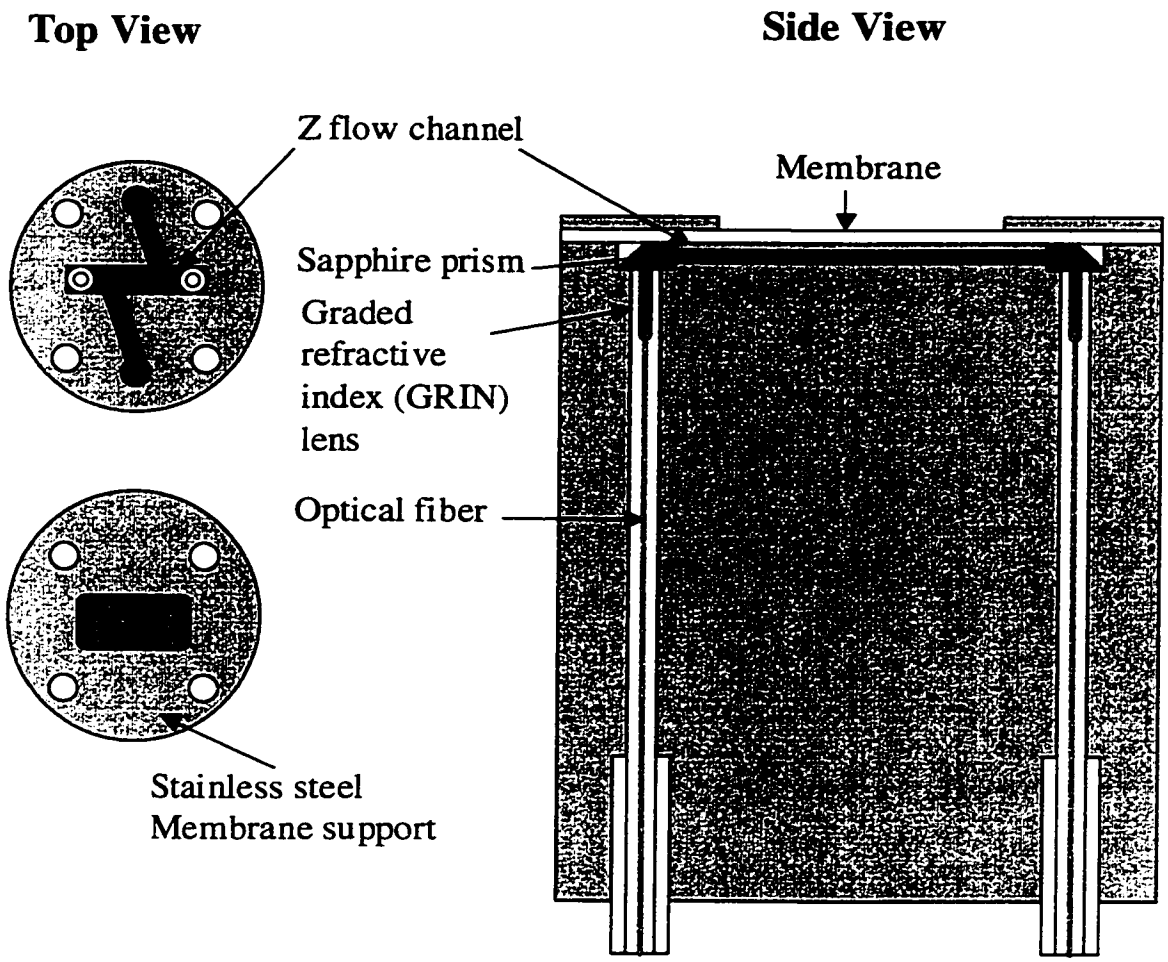

Figure 6.1 - Detail view of the FlowProbe™ probe head. The supported liquid membrane was applied as the membrane interface.

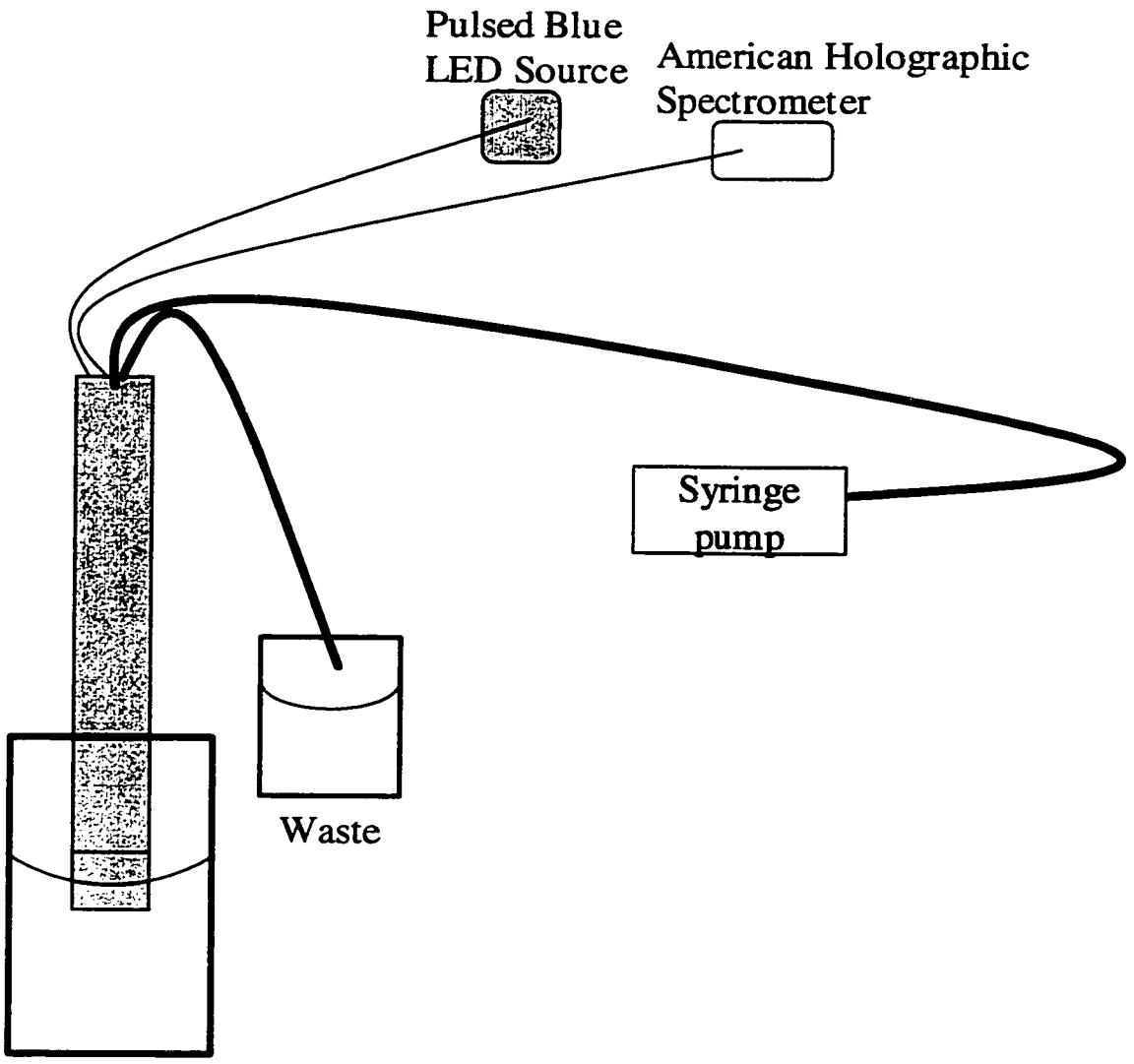

Figure 6.2 - Experiment set-up with SLM applied to the FlowProbe™. The spectra were collected on the American Holographic Spectrometer and the data were stored automatically using a LabView program.

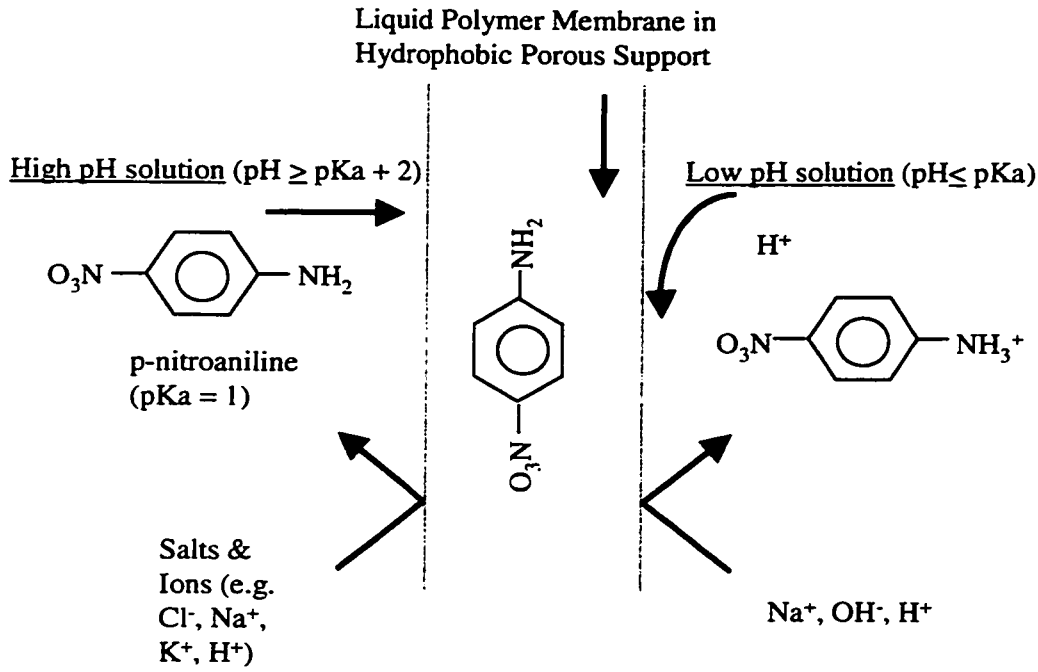

Figure 6.3 - Schematic of the p-nitroaniline SLM system with a 0.1 N HCl solution as the stripping solution.

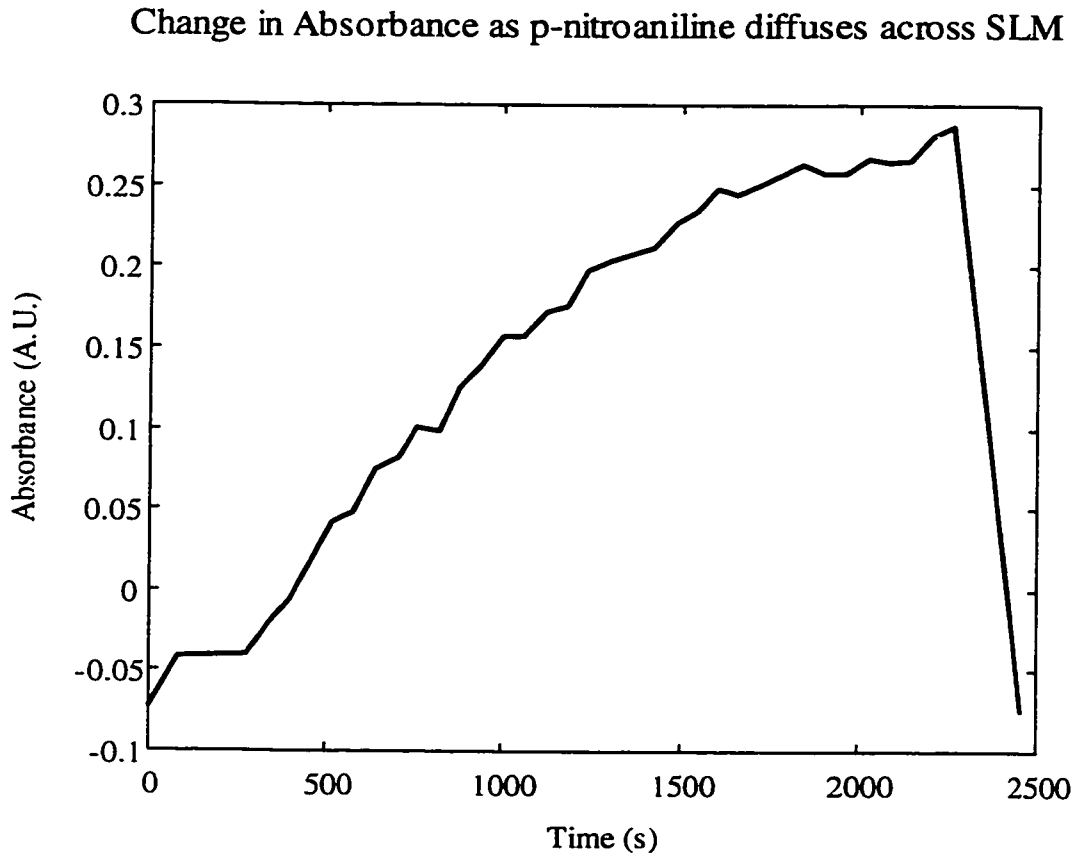

Figure 6.4 - Increase in absorbance at 380 nm as p-nitroaniline diffuses through the Supported Liquid Membrane into the FlowProbe™ head filled with 0.1M HCl. The sharp decrease just before 2500 seconds is due to the flushing out of the probe head with fresh reagent. Note that the signal returns to baseline. Similar results were obtained in the presence of possible interferents such as leaf extracts and tartaric acid.

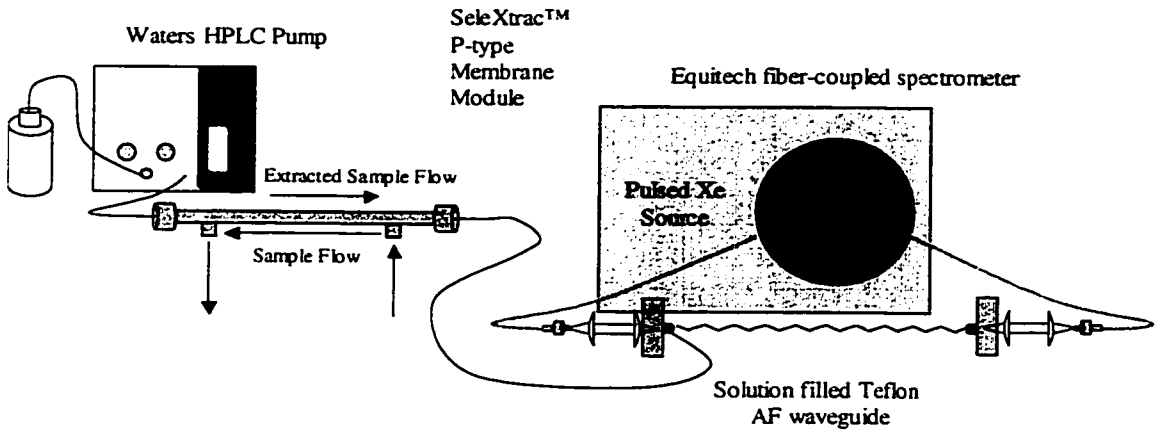

Figure 6.5 - SeleXtrac membrane module in line with LCW for detection

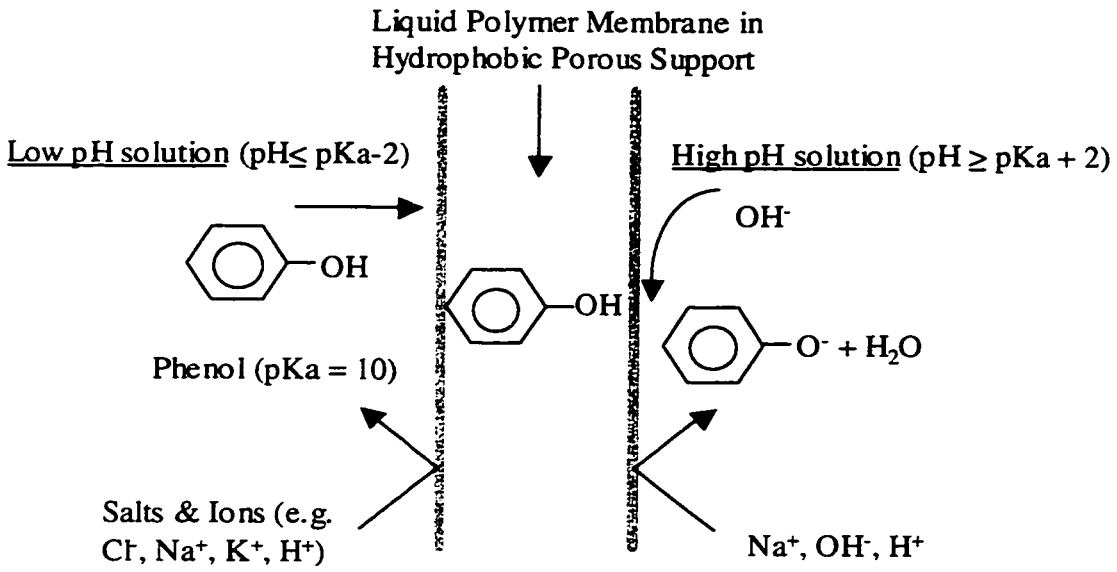

Figure 6. 6 - SLM chemistry for extraction of phenol. 0.1 N NaOH was used as the strip solution for extraction of phenol using.

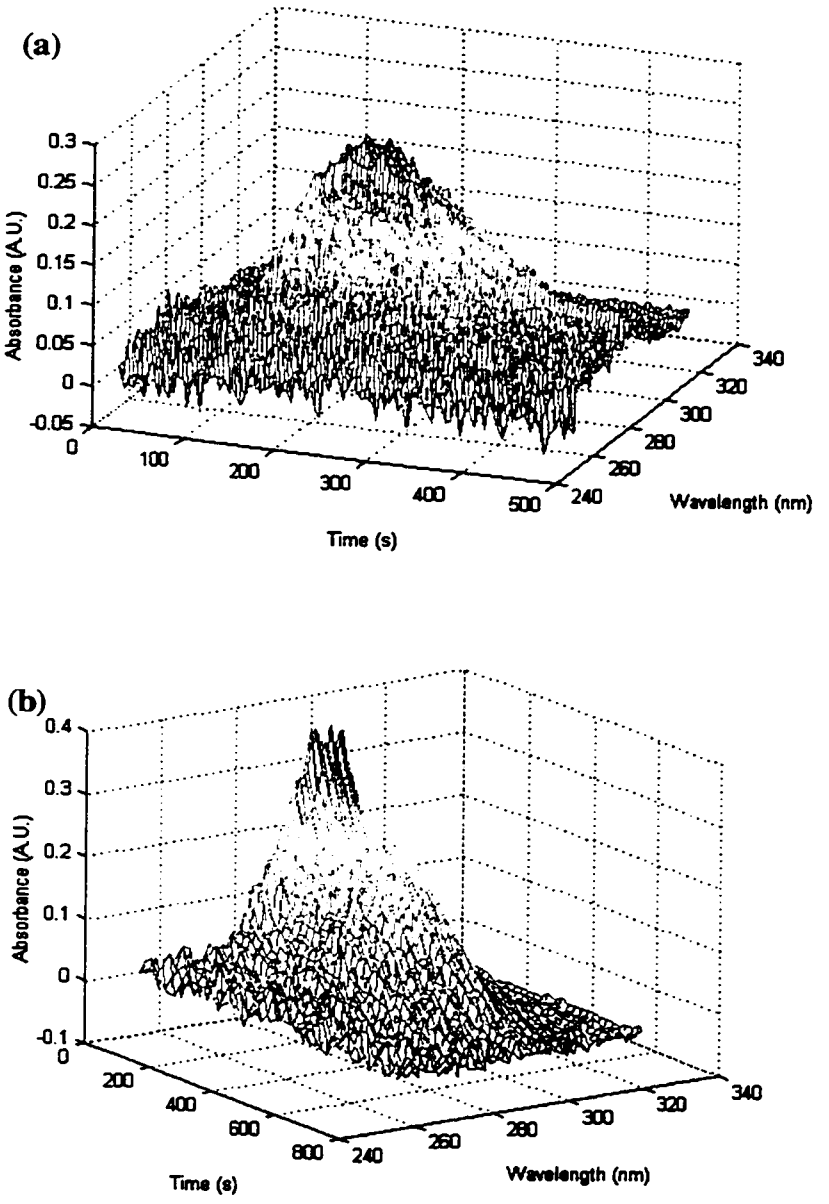

Figure 6.7 - Plot a depicts the extraction of phenol under constant flow (50 mL/min)of 0.1N NaOH solution on the strip side of the membrane. Data collection was begun as soon as an aqueous solution of 10 mM phenol was introduced into the extraction module. Phenol is extracted and converted to its anion (λ_{max}= 288 nm), and flowed through the waveguide core, where it is detected as a perturbation to the transmitted light intensity. Plot b is a similar extraction of the same concentration of aqueous phenol, but the NaOH flow was stopped for 2 minutes to allow pre-concentration of the phenol anion on the strip side of the membrane.

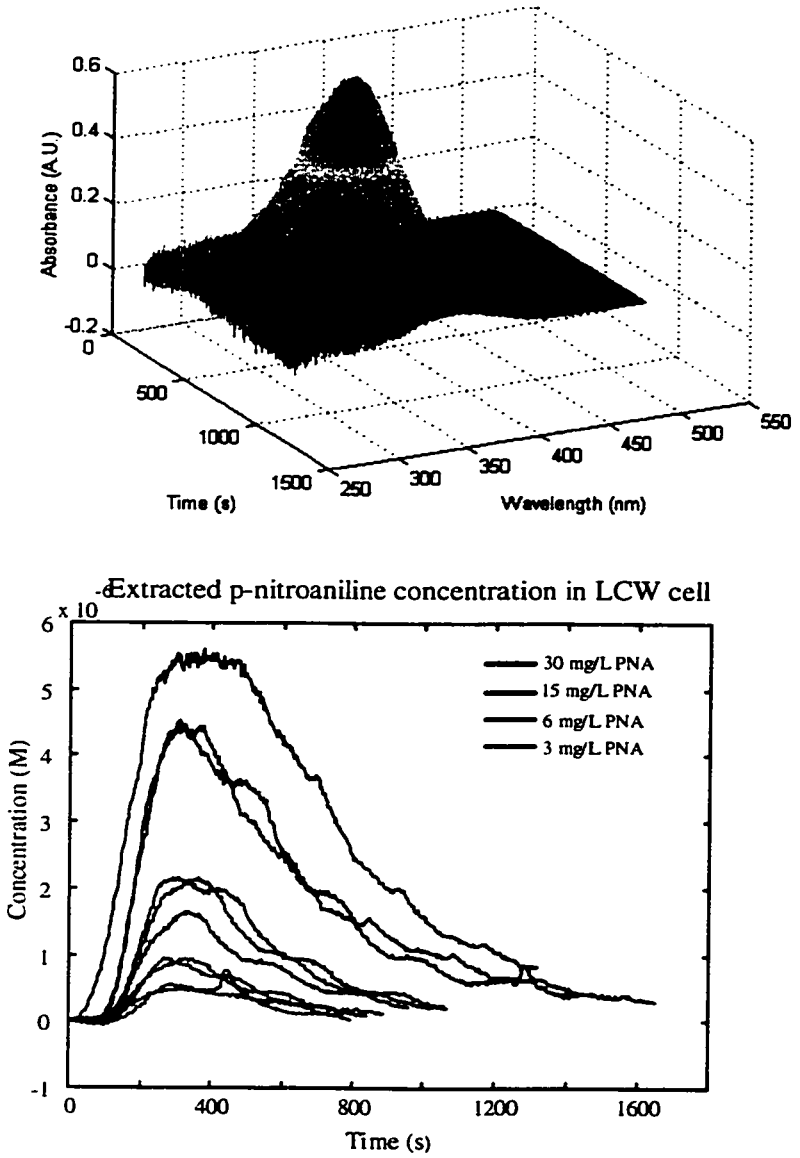

Figure 6.8 – The top plot depicts the extraction of a 15 mg/L p-nitroaniline solution. The 5 mL sample was flowed in a fast-loop through the SeleXtrac module at 2.5 mL/min while the 0.1 N HCl strip solution was flowed through the module at 50 μL/min into the waveguide. The λ_{max} of the acidic solution containing aniline is 392 nm. The bottom plot shows traces (at λ_{max}) for several concentrations of p-nitroaniline (PNA), and the measured concentration inside the waveguide. Calibration of the measured concentration was achieved by injections of p-nitroaniline in 0.1N HCl into the waveguide.

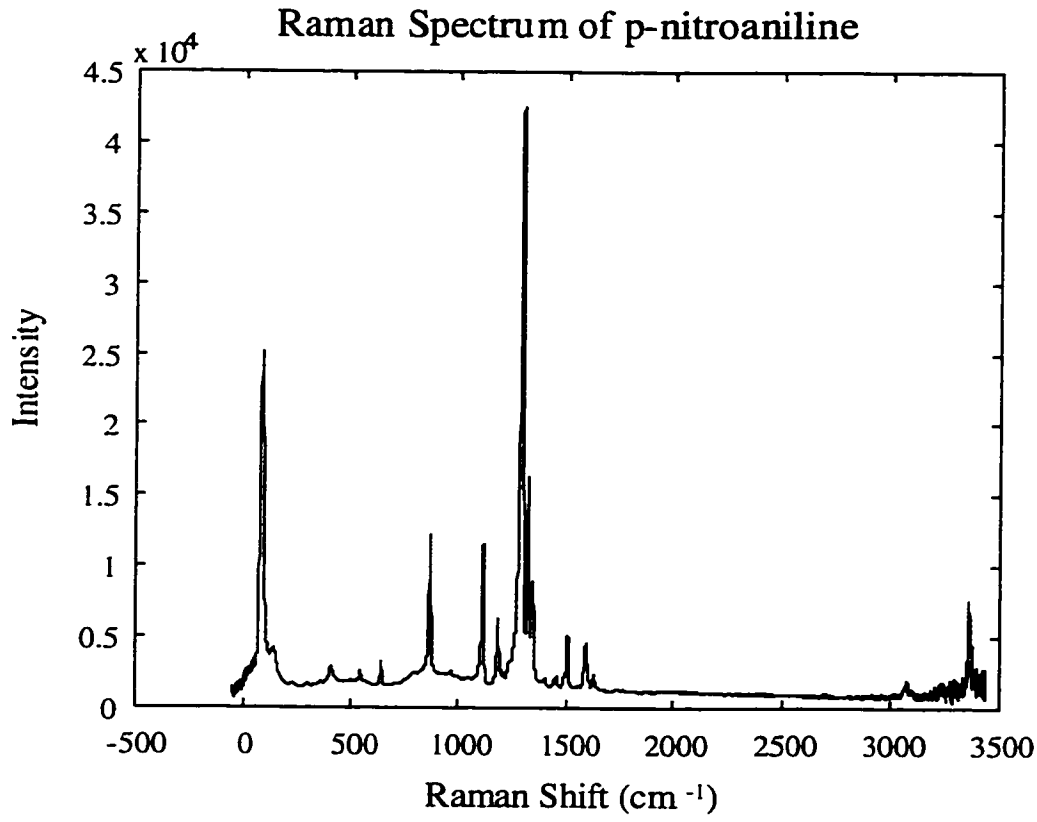

Figure 6.9 - Raman spectrum of p-nitroaniline. Note the intense emission near 1300 cm^{-1}.

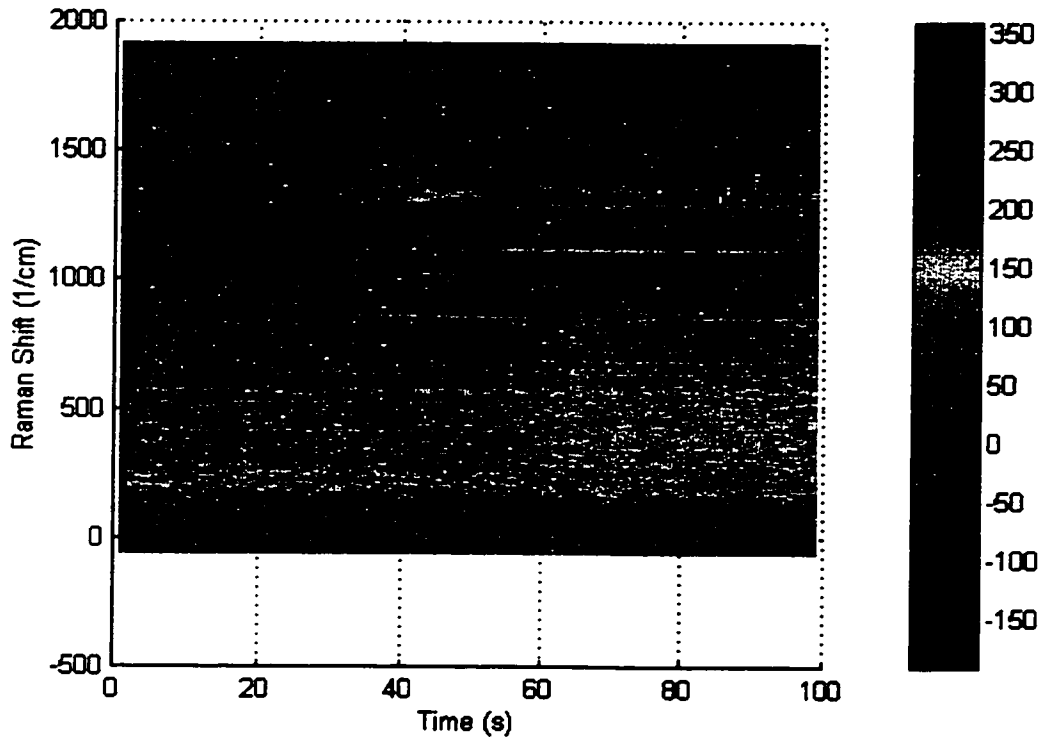

Figure 6.10 - The contour plot to the left is preliminary extraction data from the Raman waveguide system using the same chemistry as the UV/Vis experiment. The time scale is seconds. The color indicates the background-subtracted Raman intensity in counts. The PNA sample concentration was 70 mg/L which flowed at 2.5 mL/min through the module. The 0.1N HCl strip solution flowed through the Raman waveguide. Notice that several Raman bands increase in intensity as the extracted p-nitroaniline reaches the waveguide.

Chapter 7 – Conclusions

7.1 – Summary

This dissertation has described the development of modular chemical sensing systems in which the sampling interface is regenerated. The first of these systems, the chemiluminescent fiber optic biosensor, employed a non-covalently immobilized protein layer that acted as the sampling interface. Analyte was preconcentrated selectively from the bulk by the antibody layer, followed by chemiluminescent detection. In the competition assay used, the analyte concentration was inversely proportional to the chemiluminescent intensity. If the layer was no longer active, it could be stripped out of the glass tube with a solution of alcoholic KOH and replaced with a fresh layer *in situ*.

The second of the systems presented was the two-chamber dissolved oxygen sensor. This sensor's sampling interface, the electrolyte-filled silicone coil, was regenerated with each analysis by flushing fresh reagent into the coil and pushing equilibrated reagent into the sensing region of the system, the electrode cell. The two-chamber design was employed in a submersible, autonomous sensing system for marine deployment. The prototype was deployed in fresh water for a week and its stability was tested for two months. The stability test was conducted in a constant temperature, air-bubbled, salt-water tank. The data were compared to reference samples as well as modeled responses based upon the tank's temperature and salinity,

and the atmospheric pressure. The sensing system proved to be a promising alternative to traditional electrochemical oxygen sensors.

The final chemical sensing system explored was the liquid core waveguide as a chemical sensing system and as a long-path detection cell. A Teflon ™ AF-2400 waveguide containing bromthymol blue was used to detect concentrated HCl vapor as well as CO_2 in gas streams. The Teflon™ AF-2400 waveguide parameters were optimized for maximum transmission. The material is highly scattering at wavelengths below 400 nm due to the large number of microvoids that contribute to the material's unique characteristics, and this scattering limits its usefulness as a waveguide cladding material. However, Teflon AF-2400 has very rapid gas transport characteristics for small molecule gases.

The liquid core waveguide was also demonstrated as a long-path absorbance cell with a supported liquid membrane sampling interface. The supported liquid membrane was used to extract both phenol and p-nitroaniline which were detected with the liquid core waveguide under flowing conditions. Raman detection of extracted p-nitroaniline also was demonstrated. The supported liquid membranes were demonstrated as sensing system sampling interfaces that impart analyte selectivity to the sensing system. The reagent that acts as the extractant with the supported liquid membrane is a key part of the sampling interface. This reagent, and therefore sampling interface, is regenerated by pumping the extract into the waveguide.

It is possible to apply the modular components of the systems presented here in various configurations to solve chemical analysis problems. There are many common

threads between the sensing systems presented here, mainly fluidics and reagent chemistry. In addition, the sampling interface, traditionally the weakest portion of the sensing system, can be regenerated, increasing the stability of a sensing system. Unique modes of detection, such as the liquid core waveguide and the scintillation fiber probe provide for sensitive detection of analyte.

7.2 – Future Directions

This body of work presented several different sensing systems that could be studied and characterized further. This would include studying the current sensing systems further, developing them for new applications, or applying the modules to new sensing systems.

Development of the liquid core waveguides is still in its infancy. Cladding materials with less scattering are being studied as long-path detection cells, particularly for Raman detection. Ideally, the cladding material will be able to act as both a semi-permeable membrane and the liquid core waveguide material, but as we discovered with the oxygen sensing system, a single-chamber approach may not be the best approach for this. The Teflon™ AF is still a unique material due to its high diffusion rates, making it an ideal sampling coil material. In addition, further characterization of the SLM modules is required for their application as a sampling interface for a sensing system. In particular, better methods must be developed for replacing the liquid membrane material *in situ*, extending the module lifetime.

The oxygen sensing system demonstrated good stability over a two-month test. Future directions for this system include a moored deployment in a marine environment and a more detailed comparison to other oxygen sensing systems. Development of the O_2 sensor for applications such as fermentation monitoring would be another direction for research.

Bibliography

M.S. Abdel-Latif, G. G. Builbault, in Biosensor Technology Fundamentals and Applications, Marcel Dekkar, Inc., New York, (1990), 285-289.

R. Altkorn, I. Koev, R.P. Van Duyne, M. Litorja; Applied Optics, Vol. 36, (1997), 8992.

T. Araki, H. Misawa; Review of Scientific Instruments, Vol. 66, No. 12, (1995), 5469-5472.

B. Arkles, "Silane Coupling Agent Chemistry", Hüls Technical Note, (1991), 59-64.

R.J. Berman, G.D. Christian, L.W. Burgess; Analytical Chemistry; Vol. 62, (1990), 2066-2071.

R.J. Berman, Ph.D. Dissertation, University of Washington, Seattle, WA, (1990).

R.J. Berman, L.W. Burgess; Proceedings of SPIE – Chemical, Biochemical, Environmental Fiber Sensors II; Vol. 1368, (1991), 25-35.

Biogeneral Application Notes, 1999.

S. Birnbaum, S. Nilsson; Analytical Chemistry, Vol. 64, (1992), 2873.

J. Buffle, K.J. Wilkinson, M. Tercier, N. Parthasarathy; Annali di Chimica, Vol. 87, (1997), 67.

J.H. Carpenter; Limnology and Oceanography, Vol. 10, (1965), 141-143.

CRC Handbook, 71st edition, (1994).

D. Blair, H. Diehl; Talanta, Vol. 7, (1961), 163-174.

M.V. Cattaneo, K.B. Male, J.H.T. Luong; Biosensors and Bioelectronics, Vol. 7, (1992), 569-574.

P.K. Dasgupta; Analytical Chemistry, Vol. 56, (1984), 1401-1453.

M.D. DeGrandpre; Analytical Chemistry, Vol. 65, (1993), 331-337.

M.D. DeGrandpre, M.M. Baehr, T.R. Hammar; Analytical Chemistry, Vol. 71, No. 6, (1999), 1152-1159.

M.D. DeGrandpre, T.R. Hammar, S.P. Smith, F.L. Sayles; Limnology and Oceanography, Vol. 40, No. 5, (1995), 969-975.

A.B. de Haan, P.V. Bartels, J. De Graauw; Journal of Membrane Science, Vol. 45, (1989), 281-297.

J.N. Demas, B.A. DeGraff, P.B. Coleman; Analytical Chemistry, Vol. 71, No. 23, (1999), 793A-800A.

N.K. Djane, K. Ndung'u, F. Malcus, G. Johansson, L. Mathiasson; Fresnius' Journal of Analytical Chemistry, Vol. 358, (1997), 822-827.

I. Durrant; Nature, Vol. 346, (1990), 247.

T.M. Freeman, W.R. Seitz; Analytical Chemistry, Vol. 50, No. 9, (1978), 1242-1246.

K. Fuwa, W. Lei, K. Fujiwara; Analytical Chemistry, Vol. 56, (1984), 1640-1644.

Harcourt Academic Press Dictionary of Science and Technology.

H.E. Garcia, L.I. Gordon; Limnology and Oceanography, Vol. 37, No. 6, (1992), 1307-1312.

J.M. Henshaw, Ph.D. Dissertation, University of Washington, Seattle, WA (1993).

J.M. Henshaw, L.W. Burgess; Proceedings of SPIE – Chemical, Biochemical, Environmental Fiber Sensors III; Vol. 1587, 39-47.

J. Hlavay, S.D. Haemmerli, G.G. Guilbault; Biosensors and Bioelectronics, Vol. 9, (1994), 189-195.

S.V. Ho, U.S. Patent 5,507,949.

S.V. Ho, U.S. Patent 5,512,180.

S.V. Ho, P.W. Sheridan, E. Krupetsky; Journal of Membrane Science, Vol. 112, (1996), 13-27.

K. Hong, Ph.D. Dissertation, University of Washington, Seattle, WA (1995).

K. Hong, L.W. Burgess; Proceeings of SPIE, Vol. 2293, (1994), 71-79.

J. Janata, Principles of Chemical Sensors, Plenum Press, (1989), 201-206.

H.W. Jannasch, K.S. Johnson, C.M. Sakamoto, Analytical Chemistry, Vol. 66, (1994), 3352-3361.

M. Knutsson, L. Mathiasson, J.A. Jonsson; Chromatographia, Vol. 42, (1996), 165.

W. Lang, R. Zander; Ind. Eng. Chem. Fundam., Vol. 25, No. 4, (1986), 775-782.

Z. Lin, L.W. Burgess; Analytical Chemistry, Vol. 66 (1994), 2544.

C.A. Lucy, F.F. Cantwell; Analytical Chemistry, Vol. 61, (1989), 101-107.

C.A. Lucy, K. Yeung; Analytical Chemistry, Vol. 66, (1994), 2220-2225.

C.A. Lucy, S. Varkey; Analytical Chemistry, Vol. 67, (1995), 3036-3041.

Y. Luo, R. Al-Othman, J. Ruzicka, G.D. Christian; Analyst, Vol. 121, (1996), 601-606.

B.J. Marquardt, P.G. Vahey, R.E. Synovec, L.W. Burgess; Analytical Chemistry, Vol. 71, No. 21, (1999), 4808-4814.

C. McDonagh, B.D. MacCraith, A.K. McEvoy; Analytical Chemistry, Vol. 70, (1998), 45-50.

L.K. Moore, D.J. Veltkamp, J.L. Cortina, Z. Lin, L.W. Burgess; Sensors & Actuators B, Vol. 38-39, (1997), 130-135.

M.C. Moreno-Bondi, O.S. Wolfbeis, M.J.P. Leiner, b.P.H. Schaffer; Analytical Chemistry, Vol. 62, (1990), 2377-2380.

K.L. Peterson, B.K. Logan, G.D. Christian, J. Ruzicka; Analytica Chimica Acta, Vol. 99, (1997), 99.

E.P. Plueddemann, Silane Coupling Agents, 2nd Ed., Plenum Press, (1991), 242-247.

A. Sanz-Medel, J.M. Costa-Fernandez, M.E. Diaz-Garcia; Analytica Chimica Acta, Vol. 360, (1998), 17-26.

A. Sanz-Medel, M.E. Diaz-Garcia, M.R. Fernandez, W.L. Hinze; Mikrochimica Acta, Vol. 1, (1988), 269-282.

A. Sanz-Medel, Y.M. Liu, M.R. Fernandez, M.E. Diaz-Garcia; Mikrochimica Acta, Vol. 3, (1991), 53-64.

J. Setchenov; Z. Phys. Chem., Stoechiom, Verwandtschaftsl., Vol. 4, (1889), 117-125.

J.E. Sherwood, F. Stagnitti, M.J. Kokkinn; Limnology and Oceanography, Vol. 36, No. 2, (1991), 235-250.

D.L. Short, G.S.G. Shell; Journal of Physics E: Scientific Instrumentation, Vol. 18, (1985), 79-87.

L.C. Shriver-Lake, K.A. Breslin, P.T. Charles, D.W. Conrad, J.P. Golden, F.S. Ligler; Analytical Chemistry, Vol. 67, (1995), 2431-2435.

J. Stone; IEEE Journal of Quantum Electronics, QE-8, (1972), 386-388.

J. Stone; Applied Physics Letters, Vol. 20, (1972), 239-240.

K. Tsunoda, A. Nomura, J. Yamada, S. Nishi; Applied Spectroscopy, Vol. 44, (1990), 163.

R.D. Waterbury, W. Yao, R.H. Byrne; Analytica Chimica Acta, Vol. 357, (1997), 99-102.

J. Wang, J. Wang, J. Lu, B. Tian, D. MacDonald, K. Olsen; Analyst, Vol. 124, (1999), 349-352.

D.A. Weeks, K.S. Johnson; Analytical Chemistry, Vol. 68, (1996), 2717-2719.

L. Wei, K. Fujiwara, K. Fuwa; Analytical Chemistry, Vol. 55, (1983), 951-955.

J.P. Whelan, A.W. Kusterbeck, G.A. Wemhoff, R. Bredehorst, F.S. Ligler; Analytical Chemistry, Vol. 65, (1993), 3561-3565.

P. Wieczorek, J.A. Jonsson, L. Mathiasson; Analytica Chimica Acta, Vol. 346, (1997), 191-197.

D. Wijesuriya, K. Breslin, G. Anderson, L. Shriver-Lake, F.S. Ligler; Biosensors and Bioelectronics, Vol. 9, No. 8, (1994), 585-592.

L.S. Winkler; Ber. Dtsche. Chem. Ges., Vol. 21, (1988), 2843-2855.

D. Wolcott, U.S. Patent 5,317,932 (1997).

X. Zhou, M.A. Arnold; Analytica Chimica Acta; Vol. 304, (1995), 147-156.

Vita

Heather Colburn Edberg was born to James F. Colburn and Lynn G. Colburn on May 17, 1972 in Dallas, TX. In 1990, she graduated from Amador Valley High School in Pleasanton, CA, graduating in the top 10% of her class. She received a B.S. in Chemistry and a B.A. in Physics from Whitworth College in Spokane, WA in 1994, graduating *cum laude*. Her senior research project involved the sythesis and GC/MS characterization of dichlorocyclohexane products for characterization of a photo-chlorination reaction. During the summers of 1992, 1993, 1994, she participated in Lawrence Livermore National Lab's Summer Employment Program where she conducted research analyzing air and soil contamination plumes with thermal desorption GC/MS, performed simulated distillation on shale oil, and developed a miniature, portable mass spectrometer for detection of surface contaminantion on machined parts. During the summer of 1994, she married Kyle G. Edberg to whom she is still wed. In the fall of 1994, she enrolled in the University of Washington where she received her M.S. in Chemistry in 1996 and completed the requirements for a Doctor of Philosophy degree in Chemistry in January 2002. In December 2000, she began working for TraceDetect LLC in Seattle, WA where she will continue to work full-time after graduation on chemical methods development as well as instrumentation development.